Aerogels Based on Biodegradable Polymers and Clay

Liang Wang

A thesis presented to obtain the qualification of degree of Doctor

From the

Universitat Politècnica de Catalunya

Supervised by Dr. Miguel Sánchez-Soto

Department de Ciència dels Materials i Enginyeria Metal·lúrgica

Universitat Politècnica de Catalunya, Barcelona TECH

Terrassa, September 2015

Acknowledgement

In the whole life, we always say "Thanks!" to different people surrounding us, like moon to stars in the night sky…

I would like to express my sincerest appreciation to my advisor, Prof. Miguel Sánchez-Soto. He gave me a lot of encouragement and support in the past years. His patient and strict guide deeply influence me. I thank to the other members of CCP which kindly help me during these years, Prof. Maria Lluisa Maspoch, Orlando Santana, Jose Ignacio Velasco, Silvia Illescas, David Arencon, Vera Realinho, Antonio Martinez, Marcelo Antunes, Tobias Abt; Jonathan, Hakim, Gabriel, Hooman, Noel. I also want to thank to the Prof. Jordi Bou for his kind help in the degradation experiments and also to Josep Palou and Francisco Barabova for their great support. I would to say that I feel very lucky to work together with them and I had a very enjoyable life in Universitat Politecnica de Catalunya and Terrassa.

I offer my sincere appreciation to the financial support for China Scholarship Council. Finally, I want to thank my beloved parents and sisters, who always show their selfless love to me.

读万卷书，

行万里路。

Summary

Foam-like aerogels based on biodegradable polymers and sodium montmorillonite (Na^+-MMT) clay were prepared through an environmentally friendly freeze-drying process. Both synthesized and bio-based polymers were utilized in this thesis, including polyvinyl alcohol (PVOH), carboxylmethylcellulose (CMC), xanthan gum, agar, Arabic gum and starch. The morphologies of aerogels were characterized using scanning electron microscopy. The mechanical properties investigation included compression and impact tests. Porosities and solid densities were measured using a helium pycnometer while the pore size distribution was determined by automated mercury porosimeters.

Most of polymer-clay aerogels exhibited porous and layered structures that were formed via ice templating. However, high viscosity of the precursor solution may break the layered architecture by retarding the formation of ice crystals (e.g. 2.5 wt% agar aqueous solutions). The structures as well as the properties of aerogels were mainly influenced by polymer/clay proportion. Polymer molecules play a role of glue linking the clay nanoparticles, improving the structural integrity and hence the mechanical performance of the aerogels. On the other hand, clay platelets serve as a physical barrier that increases the heat endurance.

Recycled cellulose fibers (RCF) that were isolated from waste paper pulp were also used to prepare bio-based aerogels. Adding another biopolymer CMC into RCF aerogels, the resultant RCF-CMC composite aerogels showed different microstructures and enhanced mechanical properties.

Physical blending and chemical crosslinking were used to tailor the mechanical properties of xanthan gum/clay aerogels and starch/clay aerogels, respectively. Blending agar with xanthan gum in aqueous solution, the resultant aerogels displayed a significant improvement in mechanical properties compared with those containing a single biopolymer. Moreover, they exhibited tunable microstructures and mechanical

properties by changing agar/xanthan gum ratio in the aerogels. As to starch/clay aerogels, the incorporation of glutaraldehyde enhanced the structural integrity and mechanical properties of the aerogels through crosslinking reaction with starch molecules, which was proved by Fourier-Transform infrared (FT-IR) spectroscopy analysis.

The evaluation of the flammability of aerogels was conducted with a cone colorimeter while the thermal stability was obtained from the results of thermogravimetric analysis. In regard to PVOH-clay aerogel, different types of flame retardant fillers, such as aluminum trihydroxide (ALH), ammonium polyphosphate (APP), silica gel and potassium carbonate, were adopted to modify their flame retardant properties. The results showed that ALH addition enhanced the flame retardancy as well as mechanical properties. For RCF-CMC aerogels, APP and clay played a synergetic effect on the flame retardancy and thermal stability.

Resumen

En esta Tesis se han preparado diversos aerogeles usando polímeros biodegradables como matriz y arcilla como refuerzo, a través de un proceso de fabricación amigable con el medio ambiente. Los polímeros empleados han sido tanto de origen natural (goma árabiga, agar-agar, goma xantana, almidón) o sintéticos como la carboximetilcelulosa (CMC) o el alcohol polivinílico. Los compuestos formados se han caracterizado a través de diferentes técnicas con el objeto de relacionar las morfologías generadas con las propiedades térmicas y mecánicas resultantes.

La gran mayoría de los aerogeles polímero/arcilla exhiben una estructura porosa y laminar que se forma a raíz de la liofilización. Sin embargo, se ha apreciado que altas viscosidades en la solución precursora puede romper la arquitectura laminar al retardar el crecimiento de los cristales de hielo (ej. Solución acuosa de 2.5 % peso de agar). La estructura y las propiedades de los aerogeles están asimismo y en general

influenciados por la relación polímero/arcilla. En estos sistemas, las moléculas de polímero actúan a manera de pegamento uniendo las partículas de arcilla, incrementando de esa manera notablemente la capacidad mecánica de los aerogeles. Por otro lado la arcilla actúa entre otras formas, como barrera térmica incrementando la resistencia térmica y al fuego de las espumas formadas.

Dentro de este trabajo se han empleado fibras de celulosa recicladas de residuos de papel en un intento de preparar bio-aerogeles a partir de material de desecho. La unión de estas fibras con CMC permitió obtener aerogeles con propiedades mejoradas y la posibilidad de emplear estos residuos en un segundo uso. Además del mezclado físico, en algunos casos se ha realizado una reacción de entrecruzamiento para ajustar las propiedades finales, como en el caso de los aerogeles goma xantana/arcilla o almidón/arcilla. La mezcla de agar con goma xantana en solución acuosa resultó en un notable aumento de propiedades con respecto a las composiciones que contenían un único polímero, debido al cambio morfológico inducido, pasando de una estructura laminar a una de tipo panal de abeja (honeycomb). De esta forma y a través de la relación entre estos dos polímeros naturales ha sido posible balancear y definir las propiedades finales deseadas para el aerogel. En los sistemas almidón/arcilla el entrecruzamiento se ha conseguido a través de un agente externo como el glutaraldehido.

Atendiendo a su posible uso final, unas de las propiedades más relevantes en los aerogeles que se ha estudiado ha sido la estabilidad térmica y la resistencia al fuego. En este sentido, se han preparado sistemas basados en Polivinilalcohol/arcilla modificados con diferentes retardantes de llama. De los diversos aditivos probados la combinación con hidróxido de aluminio ha mostrado un efecto sinérgico incrementando tanto de la resistencia a fuego como las propiedades mecánicas. En los sistemas basados en celulosa la presencia de polifosfato de amonio y arcilla ha demostrado así mismo un efecto potenciador de la estabilidad térmica y en el retardo de llama.

CONTENTS

List of Figures

List of Tables

Abbreviations

AG	Arabic gum
ALH	Aluminium trihydroxide
Al_2O_3	Alumina
APP	Ammonium polyphosphate compound
ATR	Attenuated total reflectance
CEC	Cation exchange capacity
CMC	Carboxymethylcellulose
CNFs	Cellulose nanofibers
EPS	Expanded polystyrene
FD	Freeze-drying
FGR	Fire growth rate
FTIR	Fourier-Transform Infrared
GL	Glutaraldehyde
LDH	Layered double hydroxide
MMT	Montmorillonite
Na^+-MMT	Sodium montmorillonite
OM	Optical microscopy
PC	Potassium carbonate
PVOH	Polyvinyl alcohol
RCF	Recycled cellulose fibers
SCD	Supercritical drying
SD	Shrinkage degree
SEM	Scanning electron microscopy
SG	Silica gel
TGA	Thermogravimetric analysis
THR	Total heat release
TTPHRR	Time to peak of heat release rate
XG	Xanthan gum

Symbols

ρ_{app}	Apparent density	[g/cm^3]
ρ_{ts}	Theoretic solid density	[g/cm^3]
ρ_{es}	Experimental solid density	[g/cm^3]
σ	Compressive strength	[MPa, kPa]
$\sigma_{10\%}$	Compressive strength at 10% strain	[kPa]

$\sigma_{70\%}$	Compressive strength at 70% strain	[MPa]
σ_y	Yield strength	[kPa]
σ_{sy}	Specific yield strength	[kPa/(g/cm^3)]
ε	Compressive strain	[%]
ε_{max}	Maximum deformation	[%]
D	Pore diameter	[μm]
dW/dT_{max}	Maximum mass decomposition rate	[%/°C]
E	Compressive Young's modulus	[Mpa]
E_a	Energy absorbed	[kJ/m^3]
E_s	Specific compressive modulus	[MPa/(gcm^{-3})]
$T_{d\,5\%}$	Temperature at 5% mass loss after 150 ^{o}C	[°C]
$T_{d\,max}$	Temperature at maximum decomposition rate	[°C]
t_e	Time to flame extinguish	[s]
t_i	Time to ignite	[s]
V	Viscosity	[mpa s]
w	Mass fraction	[%]
W_R	Residue amount	[%]

Chapter 1: Introduction

1.1 Prologue

Aerogel pioneered by Kistler is a type of foam-like materials, which usually exhibit lightweight density and high porosity. The development of matrix materials and processing methods of aerogels widely expanded their properties and corresponding applications. One of most attractive research was about smectite clay aerogel prepared through a freeze-drying technique due to the cheap price as well as an environment-friendly preparation process. However, their mechanical brittleness limited their practical applications.

In order to overcome this handicap, a novel and appealing route firstly reported by Nakazawa was to infiltrate the clay aerogel with polymers. Thus polymer/clay aerogels composites were created with significantly enhanced mechanical properties. This is due to that polymer molecules interact with clay nanoplatelets through hydrogen bonding or electrostatic attraction.

In this thesis, different types of biodegradable polymers (polyvinyl alcohol, recycled cellulose fiber, sodium carboxylmethylcellulose, agar, xanthan gum, Arabic gum, starch) were utilized to prepared polymer-clay aerogels using a freeze-drying process in which the sole solvent used was water. These polymer-clay aerogels displayed the typical compressive behavior of elastic-plastic foams. Herein, they were considered as a promising alternative of non-biodegradable traditional petroleum-based foams (e.g. expanded polystyrene) that are widely used in packing, insulation, cushioning and floating.

According to the statistics for the year 2007, the global market for expanded polystyrene (EPS) was over 4 million tonnes. Because they have a density as low as 15 kg/m^3, the volume of the annual consumption is difficult to even envision. The increasing environmental problem caused by the EPS waste drives the biodegradable foam-like polymer-clay aerogels to be an interesting research topic.

The microstructures, mechanical properties and thermal stability of prepared aerogels were investigated. In addition, to realize the properties of polymer-clay aerogels can compete with traditional polymeric foams, physical blending or chemical crosslinking routes were adopted to modify their properties. It was feasible to obtain materials with tunable structures and mechanical properties.

On the other hand, petroleum-based foams are intrinsically highly flammable due to their low heat capacity, low thermal conductivity and high internal surface area. The challenges from fire hazard require developing less flammable foam materials. The fire behavior of the polymer-clay aerogels was studied, showing superior flame retardant properties than EPS due to the loading of inorganic clay. Combination flame retardant (FR) fillers (alumina trihydrate, ammonium polyphosphate, silica gel and potassium carbonate) into aerogels yielded better flame retardancy. Moreover, enhanced compatibility of mechanical properties and fire resistance was obtained when alumina trihydrate was used to modify polyvinyl alcohol (PVOH)-clay aerogel. Corresponding flame retardant mechanisms were proposed according to the experimental data.

1.2 Objectives

The purpose of this thesis is to develop biodegradable polymer/clay composite aerogels. Biodegradable synthetic polymers as well as biopolymers from renewable resource have been utilized. The mechanical properties and flame resistance of the aerogels were modified to expand the potential application of these aerogel in relevant scientific and industrial fields. A state-of-the-art (chapter 2) will be presented as a review of previous works related with the aim of the thesis. The experimental work of is divided in five parts:

(1) Raw materials information, aerogels sample preparation methods and the properties characterization techniques (chapter 3).

(2) PVOH-clay aerogels and their properties modification with different flame retardant fillers (chapter 4).

(3) Aerogels based on recycled cellulose fibers and carboxylmethylcellulose; improving their thermal stability and flame retardancy by adding clay and ammonium polyphosphate (chapter 5).

(4) Exploring and developing possibilities of preparing naturally occurring bio-based polymers/clay aerogels. The raw materials included agar, xanthan gum (chapter 6), Arabic gum (chapter 7) and starch (chapter 8).

(5) Investigation of biodegradability of prepared aerogels (chapter 9).

Chapter 2: State-of-the-art

In this chapter, a comprehensive literature review is presented. Different types of aerogels, which were prepared through supercritical carbon dioxide (CO_2) drying technique and freeze-drying process, were firstly summarized and their applications were briefly introduced. Then the state-of-the-art regarding the development of clay and polymer/clay aerogels prepared via freeze-drying technique was emphasized. The modification methods for improving the properties of polymer/clay aerogels (especially the mechanical properties and fire resistance) were discussed as well. Finally, the relationships between the processing, structures, and properties were described.

2.1 Origin of Aerogels

The term aerogel was first introduced by Kistler in 1930s to designate dry silica gels with a very high relative pore volume after a supercritical drying process [1]. During this procedure, the liquid in the gel was firstly substituted by supercritical CO_2 fluid in an autoclave under its critical temperature and pressure followed by leaking the gas. Therefore, the formation of liquid-vapor meniscuses was prevented, creating dry samples without collapsing the gel solid network. Besides silica aerogels, Kistler synthesized a series of aerogels with different natures ranging from metal oxide aerogels (tungstic, ferric, or stannic oxide and nickel tartrate) to organic aerogels (cellulose, nitrocellulose, gelatine, agar, or egg albumin) [2]. After the discovery of Kistler, aerogels have been progressively developed with various functions and applications.

2.2 Sol-gel Process

The precursor gels of aerogels can be prepared using a sol-gel process in which a colloidal solution is firstly produced by hydrolyzing raw materials followed by condensation of sol particles. An ageing process is subsequently conducted to increase the connection and strength of the gel network. The obtained gel is finally transformed into aerogel via different drying techniques [3]. A typical scheme of this process is as shown in Figure 2.1.
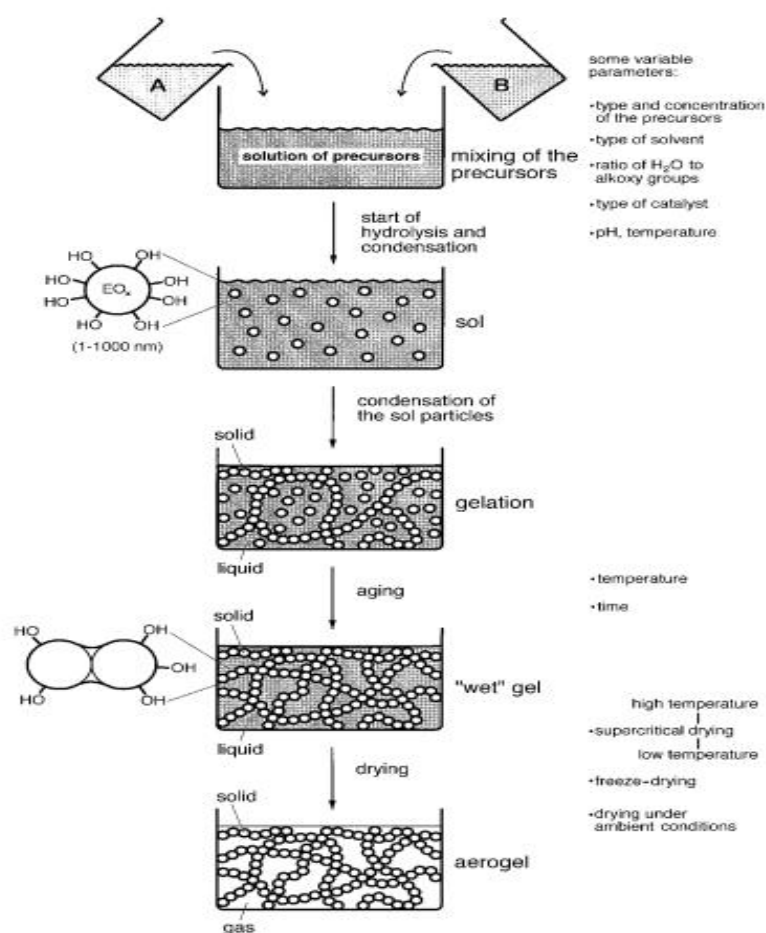
Figure 2.1 General scheme for preparing aerogels by sol-gel processing and some typical variable parameters [3]

Two pathways that are usually used to produce aerogels include supercritical drying and freeze-drying. In the following section, aerogel are categorized based on their natures as well as drying processes. This classification can help us understand the

application of two different drying techniques in preparing different aerogels. However, the emphasis is placed on the aerogels prepared using freeze-drying that is used in present work.

2.3 Supercritical Drying

Supercritical drying (SCD) is a process by which the liquid in a matrix is transformed into gas in the absence of surface tension and capillary stress, as shown in Figure 2.2 (green arrow). To attain this attempt, the gel is put in an autoclave in which the temperature and pressure exceed the critical points. It is known that the surface tension between solvent and solute molecules ceases in a supercritical fluid. The liquid in the gel is finally replaced with a gas without destroying the solid delicate networks. The vapors are then slowly released from the autoclave, until the pressure in the autoclave reaches atmospheric pressure.
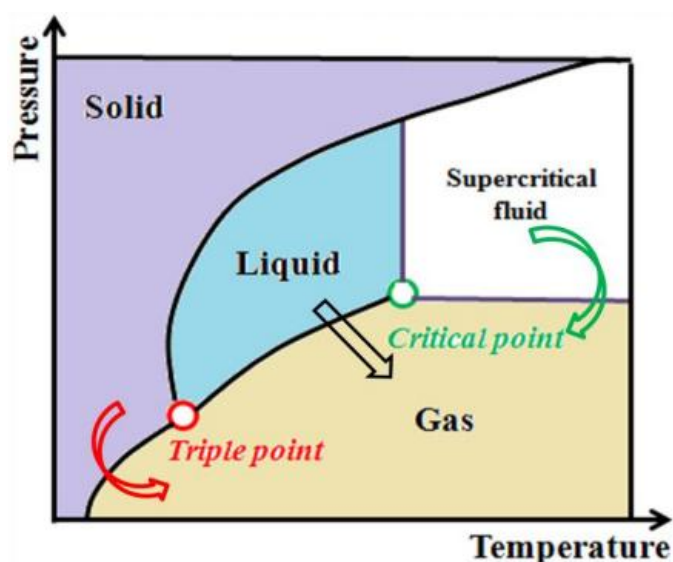
Figure 2.2 Three phase diagram: freeze drying route-red; conventional drying-black; supercritical drying-green [5]

Carbon dioxide (CO_2) is usually chosen as gas media due to its low supercritical temperature and nontoxicity. In the process of supercritical CO_2 drying, the liquid in

the gel (usually ethanol) firstly replaced by liquid CO_2 in a sealed vessel; and then CO_2 is changed to supercritical state by raising the temperature and pressure; finally the vessel is isothermally depressurized to release CO_2 gas [4]. In comparison to SCD, a high-temperature supercritical drying requires that the solvent in the vessel remains the same as the one in gel.

In the past 20 years, many aerogels have been prepared via supercritical drying technique following the scheme described in Figure 2.1. According to their chemical compositions, aerogels can be inorganic (silica, metal oxide, carbon-based aerogel), organic (polymer matrix) and organic-inoganic. These aerogels had various exceptional properties resulting in tremendous variety of applications in general or specific aspects. In this chapter, the applications of aerogels are focused in scientific experiments and engineering design, rather than in commercial products.

2.4 Aerogels Prepared via SCD

2.4.1 SiO$_2$ Aerogels

The preparation of SiO_2 aerogels from aqueous solutions of sodium silicate as described by Kistler was time-costly. Teichner et al. achieved a simple synthesis process in the 1960s [6]. In his work, tetramethoxysilane (TMOS) was dissolved in methanol, following by hydrolysis and condensation in defined amount of water. The chemical reactions during sol-gel processing of TMOS can be described by Figure 2.3. This report led to increasing interest on the researches of silica aerogel. More alkoxysilanes, such as tetraethoxysilane (TEOS), were successively used to prepare SiO_2 aerogels. The aerogels skeletons are composed of "pearl-necklace" networks [7], as seen in Figure 2.4b. Moreover, the structures of aerogels can be tailored by changing the parameters (e.g. PH value, ageing time, temperature). Due to the low-dimensional pore radii (20-150 nm) and high porosity (88-99 %), SiO_2 had superior properties, such as low bulk density (0.003-0.500 g/cm^3), high inner surface

area (100-1600 m^2/g), low thermal conductivity (0.017-0.021 W/(mK)), etc [3]. Therefore, they can be applied as thermal insulator, clean-up agents, optic elements, to name a few [8].
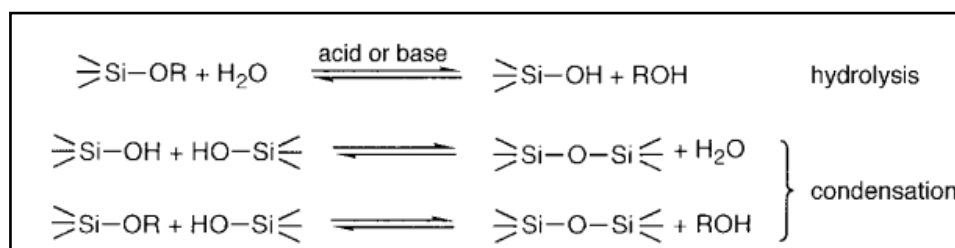
Figure 2.3 Scheme of chemical reactions for the sol-gel process of alkoxysilanes [3]
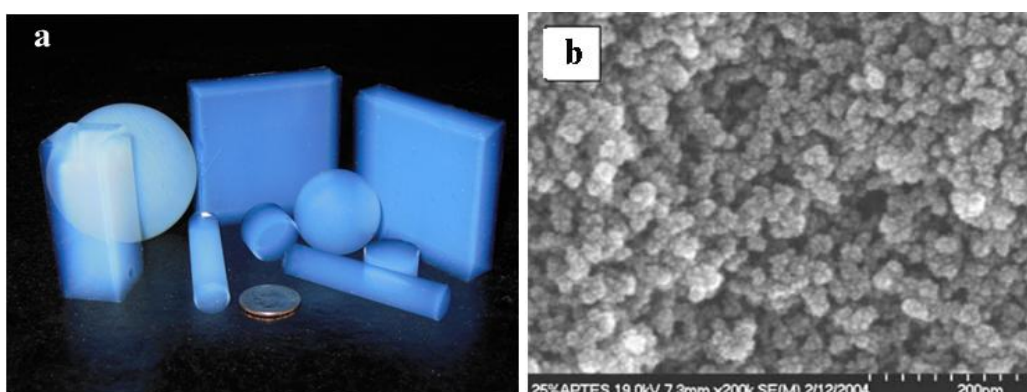
Figure 2.4 (a) Typical silica aerogels photos [9]; (b) SEM of amine modified silica aerogel from reference [10] with a apparent density of 0.19 g/cm^3

2.4.2 Metal Oxide Aerogels

Metal oxide aerogels were also first reported by Kristler. The preparation method of metal oxide aerogels is principally the same like the one of silica aerogels. However, it was developed slowly up until the 1990s due to high hydrolysis rates of the precursors (usually metal alkoxides). The late developments of new techniques [11, 12], which can control hydrolysis rate, made it possible to produce stable metal oxide gels. Unlike silica aerogels, the aerogels of various metal oxides have different morphologies, for example, V$_2$O$_5$ aerogels show fibrous structures [13] while Al$_2$O$_3$ aerogels have leaf-like ones (Figure 2.5) [14]. The metal oxide aerogels exhibit high

specific surface area (hundreds of square meters per gram) as well as their own unique properties (e.g. magnetic, electric). They have been received considerable attention because of their emerging applications in electrical engineering and electrocatalysis.
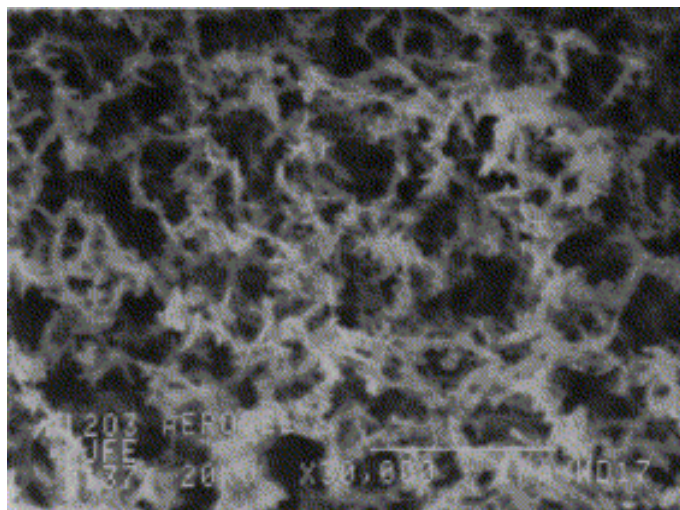
Figure 2.5 SEM of Al_2O_3 aerogel with a leaf-like morphology [14]

Multi-component metal oxides (binary or ternary metal oxide complexes) and metal doped metal oxide aerogels were also developed for expanding the functions of metal oxide family. A complete compilation is beyond the scope of this work. Some examples summarized by Husing and Schubert in 1990s [3] are listed in Table 2.1. New studies on metal oxide aerogels after them mainly focused on expanding the precursor for preparing the metal oxide aerogels or potential application of the aerogels.

Table 2.1 Examples of metal oxide aerogels, precursors for their preparation and potential applications

Aerogel	Precursor	Application
V_2O_5	$VO(OiPr)_3$, $VO(Oet)_3$	cathode in the lithium batteries
Cr_2O_3	$Cr(NO_3)_3$, $CrCl_3$, $Cr(Oac)_3$	oxidated agent, fluorination
MoO_2	$[MoO_2(acac)_2]$	electrocatalysis
Al_2O_3/SiO_2	$(AlCl_3.$ethylene oxide$).Si(OEt)_4$	catalyst support
$NiO/Al_2O_3/MgO$	$Ni(Oac)_2.ASB.Mg(OMe)_2$	nitroxidation
Pt/MoO_2	$H_2[PtCl_6]$ in MeOH	hydrogenation
Pd/Al_2O_3	$Pd(Oac)_2$	car-exhaust catalysis

2.4.3 Organic Aerogels

Pekala et al. pioneered pure organic aerogels which were synthesized by polycondensation of resorcinol-formaldehyde following by supercritical drying [15]. Sol-gel polymerization of resorcinol with formaldehyde is shown in Figure 2.6.
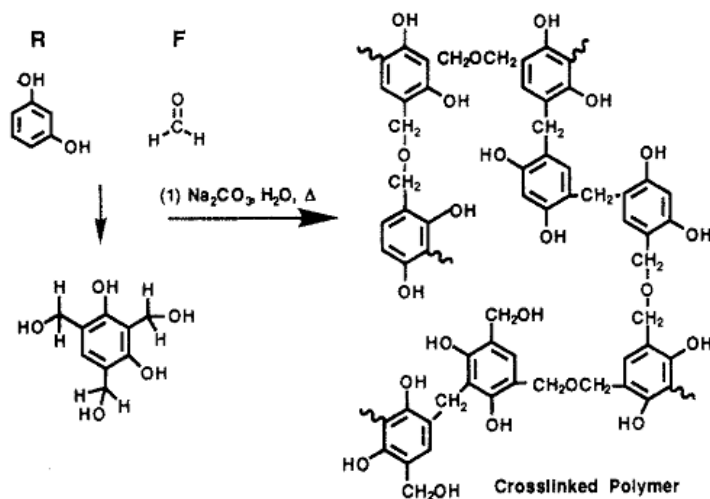
Figure 2.6 Scheme of the polymerization process for resorcinol-formaldehyde [16]

Additional development in this area was based on the polymerization reaction of phenol [17] or melamine [18] with formaldehyde. The structures of these organic aerogels were strongly influenced by the processing parameters, such as the catalyst concentration and the pH of the solution. The aerogels were dominated by micropores and mesopores (<50 nm), resulting in high specific surface area and super low thermal conductivity (as low as 0.012 W/(mK) [19]).

Except the sol-gel polymerization, precursors of aerogels can be prepared through a physical solution-gelation process as well. Firstly, hydrogels were created by gelling corresponding homogenous polymer solutions or well-dispersed particles suspensions. Then the prepared hydrogels were treated with a solvent exchange to obtain gel-ethanol mixtures before supercritical CO_2 drying [20]. These aerogels had high porosity and large specific surface area. Therefore, they were widely applied in tissue engineering, drug delivery, catalysis, absorption and separation.

Garcia et al [20] overviewed polysaccharide-based aerogels for drug delivery. Highly porous drug carriers based on starch, pectin, alginate, chitin, chitosan, carrageenan, agar and cellulose were included in their work. Quignard et al [21] summarized marine polysaccharides-based aerogel impregnated with metal nanoparticles (e.g. palladium) as catalysts and catalyst supports.

Both synthesized and natural polymers were used to prepared aerogels via this process. The structures and properties of aerogels not only depend on the nature of polymers, but also the processing parameters (e.g. temperature, drying time, solvent, etc.). Some factors will be discussed in the following sections.

2.4.4 Inorganic-organic Hybrid Aerogels

Combining organic molecules to inorganic aerogels during the sol-gel procedure can endow inorganic aerogel with exotic functions by forming inorganic-organic networks. There are four configurations of networks, as illustrated in Figure 2.7. These hybrid aerogels have been recently of great interests because some of the properties of aerogels are widened or improved without affecting the rest. For example, the hydrophobicity and the elastic properties of SiO_2 aerogels were relatively improved by incorporating organic groups [22, 23]. The publications of hybrid aerogeols (organic-silica, organic-carbon, organic-clay and organic-metal) have been boomed in last 20 years. Table 2.2 lists some of hybrid aerogel, their precursor, properties and applications.

Table 2.2 Examples of inorganic-organic aerogels, precursors of aerogels and application

Aerogel	Precursor	Key Properties	Reference
Acrylamide-SiO_2	Dimethylsiloxane, N,N-dimethylacrylamide	strong, transparent, hydrophobic	[24]
Isocyanate-SiO_2	Diisocyanate,tetramethoxysilane	flexible	[25]
Pectin-Fe_2O_3	γ-Fe2O3 nanoparticles, pectin	magnetic	[26]
Polyimide-clay	Montmorillonite, 4,4'-oxidianiline, N.N'-dimethylacetamide	heat resistant	[27]
Isocyanate-graphene	Triisocyanate, graphene oxide	high absorbent	[28]
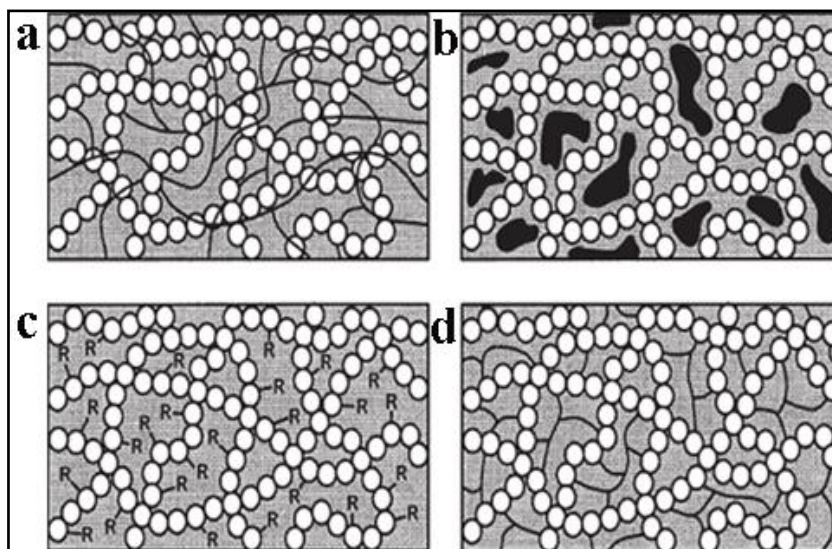
Figure 2.7 Inorganic-organic hybrid networks through sol-gel process. (a) interpenetrating inorganic and organic networks; (b) incorporation of organic molecules (enzymes, dyes, etc.); (c) functionalization of oxidic materials with organic substituents; (d) dual networks [3]

2.5 Freeze-drying Process

Freeze-drying (FD), which is also called "lyophilization", is another drying technique for avoiding phase boundaries following a three phase-diagram shown in Figure 2.2 (red arrow). The resultant porous materials are also called "cryogel".

When freeze-drying process is designed to produce aerogels, aqueous precursor solutions are needed to be prepared in advance. The pores are created by freezing the solvent into ice crystals. When the ice is sublimed under vacuum, porous materials are obtained. During the freezing process, the ice crystals nucleate and grow, expelling the impurity to the interstitial regions between those ice crystals, as shown in Figure 2.8. This process determines the structures and hence the properties of the resultant aerogels [29], which are also dependent on other factors discussed in following section. It is noted that both SCD and FD technique can be used to dry the precursors which can be prepared through the mentioned chemical sol-gel polymerization or physical solution-gelation process.
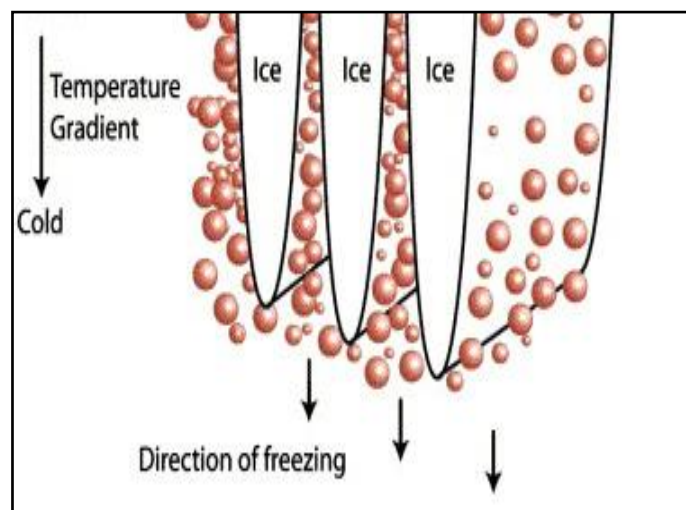
Figure 2.8 Ice crystals growth in polymer solution, inorganic nanoparticles dispersion or organic-inorganic mixture [30]

2.6 Aerogels Prepared via Freeze-drying

2.6.1 Aerogels Based on Ceramics and Carbon

Freeze-dried inorganic aerogels mainly include the ones of ceramic and carbon nature. Aerogels based on ceramic were first reported by Mahler and Bechtold in 1980. They synthesized inorganic aerogels composed of bundles of aligned silica fibers [31]. Since then, a number of works have been reported on ice-templated porous ceramics, for example, alumina aerogels were prepared by freeze-casting slurries of water [32] or water/glycerol solutions containing high loadings of alumina [33]. Deville summarized works on porous ceramics materials [34]. A wide variety of ceramic aerogels (e.g. Si_3N_4, MgO, SiC, mullite, hydroxyapatite and tricalcium phosphate) have already been prepared following the process shown in Figure 2.9. These materials usually exhibit super high mechanical properties and high porosity, herein, are considered for potential load-bearing biomaterials applications.
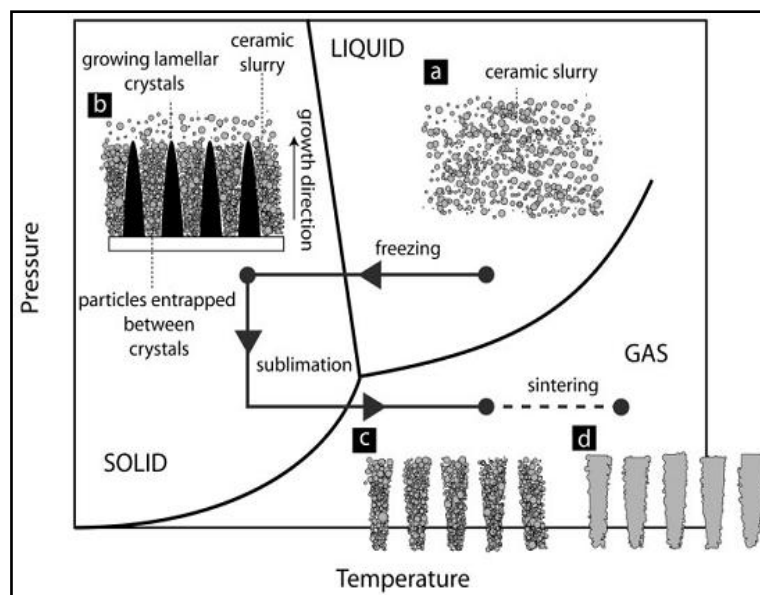
Figure 2.9 The illustration of preparation of ceramics aerogel via freeze-drying [34]

Carbon-based nano-materials, such as active carbon (black carbon), carbon nanotubes, carbon nanofibers or graphene, are nowadays the most popular topic in both frontier scientific research and industry nowadays. These advanced carbon nano-materials have been recent widely reported to make aerogels by FD process. The created foam-like carbon materials exhibit high surface area as well as high strength and electricity conductivity at extremely low density. They have been employed in various applications such as electrochemical energy storage and conversion [35], sensing [36], or catalysis [37] to name a few.

2.6.2 Clay and Clay Aerogel

Clay is a group of natural minerals mainly composed of silicate. They do exhibit great properties, such as stiffness and anti-flammability, making them a superior choice for gas barrier, reinforcement and fireproof in polymer-clay nanocomposites [38, 39]. According to the variation in the layered structure, clay can be divided into four majors groups shown in Table 2.3. The 2:1 layer type is most commonly used. They have a layered structure made up of two tetrahedrally coordinated silicon atoms fused

to an edge-shared octahedral sheet of either aluminium or magnesium hydroxide, as seen in Figure 2.10. Each layer sheet is approximate 1 nm thick and its length varies from tens of nanometers to more than one micron. Isomorphic substitution is the replacement of an element with another one inside the sheet without changing its chemical structure. For instances, Al^{3+} can be replaced by Mg^{2+} or Fe^{2+}, and Mg^{2+} by Li^+ [40]. Silicate layers stack with regular Van der Waals gap between the platelets. This gap is called the interlayer or the gallery filled with alkali cations (Na^+,Ca^{2+}, etc.), which counterbalance the negatively charged platelets.

Table 2.3 Clay types and features [41]

Group Name	Member Mineral	General Formula	Layer Type	Layer Charge
Kaolinite	kaolinite, dickite, nacrite	$Al_2Si_2O_5(OH)_5$	1:1	<0.01
Montmorillonite or smectite	montmorillonite, talc, pyrophyllite, vermiculite*, sauconite, saponite, nontronite	$(Ca,Na,H)(Al,Mg,Fe,Zn)_2(Si,Al)_4$ $O_{10}(OH)_2$ XH_2O	2:1	0.5-1.2
Illite	illite	$(K,H)Al_2(Si,Al)_4O_{10}(OH)_2$ XH_2O	2:1	1.4-2.0
Chlorite	(Ⅰ)amesite (Ⅱ)chamosite (Ⅲ)cookeite (Ⅳ)nimite	$(Mg,Fe)_4Al_4Si_2O_{10}(OH)_8$ $(Fe,Mg)_3Fe_3AlSi_3O_{10}(OH)_8$ $LiAl_5Si_3O_{10}(OH)_8$ $(Ni,Mg,Fe,Al)_6AlSi_3O_{10}(OH)_8$	2:1:1	Variable

*Layer charge of vermiculite is 1.2 to 1.8; X indicates varying level of water in mineral type.
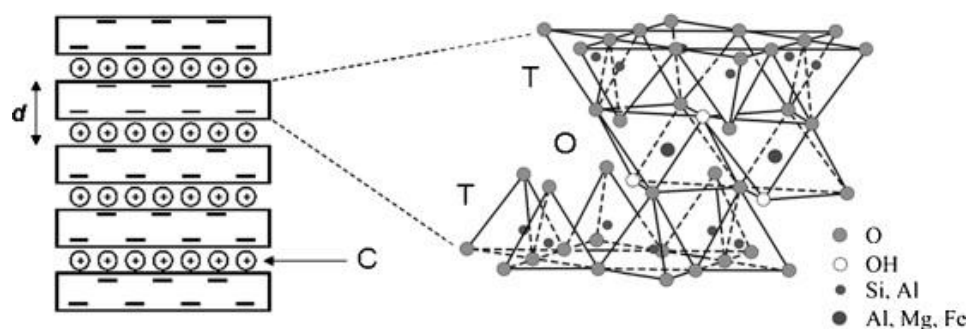
Figure 2.10 2:1 layered silicate structure (T, tetrahedral sheet; O, octahedral sheet; C, intercalated cations; d, interlayer distance) [42]

Van Olphen determined that interlayer surface and cation hydration between the galleries is a unique property of montmorillonite (MMT) [43]. This leads to high hydrophilicity and excellent swelling ability of MMT in water, which are dependent on the cation exchange ability [44]. These properties are closely related with MMT aerogels discussed in following section.

The preparation of MMT aerogel by freeze-drying clay hydrogel was firstly reported by Mackenzie [45] and Call [46] in the 1950s. Unlike the aerogels that follow sol-gel chemical condensation route as described previously, clay aerogels were formed by physical/electrostatic interactions between clay particles. This new inorganic aerogel can be formed in one step with water followed by freeze-drying process.

Van Olphen et al [47] investigated the clay nanoparticles dispersive configuration and clay swelling behaviour in aqueous suspension. It was proposed that MMT nanoparticles within the aerogels are linked edge-to-face much like a "house of cards" owing to opposite surface and edge charges that exist in clays. However, similar processing of non-swelling clays, such as kaolin, only produced fine powders.

Nakazawa et al. [48] studied the effects of processing parameters (e.g. clay concentration and freezing rate) on the structures of clay aerogels. It was found that decreases in clay concentrations and freezing rates resulted in pore shape changes from polygonal cells to thin lenses.

Bandi discussed formation mechanism and development of sodium montmorillonite (Na^+-MMT) aerogels systematically in his dissertation [49]. According to his study, Na^+-MMT aerogels exhibited a hierarchical layered structure (Figure 2.11) in various clay concentrations (3 wt% to 10 wt%) and freezing conditions (-21 ℃ to -196 ℃).

In this section, the formation mechanism of Na^+-MMT aerogels is briefly introduced according to the summarization of previous work. Na^+-MMT particles absorb water into the interlayer region and swell, forming a trixotropic fluid. Due to the physical electrostatic interactions between positive charged Na^+ within the galleries and negative charged platelet edges, clay will minimize free energy, resulting

in an edge-to-face association in water. When this Na^+-MMT suspension is frozen, clay platelets are rejected from ice crystals and stacked into the walls of aerogels which have three-dimensional highly regular, "house of cards" structures, as seen in Figure 2.12.

This type of aerogel has a great interest due to the low cost of clay. On the contrary, the alkoxide precursors for preparing the silica or metal oxide aerogel are much more expensive. On the other hand, supercritical drying process, which takes advantage of CO_2 instead of alcohol, usually requires a solvent change process before drying, and costs more time and energy than freeze-drying.
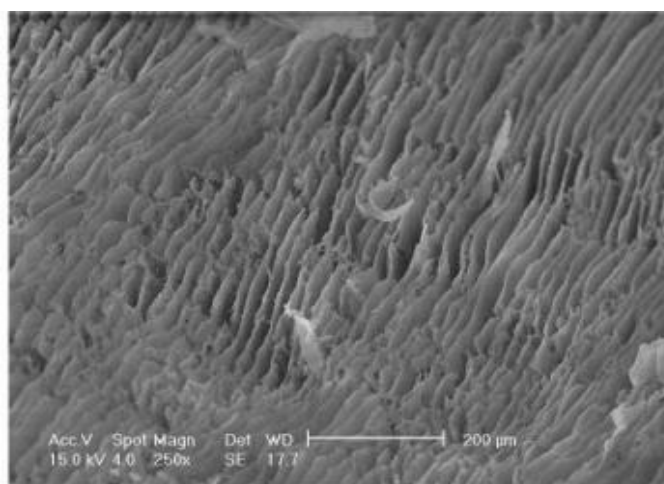
Figure 2.11 Morphology of clay aerogel (4 wt% clay, freezed at -31°C) [50]
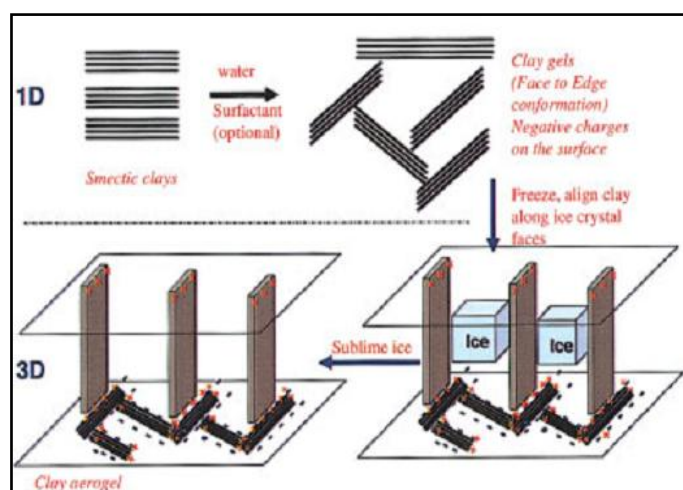
Figure 2.12 Synthesis of clay aerogels [51]

2.6.3 Polymer-based Aerogels

Aerogels of polymeric nature prepared via freeze-drying process date back to 1950s [52]. The preparation of precursor can follow the same methods used in SCD polymer aerogel. However, the drying technique has a dramatic effect on the texture of materials. SCD aerogels usually have considerably higher porosity and specific surface area than ones from lyophilization (e.g. chitosan [53]). Due to its environmentally friendly feature, freeze-drying was firstly used to produce porous polymeric materials for biomedicine applications, such as poly(L-lactic acid) and poly(DL-lactic-co-glycolic acid) porous biomaterials for tissue engineering [54].

The raw materials used to produce aerogel can be on basis of both synthetic and natural polymers [55]. Kang et al [56] produced freeze-dried gelatin sponge from a gelatin-water solution without use of any additives and organic solvents. Hsieh et al [57] reported a γ-poly(glutamic acid)/chitosan combined aerogels for culturing cells. It was found that this binary system [58] showed better hydrophilicity, cytocompatibility, and mechanical properties than chitosan aerogel. Collagen and elastin were also used to prepare tissue scaffold by Daamen et al [59].

Except as biomaterials, aerogels based on biomass are of interest as a replacement of petroleum-based polymer foams for a sustainable reason. They have been intensively developed and studied during the past decade. These foam-like materials have typical elastic-plastic behaviour and low thermal conductivity. Generally, those renewable polymers are obtained from large-scale forestry or agricultural feedstock, mainly based on polysaccharides and proteins.

Hedenqvist et al yielded aerogels from wheat gluten (a byproduct from the European ethanol industry) alkaline aqueous solutions. They studied the porous structures, mechanical properties, thermal conductivity and combustion properties of wheat gluten foams [60-62]. The thermal conductivity ranged from 0.03 to 0.08 W/(mK). However, some disadvantages (e.g. high sensitivity to moisture, poor barrier properties, and unsatisfactory mechanical performance) were found in these biofoams. Therefore, they modified the properties of wheat gluten aerogels by introducing

inorganic silica [63, 64]. Especially, the thermal stability and flame resistance were significantly improved (e.g., the temperature of the second combustion step increased by 55 ^{o}C in the presence of silica). Two more types of protein-based aerogels (whey protein and casein) were reported by Schiraldi et al [65, 66].

In comparison to the aerogels from protein, the ones from polysaccharides are much more common in scientific publications. Chen et al. [67, 68] prepared alginate aerogels with low flammability and robust pectin foam-like materials using freeze-drying process. Cellulose-based biopolymers are the most popular selection. Of particular, cellulose nanofibers (CNFs) are widely utilized to develop aerogels due to their excellent mechanical properties. Plackett summarized the sources and preparation methods [69] of CNFs, which can be obtained from wood or agricultural crops and by-products (such as wheat straw and soy hulls) by mechanical extraction and chemical or enzymatic treatment.

CNFs aerogels prepared via freeze-drying technique were firstly reported by Jin and co-workers, who prepared CNFs aerogels from CNF/Calcium thiocyanate tetrahydrate/water aqueous solution [70]. Different freeze-drying processes were investigated. It was found that a solvent-exchange freeze-drying made the aerogels have a surface area 160-190 m^{2}/g, significantly greater than those of samples from regular freeze-drying.

Instead of dissolving CNF in organic solvent, Ikkala prepared a precursor by dispersing long and entangled native cellulose Ⅰ nanofibers in water, resulting in flexible aerogels with high porosity (95-98%) and porous hierarchical structures [71]. On the basis of this work, Berglund et al. studied the mechanical performance of this CNF aerogels [72]. The compressive modulus (E) and compressive yield strength (σ_y) can reach as high as 5.31 MPa and 516 kPa, respectively. Moreover, the dependence of mechanical properties on relative density was found to match open cell foam expressions according to Gibson and Ashby scaling laws.

CNFs were also used to reinforce the cell walls of aerogels based on xyloglucan and amylopectin in the works of Berglund's research group [72-74]. By incorporating strong and flexible CNFs into the cell walls, the mechanical properties of biofoams

were strongly improved. The CNFs reinforced starch biofoams are able to reach comparable mechanical properties (E=32 MPa, σ_y=630 kPa) to expanded polystyrene (EPS) at 50% relative humidity and similar relative density.

Besides wood, CNF was able to be isolated from the other sources as mentioned previously. Bio-based aerogels were also reported based on those CNFs from waste paper [75], coconut shell [76], jute [77], wheat straw [78], and the other plants [79].

Aerogels can be fabricated from different cellulose as well, like cellulose derivatives (carboxymethylcellulose, hydroxyethylcellulose), bacterial cellulose, cellulose microcrystal, cellulose whisker, lignin and hemicelluloses. Moreover, it has been studied the effect of organic solvent types on the properties of cellulose-based aerogel which were freeze-dried from cellulose-organic solvent solution.

However, cellulose-based aerogels have some drawbacks. For example, aerogel skeleton is moisture sensitive, significantly reducing the mechanical properties. Cellulosic materials usually have hydroxyl groups dispersed on their molecules, which enables them to be easily physically or chemically modified. These modifications can endow cellulose aerogels with new functions (e.g. superhydrophobicity, high mechanical properties, electromagnetic performance, bioactivity, to name a few), which might further widen the applications. Table 2.4, which is derived from Ma's work [80], lists some of contributive works, including materials, modifying methods, properties and features.

2.6.4 Polymer-clay Aerogel Composites

The Na$^+$-MMT aerogels discussed previously have recently been of great interest. It is because not only the aerogels are based on cheap abundant minerals, but also they are prepared via an environmentally friendly freeze-drying process in which only nontoxic water is used as a dispersion media. However, one of the mainly bottlenecks of clay aerogels for application is their mechanical brittleness. An improving way is combining water soluble polymer solution into clay dispersion. A review with details is introduced in next section.

Table 2.4 Modified-cellulose-based aerogels prepared via freeze-drying process

Materials	Modifying Methods	Key Properties	Features	Ref.
Cellulose/Na-OH/thiourea	Adding GOS to cellulose solution	E=58.1 MPa, σ_y=1.13 MPa	High mechanical properties	[81]
CNF/HAp	Adding HAp to oxidized CNF dispersion	ρ: 8-11 kg/m^3	Low density	[82]
CNF	CVD of silane	Water CA: 150°	Hydrophobic, oleophilic	[83]
CNF	ALD of TiO$_2$	Water CA>90°	Hydrophobic, oleophilic, reusable	[84]
CNF	CVD of TiO$_2$	Water CA: 140°	Photoswitchable, high adhesive surface, photocatalytic acitivity	[85]
CNF	CVD of silane	Castor oil CA>>90°	Superoleophobic	[86]
CNF	CVD of silane	Water CA: 160°; paraflin oil CA: 153°	Superoleophobic, superhydrophobic	[87]
CNF	Dipping in PANI solution	EC: 10^{-2} S/cm	Electrically conducting	[71]
BC	Dipping in FeSO$_4$/CoCl$_2$ solution		Magnetic	[88]
CNF	Blending with CNT to CNF dispersion	EC: 10^{-2} S/cm; CS: 178 F/g; MPD: 13.6 mW/cm^2; ED: 20mWh/cm^2	Electrically conducting, pressure sensing	[89]
BC	In-situ formation of Ni NP in hydrogels		Ferromagnetic, superparamagnetic	[90]
Cellulose acetate	To form Ag-carbon aerogels		Antibacterial	[91]

ALD: atomic layer deposition; BC: bacterial cellulose; CA: contact angle; CNF: cellulose nanofiber; CNT: carbon nanotube; CS: specific capacitance; CVD: chemical vapor deposition; EC: Electric conductivity; ED: energy density; GOS: grapheme-oxide-sheet; HAp: hydroxyapatite; MPD: max power density; NP: nanoparticles.

To our best knowledge, the earliest work on clay-polymers aerogels was reported by Nakazawa et al. in 1990s [92]. Porous clay-organic composites were prepared by lyophylization of clay-polymer mixture. The polymers used were starch, gelatin and sodium alginate. The author pointed out these porous materials had potential application in packaging and insulation. However, the properties of different clay-polymer aerogels were not studied.
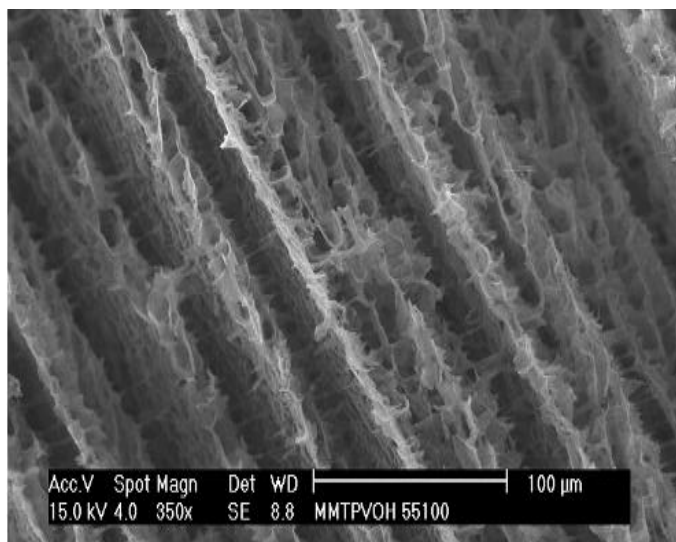
Figure 2.13 SEM micrographs of PVOH-Clay aerogel composites with 5 wt% PVOH and 5wt% clay in the precursor [93]

Alhassan et al. used the same process to obtain a polyvinyl alcohol (PVOH)/Na^+-MMT aerogels. Hydrophilic PVOH created interfacial interactions with smectic clays, as shown in Figure 2.13. Adding 5% PVOH into 5% clay aerogels, the compressive modulus and yield stress were two orders of magnitudes higher than pure clay aerogels [93]. He found the mechanical properties of aerogel composites had power-law dependence on relative density. The exponent values for elastic modulus and yield strength were 3.74 and 3.48, which were higher than the one of open cell polymeric foams (exponent=2). The reason for this behaviour was attributed to the layered structure of the aerogels.

Hostler et al. [94] studied the thermal conductivity of PVOH-clay aerogel composites, which ranged from 0.03 to 0.05 $W(mK)^{-1}$. It was found that addition of PVOH decreased the thermal conductivity of the aerogels. Moreover, the aerogels showed different thermal conductivity in horizontal and vertical direction. The possible corresponding reason is the complex anisotropic labyrinth-like pore path in the aerogels.

Arndt [95] reported the preparation of Na^+-MMT /epoxy elastic aerogels which could withstand and recover large amounts of compressive strain without failure or significant permanent deformation. The epoxy was produced through *in situ* polymerization of the water-soluble cross-linking thermoset precursors 1,4-butanediol

diglycidyl ether and triethyleneteramine.

Johnson Ⅲ [96] made branched-poly(ethylene imine) (PEI)/ Na$^+$-MMT aerogels which were modified by biomimetic mineralization of silica with tetramethyl orthosilicate. The resultant silica-encapsulated materials showed a 10-fold increase in specific compressive properties. Repeated silica/PEI treatment resulted in further enhancement of mechanical properties.

Pojanavaraphan [97, 98] produced prevulcanized natural rubber/Na$^+$-MMT aerogels. The extent of interface bonding between Na$^+$-MMT nanoparticles and rubber molecules were found to be key factor to influence the mechanical behaviour and viscoelasticity of the aerogel composites.

Wu and co-workers reported a low-density polyimide-Na$^+$-MMT aerogels with a high onset decomposition temperature (>410 ^{o}C). The aerogel composites had considerable promising applications in structural and high-temperature insulations.

The aforementioned polymers are petroleum-based and synthetic. Naturally occurring biopolymer were also utilized to develop polymer/clay aerogels.

Gwaryla et al pioneered a new application of biopolymers in preparing casein/clay aerogels [99]. Casein, a type of natural protein, was combined with Na$^+$-MMT in aqueous precursor. The resultant freeze-dried aerogels had densities in the range of 0.08-0.15 g/cm^3 and exhibited foam-like elastic-plastic properties similar to typical polymeric foams. The biodegradability of these aerogels was investigated as well. All the samples decomposed rapidly within 3 weeks and reached the highest degree of biodegradability after 30 days. They also created cellulose whisker/clay aerogels via simple freeze-drying of aqueous dispersions of clay and cellulose whiskers [100]. It was revealed these materials exhibited compressive strengths that were significantly higher than predicted by simple additive behavior of the properties of the individual components due to the formation of a nanoscale ''wattle-and-daub'' effect, as seen in Figure 2.14.
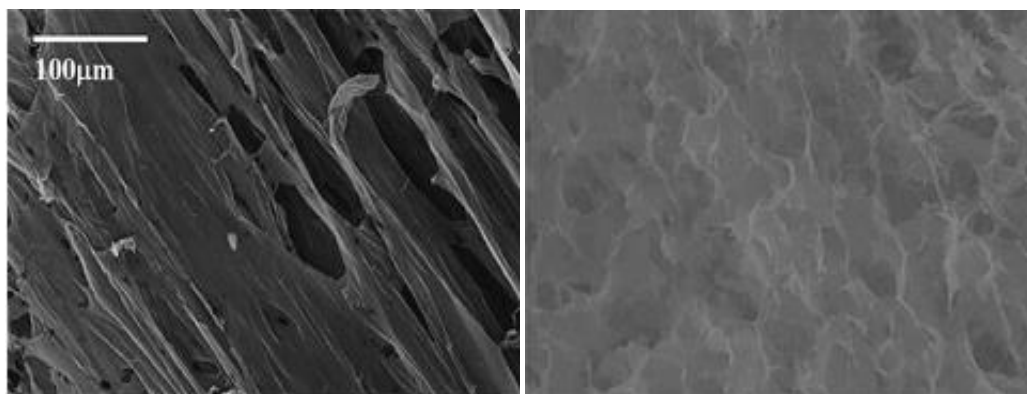
Figure 2.14 SEM photos of pure whisker aerogels (left) and whisker-clay aerogels (right)

Chen et al. [67] prepared ammonium alginate-clay aerogel composites with a low flammability. The aerogel structures changed from a layered architecture to network-like microstructure by increasing the solid content in the precursor solutions. This is because the increase of viscosity affects the ice growth. Herein, these aerogels exhibited tuneable properties (compressive moduli: 1-97 MPa; apparent densities: 0.047-0.174 g/cm^3). Due to the inherently low flammability of alginate and barrier function of clay platelets, the aerogels composites showed very excellent flame resistance (no open fire in the tests). They also used bio-based pectin and whey protein (WP) to prepare pectin/ Na^+-MMT or WP/Na^+-MMT aerogels as mentioned previously.

Donius et al. [101] reported CNF-Na^+-MMT aerogels which could show two architectures. Isotropic foam and anisotropic honeycombs were fabricated by non-directional and directional freezing, respectively. In comparison to isotropic one, the anisotropic aerogels have superior mechanical properties. Moreover, these properties spanned multiple magnitudes by changing composition, architecture and processing.

The polymer/clay aerogels, in which polymer molecules play a role of glue linking the Na^+-MMT nanoparticles, exhibit better mechanical performance than pure clay aerogels. Figure 2.15 shows a comparison of the compressive moduli of the polymer-clay aerogels as a function of their apparent densities. Actually, the modulus

is dependent on the interaction between each component. On the other hand, Na$^+$-MMT platelets serve as a physical barrier that increases the heat endurance of the aerogels, resulting in a higher thermal stability than pure polymer aerogels. This function of clay has been also widely reported in clay modified polymer based composites [38, 42].
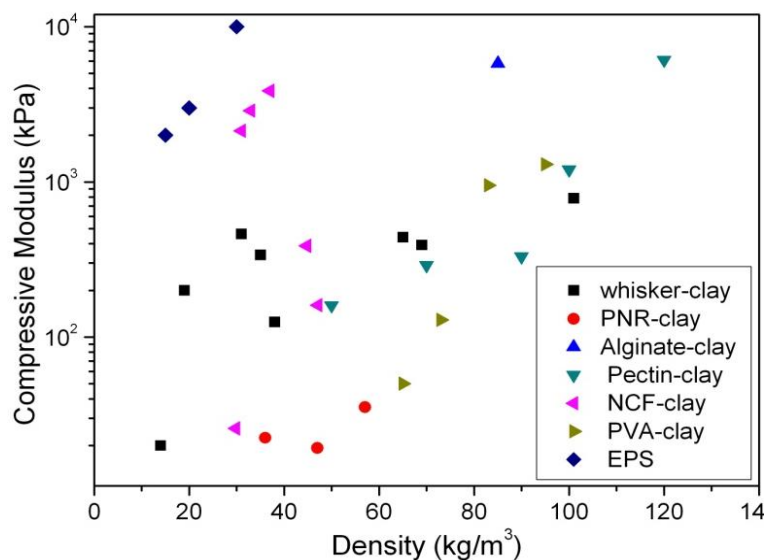
Figure 2.15 Comparison of the compressive modulus vs density of the polymer-clay aerogels

Virtually, any polymer can be selected to prepared polymer-clay aerogels from the previous experience if it can meet two conditions: (1) a thermo-dynamically stable polymer-clay suspension or colloid should be formed and frozen without phase separation; (2) the solvent must be capable of undergoing crystallization during the freezing process.

The majority of biopolymers have molecular chains containing hydrophilic groups, such as hydroxyl and carboxyl. They or their derivatives are water-soluble. In addition, the hydrophilicity of MMT clay makes water the best media for dispersion. So biopolymers match the two requirements discussed above for preparing polymer/clay aerogels. Moreover, all the raw materials used (biopolymers, Na$^+$-MMT and water) are not toxic and environmental-friendly.

Although some biopolymers from renewable sources, especially cellulose, have been used to prepare aerogels as discussed previously, very little research was

reported on produce green biopolymer/clay aerogels apart of the mentioned works. According to the survey on their properties, polymer/clay aerogels have potential application in packaging and insulation as a substitution candidate of traditional petroleum-based foams. The aerogels based on biopolymers and clay may become a new way to decrease the carbon footprint.

A wide range of biopolymers are available for building new materials, as shown in Table 2.5. Some of them, such as cellulose and starch, are actively used in products today. However, many others remain underutilized and may be used to prepared biopolymer/clay aerogels.

Table 2.5 List of biopolymers [102]

Polysaccharides		
Polysaccharides (plant)	Polysaccharides (animal)	Polysaccharides (bacterial)
starch	hyaluronic acid	chitin, chitosan (fungal)
cellulose	Polysacchaides (fungal)	levan
pectin	pullulan	xanthan
konjac	elsilan	polygalactosamine
alginite	scleroglucan	curdlan
carageenan		gellan
gums		dextran
Proteins		
soy	albumin	polylysine
zein	resilin	poly (γ-glutamic acid)
wheat gluten	polyamino acids	polyarginyl-polyaspartic acid
casein	collagen/gelation	elastin
silks	adhesives	
Polyesters		
polyhydroxyalkanoates	polylactic acid	polymatic acid
Lipids/Surfactants		
acetoglycerides, waxes, surfactants		emulsan
Speciality Polymers		
lignin	shellac	natural rubber

2.7 Modification of Polymer/clay Aerogels

As described previously, the structures and properties polymer aerogels can be tailored by chemical or physical routes. Similar processes could be applied to modify the properties of polymer/clay aerogel composites.

Functional fillers and nanoparticles have been used as reinforcement additives in polymer-clay aerogels. Finlay et al [103] reported a woven-like structure by incorporating short-cut natural fibers into PVOH-clay aerogels. Both compressive modulus and strengths were increased by as much as 5-fold at 5wt % fiber loadings, while bulk densities were increased by a factor of <2. Gawryla [104] studied single-walled carbon nanotubes (SWNT) reinforced Poly(acrylic acid) (PAA)-clay aerogels. It was found that SWNT significantly improved mechanical behavior. Incorporating 0.05 wt% SWNT increased the compressive modulus by nearly 8 times. Moreover, it imparted electrical conductivity to these aerogels.

Chemical crosslinking is another method to improve the properties of polymer-clay aerogels. Pojanvaraphan et al used DL-glyceraldehyde (GC) and sulfur monochloride to crosslink casein-clay [99] (Fig.2.16) and natural rubber-clay aerogels [105], respectively. Chen et al also modified the PVOH-clay aerogels via cross linging with divinylsulfone (DVS) [106]. A network was formed within the aerogels after crosslinking treatment (Fig. 2.17), resulting in great enhancement in their structural integrity.
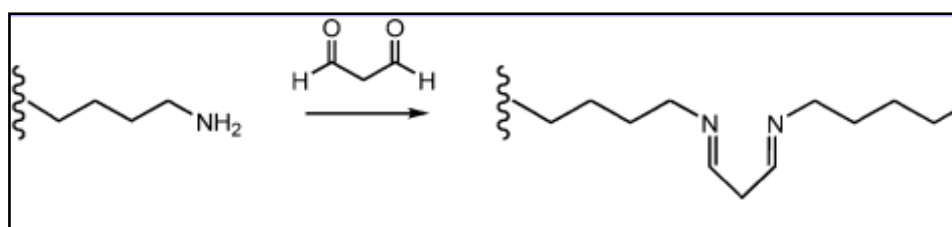
Figure 2.16 Proposed Cross-Linking Mechanism of Casein with GC through the Maillard Reaction
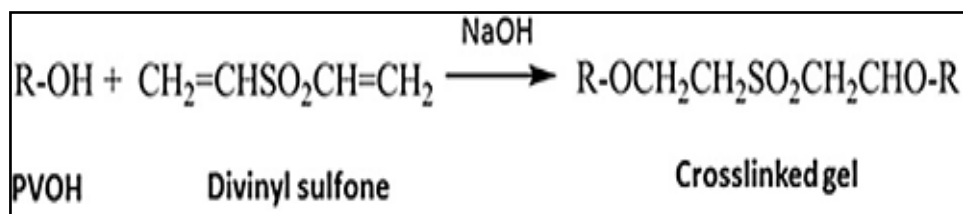
Figure 2.17 Chemical reaction of PVOH and DVS

2.8 Factors Influencing Aerogel Structure and Properties

The aerogel structures (i.e. pore size, pore volume and morphology) and properties are dependent on variables, such as the freezing direction, freezing temperature, solution concentration, and the nature of solvent and solute. The effect of these variables is discussed in the following sections.

2.8.1 Freezing Rate and Freezing Direction

Macropores are created by the ice crystals in the aerogels prepared via freeze-drying process. The size of the ice crystals can be adjusted by varying the freezing temperature and the freezing rate; while orientation alignment of pores can be realized by controlling the freezing direction [107].
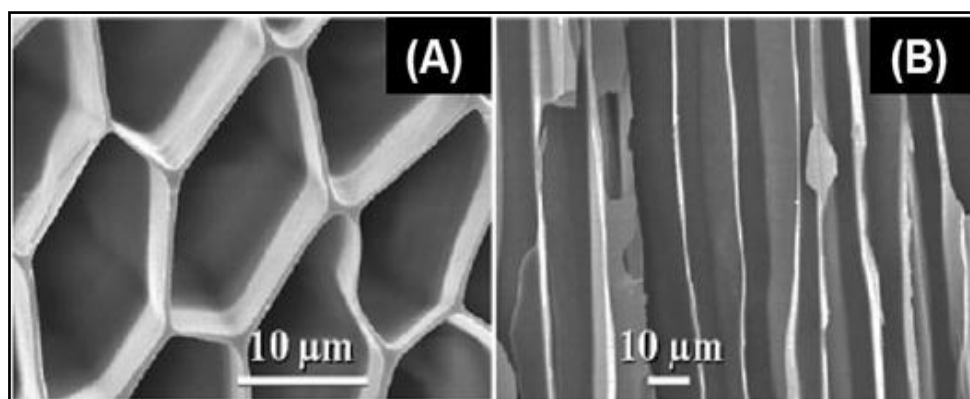
Figure 2.18 SEM images of monolithic silica microhoneycombs. (A) Cross section of a channel structure; (B) Vertical section along an aligned axis [108]

28

Mukai et al [108] reported the preparation of silica aerogels by use of unidirectional freezing at a controlled immersion rate. Unidirectional freezing allows for the achievement of micro-channelled structure in the longitudinal direction and micro-honeycomb architecture in the cross-sectional direction, as shown in Figure 2.18. The produced silica aerogels had surface area ranged between 400 and 700 m^2/g. Kim and co-workers [109] used the same process to prepare a porous poly(L-lactic acid) monolith having similar structures with silica aerogels from Mukai's work. Moreover, they proposed an ice formation mechanism during unidirectional freezing, as shown in Figure 2.19.
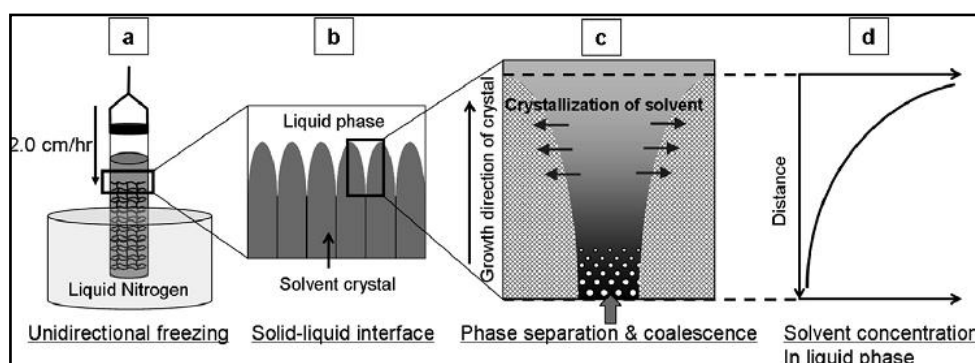
Figure 2.19 Schematic diagram of unidirectional freezing, phase separation, and coalescence [109]

Gutiérrez et al [110] studied the effects of freezing rate on the structure of PVOH aerogels. It was observed that the porous channel size decreased with the increase of freezing rate, as seen in Figure 2.20. This is because higher freezing rates allow smaller ice crystals formation, ultimately producing samples with smaller pores.

O'Brien et al. [111] proposed that collagen-glycosaminoglycan aerogel scaffolds obtained with a constant freezing rate had a more homogenous pore size than the one at a rapid quench freezing, which instead led to heterogeneity in pore size due to the varying freezing rate.
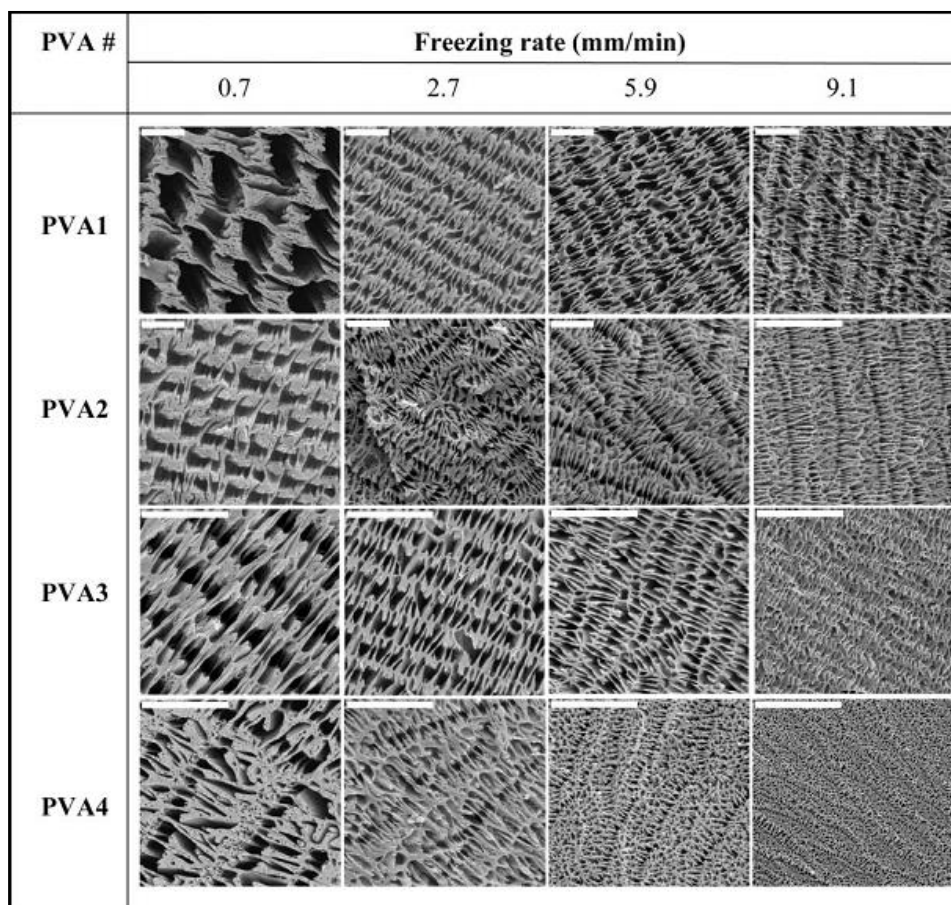
Figure 2.20 SEM images of cross-sectioned PVA aerogels. Tailored morphologies are obtained by using PVA with different molecular weights (M_w: PVA1 > PVA2 > PVA3 > PVA4) and by processing the PVA solution at different freezing rates. All scale bars are 20 microns. The PVA content was 7.8 wt% for every sample [110]

Tomsia and co-workers [30] studied the evolution of the ice front morphology during bottom-up freezing alumina slurries, as described in Figure 2.21. In the vertical cross-section, the layer thickness increased progressively with the height up to approximate 250 μm and then became constant. The horizontal cross-sections (parallel to ice front) revealed the corresponding evolution of the porous structure and hence the interface morphology. The pore dimension depended on the distance from cooling liquid immersion level.

Svagan et al. [112] prepared starch-NFC biofoams through a freeze-drying process in which a quench freezing was conducted at different freezing temperatures. They also suggested a relationship between mechanical properties and cell wall structures [74]. A lower freezing temperature would bring in aerogels with smaller

and more numerous pores, which are more favorable for reducing local stress. Therefore, higher Young's moduli, yield strengths and toughness were attained in these materials. Similar trend was found the in the PVOH-clay aerogel composites which exhibited layered structures [113]. As the freezing temperature decreased, the compressive modulus increased generally yielding more compacted layers.
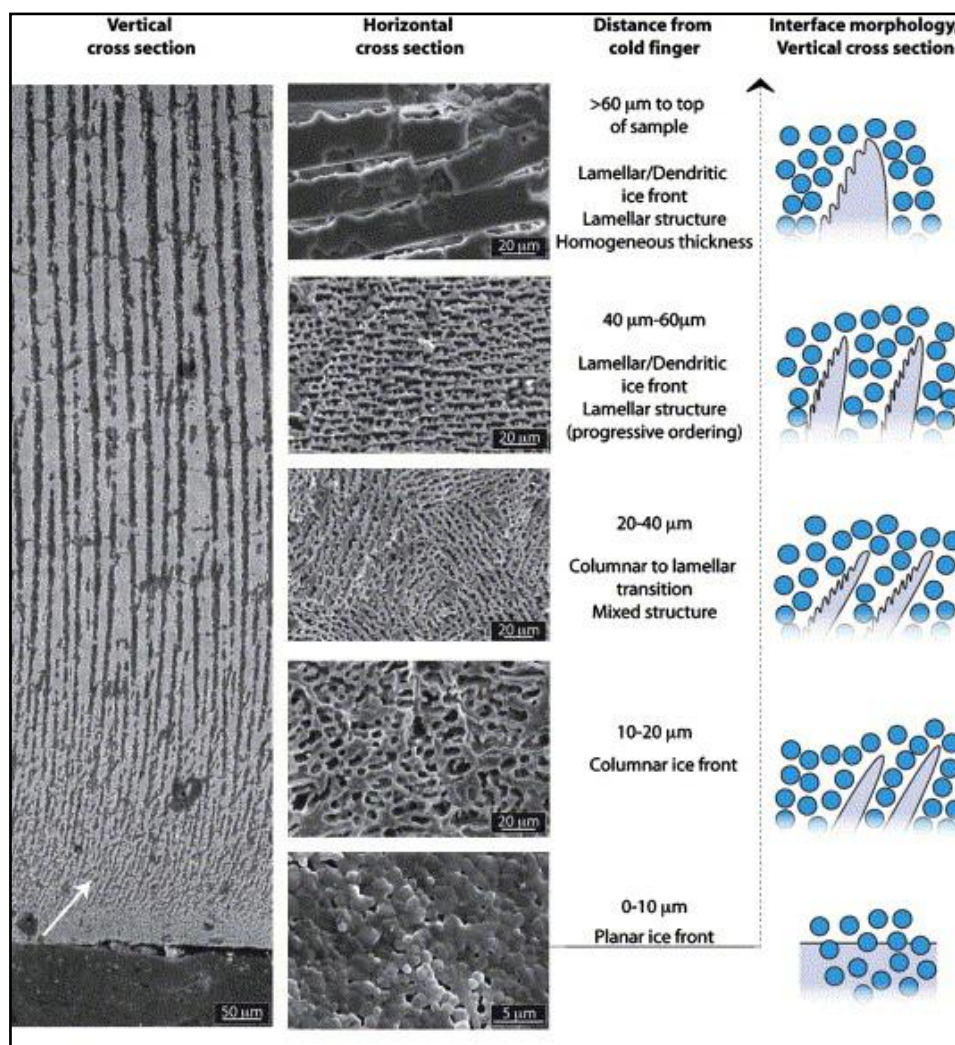
Figure 2.21 SEM micrograph of the final microstructure and evolution of the ice front morphology. The black portion at the bottom (left) is the epoxy that was used to embed the sample for cross-sectioning and polishing. The evolution was depicted on the right [30]

2.8.2 Solid Concentration and Nature of Solvent and Solid

With different nature and solid content, aerogels showed different structures. In regard

to polymeric-inorganic composite aerogels, the morphologies are also related to the polymer/inorganic particles ratios.

Gutiérrez summarized the morphologies of aerogels based on various natures (ceramics, polymer, CNT composites) prepared via freezing drying technique, as shown in Figure 2.22. In the direction vertical to freezing one, ceramic and CNT aerogels displayed honeycomb and lamellar structures, respectively. However, PVOH aerogels, which were fabricated using the same method, had irregular porous structures. He also studied the effects of molecular weight and polymer concentration in solution on the structures and properties of PVOH aerogels (The effect of M_w on aerogels morphologies was shown in Figure 2.20). Both increase in M_w and concentration would increase the solutions viscosities, retarding the ice crystals growth. As a result, the dimension of pores reduced, leading to an improvement in mechanical properties, as suggested by Figure 2.23.

Colard et al. [114] obtained porous poly(vinyl laurate) (PVL)-silica with different morphologies by changing the silica/polymer ratio. As observed from Figure 2.24, pure PVL foams collapsed at ambient temperature because glass-transition temperature of PVL is far below ambient temperatures. Adding silica nanoparticles, structures with elongated and parallel sheets appeared.
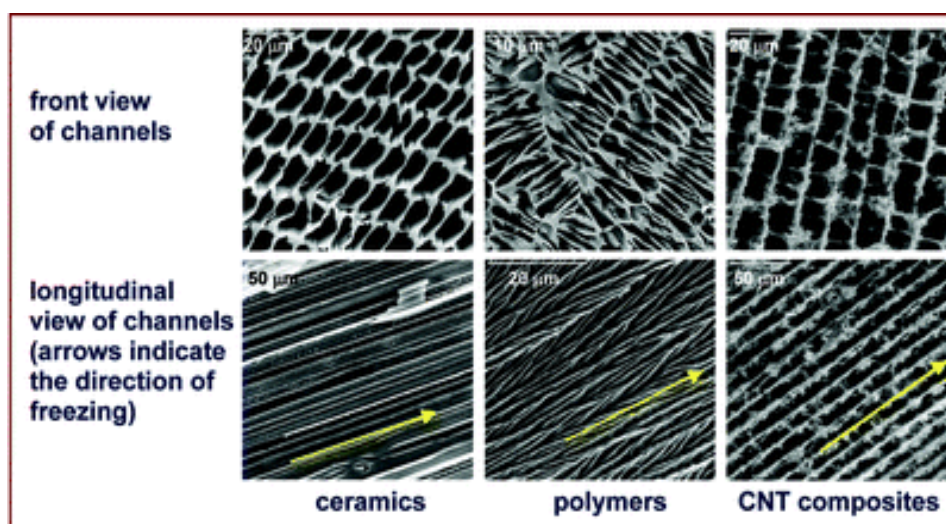
Figure 2.22 SEM micrographs of cross and longitudinal sections of aerogels with different natures formed by freeze-drying process [29]
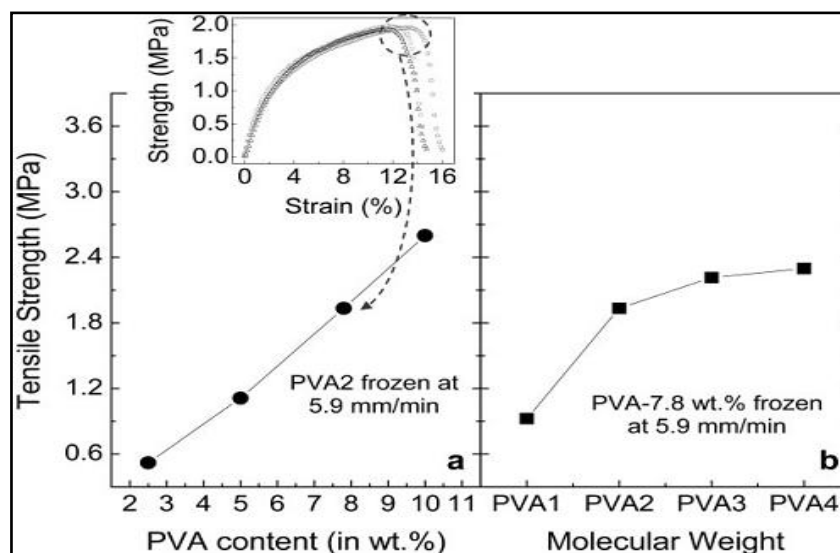
Figure 2.23 Tensile strength of PVA aerogels prepared with different conditions [110]
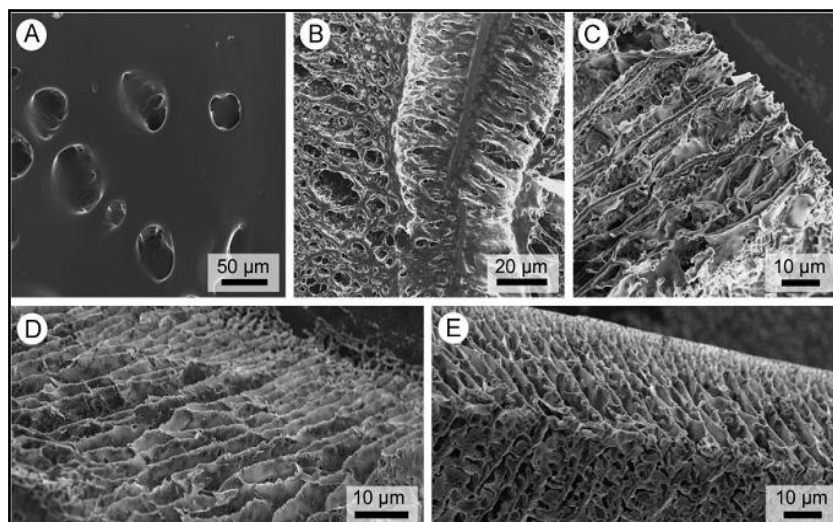
Figure 2.24 Field-emission-gun SEM images of PVL-silica foams with silica/polymer mass ratio A=0, B=0.22, C=0.38, D=0.46, E=2.22 in the perpendicular direction. Overall solid contents of the samples are: A=9.3, B=12.1, C=13.0, D=13.6, E=19.7

Hu et al. [115] fabricated PLA foams from PLA/dioxane/water mixture. Ice crystals growth leads to a phase separation which is a mass and heat transfer process. In different solvent systems, the crystals nucleation and growth mechanism are distinct. Adjusting the volume fraction of water in mixture, the resultant PLA aerogels showed different morphologies. When only dioxane was used, a closed-pore structure was observed. Increasing the water content, the closed pores were gradually turned

into an open stage and the configurations of pores changed from circular to fibrous or flaky.

2.9 Conclusion

Polymer/clay aerogels are a promising alternative for traditional petroleum-based foams which are widely used in packaging but not are biodegradable. Freeze-drying is simple and environmentally friendly technique to prepare foam-like aerogels. This art-of-stage reviewed the effects of processing parameters as well as raw materials on the structures and properties of aerogels. Moreover, it pointed out bio-based polymer could be widely used to developed bio-based polymer/clay aerogels. Some physical and chemical methods were proposed to improve the properties of polymer/clay aerogels, although further research is needed before the industrial application of this type of materials.

References

[1] Kistler S. Coherent expanded-aerogels. The Journal of Physical Chemistry. 1932;36:52-64.

[2] Aegerter MA, Leventis N, Koebel MM. Aerogels handbook. Springer Science & Business Media; 2011. p. 3-18.

[3] Hüsing N, Schubert U. Aerogels-airy materials: chemistry, structure, and properties. Angewandte Chemie International Edition. 1998;37:22-45.

[4] Wang P, Emmerling A, Tappert W, Spormann O, Fricke J, Haubold H-G. High-temperature and low-temperature supercritical drying of aerogels-structural

investigations with SAXS. Journal of Applied Crystallography. 1991;24:777-80.

[5] Abdelwahed W, Degobert G, Stainmesse S, Fessi H. Freeze-drying of nanoparticles: formulation, process and storage considerations. Advanced drug delivery reviews. 2006;58:1688-713.

[6] Nicolaon G, Teichner S. Chemical composition of silica aerogels prepared from hydrogels converted into alcogels. Bulletin de la Societe Chimique de France. 1968:1906.

[7] Pajonk G. Catalytic aerogels. Catalysis Today. 1997;35:319-37.

[8] Hrubesh LW. Aerogel applications. Journal of Non-Crystalline Solids. 1998;225:335-42.

[9] Inc. MI. Silica aerogel. Aerogel and nanofoams, available online: http://mkt-intl.com/aerogel. [Accessed August 30, 2015].

[10] Ilhan F, Fabrizio EF, McCorkle L, Scheiman DA, Dass A, Palczer A, et al. Hydrophobic monolithic aerogels by nanocasting polystyrene on amine-modified silica. Journal of Materials Chemistry. 2006;16:3046-54.

[11] Kickelbick G, Schubert U. Oxozirconium Methacrylate Clusters: $Zr_6(OH)_4O_4$ $(OMc)_{12}$ and $Zr_4O_2(OMc)_{12}$ (OMc=Methacrylate). Chemische Berichte. 1997;130:473-8.

[12] Gash AE, Tillotson TM, Satcher Jr JH, Hrubesh LW, Simpson RL. New sol-gel synthetic route to transition and main-group metal oxide aerogels using inorganic salt precursors. Journal of Non-Crystalline Solids. 2001;285:22-8.

[13] Sudoh K, Hirashima H. Preparation and physical properties of V_2O_5 aerogel. Journal of Non-Crystalline Solids. 1992;147:386-8.

[14] Poco J, Satcher J, Hrubesh L. Synthesis of high porosity, monolithic alumina aerogels. Journal of Non-Crystalline Solids. 2001;285:57-63.

[15] Pekala R. Organic aerogels from the polycondensation of resorcinol with formaldehyde. Journal of Materials Science. 1989;24:3221-7.

[16] Pekala R, Schaefer D. Structure of organic aerogels. 1. Morphology and scaling. Macromolecules. 1993;26:5487-93.

[17] Pekala R, Alviso C, Lu X, Gross J, Fricke J. New organic aerogels based upon a

phenolic-furfural reaction. Journal of Non-Crystalline Solids. 1995;188:34-40.

[18] Pekala RW. Melamine-formaldehyde aerogels. Google Patents; 1992.

[19] Lu X, Arduini-Schuster M, Kuhn J, Nilsson O, Fricke J, Pekala R. Thermal conductivity of monolithic organic aerogels. Science. 1992;255:971-2.

[20] García-González C, Alnaief M, Smirnova I. Polysaccharide-based aerogels-Promising biodegradable carriers for drug delivery systems. Carbohydrate Polymers. 2011;86:1425-38.

[21] Quignard F, Valentin R, Di Renzo F. Aerogel materials from marine polysaccharides. New Journal of Chemistry. 2008;32:1300-10.

[22] Schwertfeger F, Glaubitt W, Schubert U. Hydrophobic aerogels from $Si(OMe)_4/MeSi(OMe)_3$ mixtures. Journal of Non-Crystalline Solids. 1992;145:85-9.

[23] Schwertfeger F, Hüsing N, Schubert U. Influence of the nature of organic groups on the properties of organically modified silica aerogels. Journal of sol-gel science and technology. 1994;2:103-8.

[24] Novak BM, Auerbach D, Verrier C. Low-density, mutually interpenetrating organic-inorganic composite materials via supercritical drying techniques. Chemistry of Materials. 1994;6:282-6.

[25] Leventis N, Sotiriou-Leventis C, Zhang G, Rawashdeh A-MM. Nanoengineering strong silica aerogels. Nano letters. 2002;2:957-60.

[26] García-González CA, Carenza E, Zeng M, Smirnova I, Roig A. Design of biocompatible magnetic pectin aerogel monoliths and microspheres. RSC Advances. 2012;2:9816-23.

[27] Wu W, Wang K, Zhan MS. Preparation and performance of polyimide-reinforced clay aerogel composites. Industrial & Engineering Chemistry Research. 2012;51:12821-6.

[28] Li J, Wang F, Liu C-y. Tri-isocyanate reinforced graphene aerogel and its use for crude oil adsorption. Journal of colloid and interface science. 2012;382:13-6.

[29] Gutiérrez MC, Ferrer ML, del Monte F. Ice-Templated Materials: Sophisticated Structures Exhibiting Enhanced Functionalities Obtained after Unidirectional Freezing and Ice-Segregation-Induced Self-Assembly. Chemistry of Materials.

2008;20:634-48.

[30] Deville S, Saiz E, Tomsia AP. Ice-templated porous alumina structures. Acta Materialia. 2007;55:1965-74.

[31] Mahler W, Bechtold MF. Freeze-formed silica fibres. Nature. 1980; 285: 27-8.

[32] Fukasawa T, Ando M, Ohji T, Kanzaki S. Synthesis of Porous Ceramics with Complex Pore Structure by Freeze-Dry Processing. Journal of the American Ceramic Society. 2001;84:230-2.

[33] Sofie SW, Dogan F. Freeze casting of aqueous alumina slurries with glycerol. Journal of the American Ceramic Society. 2001;84:1459-64.

[34] Deville S. Freeze-casting of porous ceramics: a review of current achievements and issues. Advanced Engineering Materials. 2008;10:155-69.

[35] Ji H, Zhang L, Pettes MT, Li H, Chen S, Shi L, et al. Ultrathin graphite foam: a three-dimensional conductive network for battery electrodes. Nano letters. 2012;12:2446-51.

[36] Gui X, Cao A, Wei J, Li H, Jia Y, Li Z, et al. Soft, highly conductive nanotube sponges and composites with controlled compressibility. ACS nano. 2010;4:2320-6.

[37] Long Y, Zhang C, Wang X, Gao J, Wang W, Liu Y. Oxidation of SO_2 to SO_3 catalyzed by graphene oxide foams. Journal of Materials Chemistry. 2011;21:13934-41.

[38] Alexandre M, Dubois P. Polymer-layered silicate nanocomposites: preparation, properties and uses of a new class of materials. Materials Science and Engineering: R: Reports. 2000;28:1-63.

[39] Rao Y, Pochan JM. Mechanics of polymer-clay nanocomposites. Macromolecules. 2007;40:290-6.

[40] Lagaly G. From clay mineral crystals to colloidal clay mineral dispersions. Surfacant Science Series. 1993:P427.

[41] Uddin F. Clays, nanoclays, and montmorillonite minerals. Metallurgical and Materials Transactions A. 2008;39:2804-14.

[42] Bordes P, Pollet E, Avérous L. Nano-biocomposites: biodegradable polyester/nanoclay systems. Progress in Polymer Science. 2009;34:125-55.

[43] Van Olphen H. An introduction to clay colloid chemistry: for clay technologists, geologists, and soil scient ists: Wiley; 1977.

[44] Norrish K. Crystalline swelling of montmorillonite: manner of swelling of montmorillonite. 1954;173:256-7.

[45] MacKenzie RC. Clay-water relationships. Nature. 1952;171:681-3.

[46] Call F. Preparation of dry clay-gels by freeze-drying. nature. 1953.

[47] H VO. Polyelectrolyte reinforced aerogels of clays-application as chromatographic adsorbents. Clay Miner. 1967:423-35.

[48] Nakazawa H, Yamada H, Fujita T, Ito Y. Texture control of clay-aerogel through the crystallization process of ice. Clay Science. 1987;6:269-76.

[49] Bandi SA. High preformance blends and composites: Part (1) clay aerogel/poly,er composites   Part (II) Mechanistic investigation of color generation in PET/MXD6 barrier blends: Case Western Reserve University; 2006.

[50] Bandi S, Schiraldi DA. Glass transition behavior of clay aerogel/poly(vinyl alcohol) composites. Macromolecules. 2006;39:6537-45.

[51] Somlai LS, Bandi SA, Schiraldi DA, Mathias LJ. Facile processing of clays into organically-modified aerogels. Aiche Journal. 2006;52:1162-8.

[52] Pate JW, Sawyer PN. Freeze-dried aortic grafts: a preliminary report of experimental evaluation. The American Journal of Surgery. 1953;86:3-13.

[53] Valentin R, Molvinger K, Quignard F, Brunel D. Supercritical CO_2 dried chitosan: an efficient intrinsic heterogeneous catalyst in fine chemistry. New Journal of Chemistry. 2003;27:1690-2.

[54] Chen G, Ushida T, Tateishi T. Preparation of poly (L-lactic acid) and poly (DL-lactic-co-glycolic acid) foams by use of ice microparticulates. Biomaterials. 2001;22:2563-7.

[55] Lozinsky VI. Cryogels on the basis of natural and synthetic polymers: preparation, properties and application. Russian chemical reviews. 2002;71:489-511.

[56] Kang H-W, Tabata Y, Ikada Y. Fabrication of porous gelatin scaffolds for tissue engineering. Biomaterials. 1999;20:1339-44.

[57] Hsieh C-Y, Tsai S-P, Wang D-M, Chang Y-N, Hsieh H-J. Preparation of

γ-PGA/chitosan composite tissue engineering matrices. Biomaterials. 2005;26:5617-23.

[58] Hsieh C-Y, Tsai S-P, Ho M-H, Wang D-M, Liu C-E, Hsieh C-H, et al. Analysis of freeze-gelation and cross-linking processes for preparing porous chitosan scaffolds. Carbohydrate Polymers. 2007;67:124-32.

[59] Daamen W, Van Moerkerk HTB, Hafmans T, Buttafoco L, et al. Preparation and evaluation of molecularly-defined collagen-elastin-glycosaminoglycan scaffolds for tissue engineering. Biomaterials. 2003;24:4001-9.

[60] Blomfeldt TO, Olsson RT, Menon M, Plackett D, Johansson E, Hedenqvist MS. Novel Foams Based on Freeze-Dried Renewable Vital Wheat Gluten. Macromolecular Materials and Engineering. 2010;295:796-801.

[61] Blomfeldt TO, Kuktaite R, Johansson E, Hedenqvist MS. Mechanical properties and network structure of wheat gluten foams. Biomacromolecules. 2011;12:1707-15.

[62] Blomfeldt TOJ, Nilsson F, Holgate T, Xu J, Johansson E, Hedenqvist MS. Thermal Conductivity and Combustion Properties of Wheat Gluten Foams. ACS applied materials & interfaces. 2012;4:1629-35.

[63] Wu Q, Andersson RL, Holgate T, Johansson E, Gedde UW, Olsson RT, et al. Highly porous flame-retardant and sustainable biofoams based on wheat gluten and in situ polymerized silica. Journal of Materials Chemistry A. 2014;2:20996-1009.

[64] Türe H, Blomfeldt TO, Gällstedt M, Hedenqvist MS, Farris S. Nanostructured Silica/Wheat Gluten Hybrid Materials Prepared by Catalytic Sol-Gel Chemistry. Macromolecular Chemistry and Physics. 2013;214:1131-9.

[65] Chen H-B, Wang Y-Z, Schiraldi DA. Foam-like materials based on whey protein isolate. European polymer journal. 2013;49:3387-91.

[66] Gawryla MD, Nezamzadeh M, Schiraldi DA. Foam-like materials produced from abundant natural resources. Green Chemistry. 2008;10:1078-81.

[67] Chen H-B, Wang Y-Z, Sánchez-Soto M, Schiraldi DA. Low flammability, foam-like materials based on ammonium alginate and sodium montmorillonite clay. Polymer. 2012;53:5825-31.

[68] Chen H-B, Chiou B-S, Wang Y-Z, Schiraldi DA. Biodegradable Pectin/Clay

Aerogels. ACS applied materials & interfaces. 2013;5:1715-21.

[69] Siró I, Plackett D. Microfibrillated cellulose and new nanocomposite materials: a review. Cellulose. 2010;17:459-94.

[70] Jin H, Nishiyama Y, Wada M, Kuga S. Nanofibrillar cellulose aerogels. Colloids and surfaces A: Physicochemical and engineering aspects. 2004;240:63-7.

[71] Pääkkö M, Vapaavuori J, Silvennoinen R, Kosonen H, Ankerfors M, Lindström T, et al. Long and entangled native cellulose I nanofibers allow flexible aerogels and hierarchically porous templates for functionalities. Soft Matter. 2008;4:2492-9.

[72] Sehaqui H, Salajkova M, Zhou Q, Berglund LA. Mechanical performance tailoring of tough ultra-high porosity foams prepared from cellulose I nanofiber suspensions. Soft Matter. 2010;6:1824-32.

[73] Svagan AJ, Samir MA, Berglund LA. Biomimetic foams of high mechanical performance based on nanostructured cell walls reinforced by native cellulose nanofibrils. Advanced Materials. 2008;20:1263-9.

[74] Svagan AJ, Berglund LA, Jensen P. Cellulose Nanocomposite Biopolymer Foam Hierarchical Structure Effects on Energy Absorption. ACS applied materials & interfaces. 2011;3:1411-7.

[75] Nguyen ST, Feng J, Le NT, Le AT, Hoang N, Tan VB, et al. Cellulose aerogel from paper waste for crude oil spill cleaning. Industrial & Engineering Chemistry Research. 2013;52:18386-91.

[76] Wan C, Lu Y, Jiao Y, Jin C, Sun Q, Li J. Ultralight and hydrophobic nanofibrillated cellulose aerogels from coconut shell with ultrastrong adsorption properties. Journal of applied polymer science. 2015;132.

[77] Lin J, Yu L, Tian F, Zhao N, Li X, Bian F, et al. Cellulose nanofibrils aerogels generated from jute fibers. Carbohydrate Polymers. 2014;109:35-43.

[78] Perez-Cantu L, Liebner F, Smirnova I. Preparation of aerogels from wheat straw lignin by cross-linking with oligo (alkylene glycol)-α, ω-diglycidyl ethers. Microporous and Mesoporous Materials. 2014;195:303-10.

[79] Wan C, Lu Y, Cao J, Sun Q, Li J. Preparation, characterization and oil adsorption properties of cellulose aerogels from four kinds of plant materials via a NaOH/PEG

aqueous solution. Fibers and Polymers. 2015;16:302-7.

[80] Shurong M, Qinyong M, Jian Y, Jiasong H, Jun Z. Aerogel Materials Based on Cellulose. Progress in Chemistry. 2014;26:796-809.

[81] Zhang J, Cao Y, Feng J, Wu P. Graphene-oxide-sheet-induced gelation of cellulose and promoted mechanical properties of composite aerogels. The Journal of Physical Chemistry C. 2012;116:8063-8.

[82] Silva TCF, Habibi Y, Colodette JL, Elder T, Lucia LA. A fundamental investigation of the microarchitecture and mechanical properties of tempo-oxidized nanofibrillated cellulose (NFC)-based aerogels. Cellulose. 2012;19:1945-56.

[83] Cervin NT, Aulin C, Larsson PT, Wågberg L. Ultra porous nanocellulose aerogels as separation medium for mixtures of oil/water liquids. Cellulose. 2012;19:401-10.

[84] Korhonen JT, Kettunen M, Ras RH, Ikkala O. Hydrophobic nanocellulose aerogels as floating, sustainable, reusable, and recyclable oil absorbents. ACS applied materials & interfaces. 2011;3:1813-6.

[85] Kettunen M, Silvennoinen RJ, Houbenov N, Nykänen A, Ruokolainen J, Sainio J, et al. Photoswitchable superabsorbency based on nanocellulose aerogels. Advanced Functional Materials. 2011;21:510-7.

[86] Aulin C, Netrval J, Wagberg L, Lindstrom T. Aerogels from nanofibrillated cellulose with tunable oleophobicity. Soft Matter. 2010;6:3298-305.

[87] Jin H, Kettunen M, Laiho A, Pynnönen H, Paltakari J, Marmur A, et al. Superhydrophobic and superoleophobic nanocellulose aerogel membranes as bioinspired cargo carriers on water and oil. Langmuir. 2011;27:1930-4.

[88] Olsson RT, Samir MA, Salazar-Alvarez G, Belova L, Ström V, Berglund LA, et al. Making flexible magnetic aerogels and stiff magnetic nanopaper using cellulose nanofibrils as templates. Nature nanotechnology. 2010;5:584-8.

[89] Gao K, Shao Z, Wang X, Zhang Y, Wang W, Wang F. Cellulose nanofibers/multi-walled carbon nanotube nanohybrid aerogel for all-solid-state flexible supercapacitors. Rsc Advances. 2013;3:15058-64.

[90] Thiruvengadam V, Vitta S. Ni–bacterial cellulose nanocomposite; a magnetically

active inorganic-organic hybrid gel. RSC Advances. 2013;3:12765-73.

[91] Luong ND, Lee Y, Nam J-D. Highly-loaded silver nanoparticles in ultrafine cellulose acetate nanofibrillar aerogel. European Polymer Journal. 2008;44:3116-21.

[92] Ohta S-i, Nakazawa H. Porous clay-organic composites: Potential substitutes for polystyrene foam. Applied Clay Science. 1995;9:425-31.

[93] Alhassan SM, Qutubuddin S, Schiraldi D. Influence of Electrolyte and Polymer Loadings on Mechanical Properties of Clay Aerogels. Langmuir. 2010;26:12198-202.

[94] Hostler SR, Abramson AR, Gawryla MD, Bandi SA, Schiraldi DA. Thermal conductivity of a clay-based aerogel. International Journal of Heat and Mass Transfer. 2009;52:665-9.

[95] Arndt EM, Gawryla MD, Schiraldi DA. Elastic, low density epoxy/clay aerogel composites. Journal of Materials Chemistry. 2007;17:3525-9.

[96] Johnson JR, III, Spikowski J, Schiraldi DA. Mineralization of Clay/Polymer Aerogels: A Bioinspired Approach to Composite Reinforcement. Acs Applied Materials & Interfaces. 2009;1:1305-9.

[97] Pojanavaraphan T, Magaraphan R. Prevulcanized natural rubber latex/clay aerogel nanocomposites. European Polymer Journal. 2008;44:1968-77.

[98] Pojanavaraphan T, Schiraldi DA, Magaraphan R. Mechanical, rheological, and swelling behavior of natural rubber/montmorillonite aerogels prepared by freeze-drying. Applied Clay Science. 2010;50:271-9.

[99] Pojanavaraphan T, Magaraphan R, Chiou B-S, Schiraldi DA. Development of biodegradable foamlike materials based on casein and sodium montmorillonite clay. Biomacromolecules. 2010;11:2640-6.

[100] Gawryla MD, van den Berg O, Weder C, Schiraldi DA. Clay aerogel/cellulose whisker nanocomposites: a nanoscale wattle and daub. Journal of Materials Chemistry. 2009;19:2118-24.

[101] Donius AE, Liu A, Berglund LA, Wegst UG. Superior mechanical performance of highly porous, anisotropic nanocellulose-montmorillonite aerogels prepared by freeze casting. Journal of the Mechanical Behavior of Biomedical Materials. 2014;37:88-99.

[102] Kaplan DL. Biopolymers from renewable resources: Springer Verlag; 1998.

[103] Finlay K, Gawryla MD, Schiraldi DA. Biologically based fiber-reinforced/clay aerogel composites. Industrial & Engineering Chemistry Research. 2008;47:615-9.

[104] Gawryla MD, Liu L, Grunlan JC, Schiraldi DA. pH Tailoring Electrical and Mechanical Behavior of Polymer-Clay-Nanotube Aerogels. Macromolecular Rapid Communications. 2009;30:1669-73.

[105] Pojanavaraphan T, Liu L, Ceylan D, Okay O, Magaraphan R, Schiraldi DA. Solution Cross-Linked Natural Rubber (NR)/Clay Aerogel Composites. Macromolecules. 2011;44:923-31.

[106] Chen H-B, Hollinger E, Wang Y-Z, Schiraldi DA. Facile fabrication of poly (vinyl alcohol) gels and derivative aerogels. Polymer. 2014;55:380-4.

[107] Zhang H, Cooper AI. Aligned porous structures by directional freezing. Advanced Materials. 2007;19:1529-33.

[108] Mukai SR, Nishihara H, Tamon H. Formation of monolithic silica gel microhoneycombs (SMHs) using pseudosteady state growth of microstructural ice crystals. Chemical communications. 2004:874-5.

[109] Kim J-W, Taki K, Nagamine S, Ohshima M. Preparation of poly (L-lactic acid) honeycomb monolith structure by unidirectional freezing and freeze-drying. Chemical Engineering Science. 2008;63:3858-63.

[110] Gutiérrez MC, García-Carvajal ZY, Jobbágy M, Rubio F, Yuste L, Rojo F, et al. Poly (vinyl alcohol) scaffolds with tailored morphologies for drug delivery and controlled release. Advanced Functional Materials. 2007;17:3505-13.

[111] O'Brien FJ, Harley BA, Yannas IV, Gibson L. Influence of freezing rate on pore structure in freeze-dried collagen-GAG scaffolds. Biomaterials. 2004;25:1077-86.

[112] Svagan AJ, Jensen P, Dvinskikh SV, Furo I, Berglund LA. Towards tailored hierarchical structures in cellulose nanocomposite biofoams prepared by freezing/freeze-drying. Journal of Materials Chemistry. 2010;20:6646-54.

[113] Wang Y, Gawryla MD, Schiraldi DA. Effects of freezing conditions on the morphology and mechanical properties of clay and polymer/clay aerogels. Journal of applied polymer science. 2013;129:1637-41.

[114] Colard CA, Cave RA, Grossiord N, Covington JA, Bon SA. Conducting Nanocomposite Polymer Foams from Ice-Crystal-Templated Assembly of Mixtures of Colloids. advanced materials. 2009;21:2894-8.

[115] Hu Y, Grainger DW, Winn SR, Hollinger JO. Fabrication of poly (α-hydroxy acid) foam scaffolds using multiple solvent systems. Journal of biomedical materials research. 2002;59:563-72.

Chapter 3: Materials, Samples Preparation and Characterization Techniques

3.1 Materials

3.1.1 Polymers

Polyvinyl Alcohol

98% hydrolyzed polyvinyl alcohol (referred to as PVOH) was purchased from Sigma-Aldrich (St. Louis, MO, USA) and was used as received. It has a molecular weight of 40000 g/mol and a density of 1.26 g/cm^3. Its chemical structure is shown in Figure 3.1.
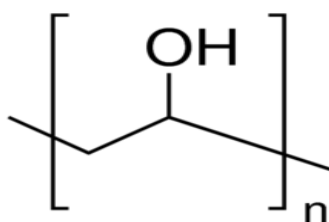
Figure 3.1 Chemical structure of PVOH [1]

Recycled Cellulose Fiber

Recycled cellulose fibers (RCF) were disintegrated from waste paper through a bioprocess involving enzymatic treatment of waste paper pulp [2]. The waste paper for preparing pulp was based on two sources. The first component (75% wt) was obtained from the output of different paper industry purifying plants consisting of mainly short fibers (0.81±0.33 mm); the second component (25% wt) was formed by long fibers (1.62±0.47 mm) coming from cardboard residues. After a mechanical shredding, the material was hydrated by adding 85 wt% water at 50 $^{\circ}$C. Then an

enzymatic bioprocess was carried out using hydrolasas and oxidorectuctases that were left to react for 1 hour at the same temperature. The pulp containing 10% solids was finally obtained and put in the fridge (4 ^{o}C) for further use.

Sodium Carboxylmethylcellulose

Sodium Carboxymethylcellulose (CMC, Walocel CRT 1000 PA 07) was received from Dowwolff Cellulosic. According to the producer, the chemical structure is shown in Figure 3.2. The degree of carboxymethyl groups substitution is 0.65-0.8. Aqueous solution containing 2 wt% of CMC at 25°C has a viscosity of 300-600 cps.
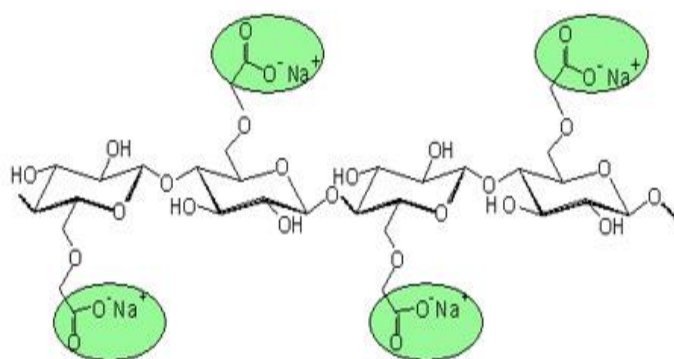
Figure 3.2 Chemical structure of sodium carboxymethylcellulose [3]
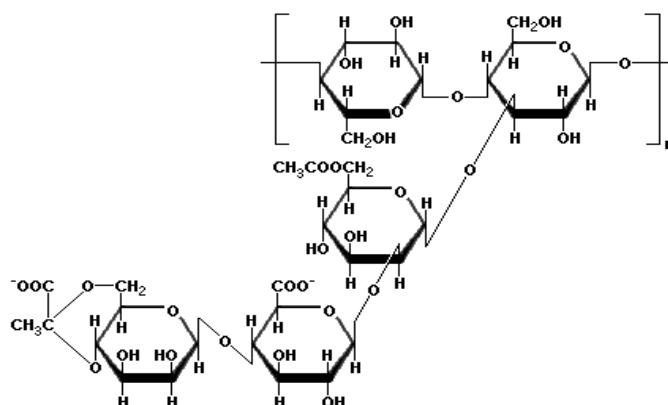
Figure 3.3 Chemical structure of xanthan gum [4]

Xanthan gum

Xanthan gum is a heteropolysaccharide produced by *Xanthomonas campestris* and the molecular structure is shown in Figure 3.3. Commercial xanthan gum (E415) was

46

bought from Vedeqsa Inc (MO, USA) and was used as received. PH value and viscosity at 25 ^{o}C of 1% solution are 7.2 and 1610 cps, respectively.

Agar

Agar is a polysaccharide that accumulates in the cell walls of agarophyte algae [5]. Its chemical structure is shown in Figure 3.4. Agar (BP grade) were brought from Merck Millipore (Darmstadt, Germany), having a melting point of 90 ^{o}C and bulk density of 550 kg/m^{3}.
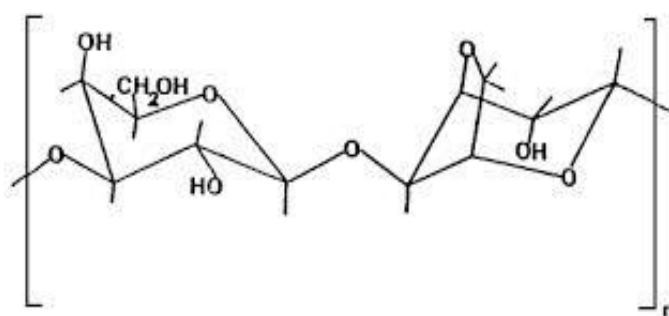
Figure 3.4 Chemical structure of agar [5]

Arabic Gum

Arabic gum powder (PRS grade) was provided by T3Q Quimica (Barcelona, Spain) with 6.9% of humidity and 4.6 of PH value for 25% aqueous solution. The exact molecular structure of Arabic gum is complex and still rather uncertain. However, it is thought that Arabic gum consists of a mixture of lower molecular weight polysaccharide (major component) and higher molecular weight hydroxyproline-rich glycoprotein (minor component) [6].

Starch

Starch generally contains 20 to 25% amylose and 75 to 80% amylopectin by weight. The molecular structures of amylose and amylopectin are displayed in Figure 3.5. Modified Potato Starch (E1442) was brought from Tradíssimo (Tarragona, Spain).
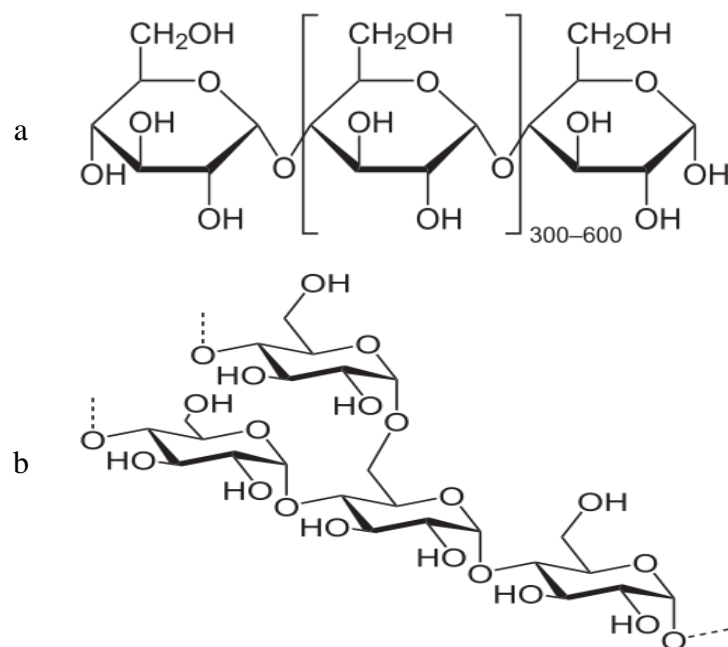
Figure 3.5 Chemical structure of amylase (a) and amylopectin (b) [7]

3.1.2. Fillers

Sodium Montmorillonite

A type of natural clay named Sodium Montmorillonite (Na^+-MMT, PGW grade) was purchased from Southern clay (Gonzales, Texas, USA). It was characterized by a density of 2.6 g/cm^3, cation exchange capacity (CEC) 145 meq/100 g and aspect ratio of 200-400. The chemical structure is illustrated in Figure 3.6. The 2:1 layer type has two tetrahedral sheets fused to an octahedral sheet [8].

Flame Retardant Agents

Aluminium trihydroxide (ALH) was obtained from Albemarle Corporation (Baton Rouge, USA). ALH platelet (Martinal 0L-111/LE) had a purity about 99.4% and solubility in water (20 ℃, pH=7) of 1.5g/ml.

Ammonium polyphosphate (APP) compound, Budit3079 was received from Budenheim Ibérica (Zaragoza, Spain). It contained approximate 42.5% P_2O_5 and 21.5% nitrogen. Figure 3.7 illustrates its chemical structure.
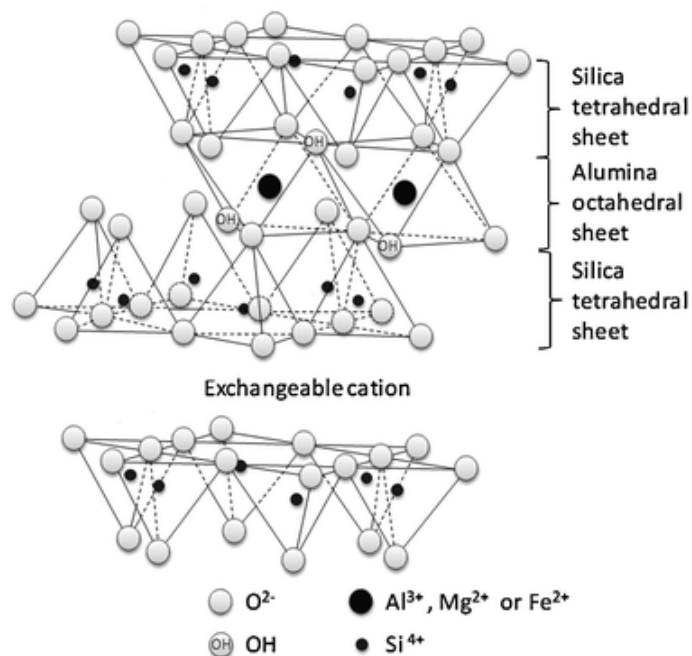
Figure 3.6 Chemical structure of MMT [9]
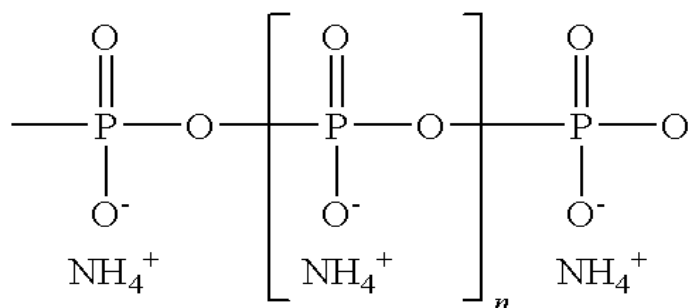
Figure 3.7 Molecular structure of ammonium polyphosphate [10]

Silica Gel (SG) with diameter 40-63 microns and Potassium Carbonate (PC) (99% purity) were purchased from Panreac (Barcelona, Spain).

All the flame retardant agents were used as received.

3.1.3 Additives

Glutaraldehyde

Glutaraldehyde, 50% (w/v), was a Sigma product. The chemical structure is shown in Figure 3.8. It was used as received.
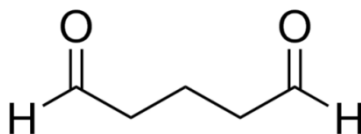
Figure 3.8 Chemical structure of glutaraldehyde [11]

Glycerin

1,2,3-Propanetriol, Glycerin (ρ=1.26 g/ml), for molecular biology, ≥99% purity, was obtained from Sigma-Aldrich. It was used as received. The chemical structure is shown in Figure 3.9.
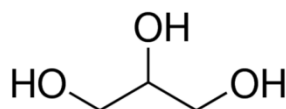
Figure 3.9 Chemical structure of glycerin [12]

3.2 Sample Preparation

Polymer-clay composite aerogels were prepared through freeze-drying polymer-clay frozen precursor mixtures. The procedure is illustrated in Figure 3.10. Na$^+$-MMT clay nanoparticles were dispersed in deionised (DI) water using an IKA Ultra-turrax disperser. In the meanwhile, polymers were dissolved in another beaker containing DI water. The conditions for dissolving different polymers will be explained in their corresponding chapter. Then the desired polymer solution and clay gel were mixed and stirred slowly to achieve homogenous mixture. Finally, the polymer-clay mixtures were transferred into cylinder vials (diameter=30 mm) or square-shaped molds (10x10 cm) before being frozen. The freezing process were conducted at -80℃ in an ethanol/solid CO_2 bath for 30 min or -27 ^{o}C in a freezer over night. Aerogels samples were obtained after the ice sublimation in a lyophilizer (Telstar Lyoquest) for 96 hours under a condenser temperature of -80 ^{o}C and vacuum of 0.01mbar. Modified aerogels required their precursor solutions to be treated with functional fillers or cross-linking

agents. The details of the corresponding preparation will be discussed separately.
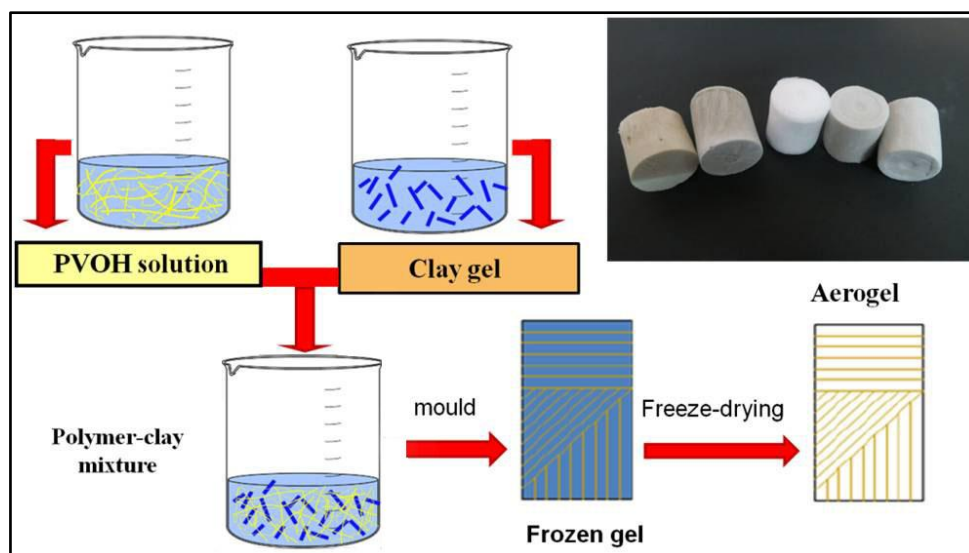
Figure 3.10 The general process of aerogels preparation

3.3 Characterization Techniques

Apparent Density

The apparent density (ρ_{app}) was calculated by measuring the mass of the specimen on a Cobos balance (Cobos, Spain, ±0.01 mg precision) and the by measuring aerogel volume using a digital caliper. Five replicas were taken for each composition.

Theoretic solid densities (ρ_{ts}) of polymer-clay composite aerogels were calculated according to equation 3.1.

$$\rho_{ts} = \frac{1}{\sum\limits_{n}^{i=1} W_i \big/ \rho_i} \qquad\qquad 3.1$$

Where, w_i and ρ_i are the mass fraction and densities of each components, respectively.

Helium Pycnometry

The experimental solid density as well as the porosity of aerogel was determined using helium pycnometer (Accupyc 1330, Norcross, GA, USA). The samples were put into the 1 cm^3 chamber and then weighted before and after analysis. During the tests, open pores were occupied by helium gas. Therefore, the volume of the open pores was recorded as the penetrated gas volume. The final volumes of solid skeleton and close pores (V_s) were calculated as the volume difference of the chamber and open pores. The experimental solid densities of the aerogels (ρ_{es}) were calculated according to eq. 3.2 and the porosities of the samples (P) were calculated by eq. 3.3 [13].

$$\rho_{es} = \frac{W_{C+S} - W_C}{V_S} \qquad\qquad 3.2$$

$$P = \left(1 - \frac{\rho_{app}}{\rho_{es}}\right) \times 100\% \qquad\qquad 3.3$$

Where, W_{c+s} is the weight of chamber with samples; W_c is the weight of empty chamber; ρ_{es} and ρ_{app} is the experimental solid density and the apparent density, respectively.

Mercury Intrusion

The pore size distribution within aerogels was determined by automated mercury porosimeters (AutoPore IV 9500 V1.07, Norcross, GA, USA). The equipment showed a testing range of 3.6-360 μm at low pressure (0-50 psia) and 0.005-6 μm (atmosphere to 33000 psia) at high pressure. The samples were firstly conducted at low pressure. Once it was finished, the tests were transferred into high pressure step. Pore diameter (D) was calculated from the Washburn equation as shown in eq. 3.4 [14].

$$D = \frac{-4\gamma\cos\theta}{P} \qquad\qquad 3.4$$

Where, γ, θ and P are surface tension, contact angle and applied pressure, respectively.

Moisture Content

Samples were weighed after five days exposure at 25 °C and 50% of relative humidity (W), and then put into a vacuum desiccator operating at 80 $^{\circ}$C. Once a constant weight was reached, the mass was again recorded (W_d). The moisture content (M) was obtained from eq. 3.5. Five replicates of each sample were used.

$$M = \frac{W - W_d}{W} \times 100\% \qquad\qquad 3.5$$

Scanning Electron Microscopy (SEM)

The microstructures of the aerogels were investigated by SEM (Jeol JSM-5610, Japan) at an acceleration voltage of 10 kV. Prior to its observation, the samples were submerged in liquid Nitrogen and equilibrated for 15 minutes. The specimens were then quickly extracted and cryo-fractured. The fracture surfaces were sputter coated with a thin Au/Pd layer using a Bal-Tec SCD005 Sputter Coater (Bal-Tec, Liechtenstein).

Optical Microscopy (OM)

The morphology of aerogels was firstly fixed in a platform and then directly observed by optical microscopy (Leica MEF4, Leica Microsystems GmbH, Wetzlar, Germany).

Fourier-Transform Infrared (FT-IR) Spectroscopy

Infrared spectra were recorded on a Nicolet 6700 spectrophotometer in the attenuated total reflectance (ATR) mode (Thermo Fisher Scientific, Waltham, MA, USA). Each sample had a spectral result based on 30 scans with a 1 cm^{-1} resolution across a wavenumber interval between 4000 and 400 cm^{-1}.

Compression Test

Compression testing was carried out in a Galdabini (Italy) universal testing machine using a load cell of 1kN following ISO 604 standard [15]. The crosshead rate and maximum strain were set to 1 mm/min and 70%, respectively. The Young's modulus was calculated from the slopes of the initial linear region of the stress-strain curves. The yield stress was taken as the stress at the intersection between the tangent line of the elastic region and the tangent line of the stress plateau segment. The energy absorbed was measured as the area below the stress-strain curve. Five replicas of each sample were used.

Impact

Impact testing were carried out in instrumented impact tester (Dartvis 16000, Ceast, Italy), using a 50 mm diameter flat headstock and a falling mass of about 2 kg that was dropped from a position 100 mm height. The maximum impact energy was of 1.962 J.

Thermogravimetric Analysis (TGA)

TGA was carried out on a Mettler Toledo TGA/DSC1 equipment (Columbus, OH, USA) to study the thermal stability of aerogels. Samples are loaded in alumina pans and heated at a rate of 10 °C/min from 30 to 900 °C under dry nitrogen or air atmosphere.

Cone Calorimetry

A cone calorimeter (Ineltec BECC model, Spain) was used to study the fire behavior of the aerogels following ISO 5660 procedure [16]. Square samples (100×100mm) with an average thickness of 7 mm were located in a steel support and exposed to an external heat flux of 50 kW/m^2.

Thermal Conductivity

Thermal conductivity of aerogels was determined by a QuickLine-30 (Anter Corporation, Pittsburgh, USA) thermal properties analyzer. The experiments were conducted according to the ASTM D5930 by using a planar sensor with a radius of 60 mm at room temperature [17]. Square specimens (6 x 6 cm) with thickness of 1 cm were prepared for the tests.

Viscosity of Solution

The viscosities of the precursor solutions were determined using dial reading Brookfield-type viscometer (RVT model, Middleboro, MA, USA). Homogenous suspensions were prepared and put in the refrigerator (4 ^{o}C) for future use. Before the test, the prepared suspension were firstly exposed to ambient condition, and then conducted at room temperature. Proper rotation speed and spindle were selected for obtaining precise viscosity values. The meniscus of the spindle was required to be immersed in the tested fluid. The torque values (T) were recorded after 30 seconds of spindle rotation. The viscosity of the solution (V) was calculated according the eq. 3.6.

$$V = T \times GF \qquad\qquad 3.6$$

Where GF is the tool geometry factor, which is obtained according to literature [18].

References

[1] Sigma-Aldrich. Poly(vinyl alcohol)**.** Datasheet, available online: www.sigmaaldrich.com. [Accessed Jan. 18, 2015].

[2] Monfort, M. C.. Process for recycling waste paper, product obtained therefrom and its uses. US Patents: 2011.

[3] Dow. Carboxymethylcellulose. Structure of WALOCEL™, available online: www.dow.com.   [Accessed Jan. 18, 2015].

[4] Garcıa-Ochoa F, Santos V E, Casas J A, et al. Xanthan gum: production, recovery, and properties. Biotechnology advances, 2000, 18(7), 549-579.

[5] Armisen, R. Agar. In Thickening and Gelling Agents for Food; Springer: Dordrecht, The Netherlands, 1997.

[6] GO Phillips, PA Williams (Eds.), Handbook of hydrocolloids, CRC Press, Cambridge, UK, 2000, p:155–168.

[7] Advances in Biopolymers; Fishman, M. L., Qi, P. X., Wicker, L., Eds.; ACS Publications: Washington DC, 2006.

[8] Van Olphen, H.. An introduction to clay colloid chemistry: for clay technologists, geologists, and soil scientists; Wiley, 1977.

[9] R. E. Grim, Clay Mineralogy, McGraw-Hill, New York, 2nd edn, 1968.

[10] Budenheim. BUDIT 3079. Buddenheim Inc, available online: www.budenheim.com. [Accessed Jan. 20, 2015].

[11] Sigma-Aldrich. Glutaraldehyde, available online: www.sigmaaldrich.com. [Accessed Jan. 20, 2015]

[12] Sigma-Aldrich. 1,2,3-Propanetriol, Glycerin, available online: www.sigmaaldrich.com. [Accessed Jan. 20, 2015]

[13] Gibson, L. J., & Ashby, M. F. Cellular solids: structure and properties. Cambridge university press. Ed2, 1999.

[14] Webb PA, Orr C. Analytical methods in fine particle technology. Micromeritics Instrument Corp; 1997: p157.

[15] ISO 604:2002, Plastics: Determination of compressive properties. International Organization for Standardization, July 2003.

[16] ISO 5660-1:2002(E), Reaction-to-fire test: Heat release, smoke production and mass loss rate-Part 1: Heat release rate (cone calorimeter method). International Organization for Standardization, 2002.

[17] ASTM D 5930-01. Standard test method for thermal conductivity of plastics by means of a transient line-source technique. Philadelphia: American Society for Testing and Materials; 2002.

[18] Brookfield. RV Series Viscometer, datasheet. Available online: www.brookfieldengineering.com. [Accessed Jan. 20, 2015]

Chapter 4: PVOH-clay Aerogels and Flame Retardant Modified PVOH-clay Aerogels

4.1 Introduction

Polyvinyl alcohol (PVOH) is a water-soluble synthetic polymer, which is widely used in papermaking, textile and a variety of coatings [1]. Due to its relatively low cost, excellent water-solubility and biodegradability, PVOH has been a subject of research interest. Recently, PVOH was utilized for creating polymer/Na^+-MMT aerogels because of its strong molecular affinity with clay [2]. The resulting properties are similar to those of conventional polystyrene expanded foam, or polyurethane foams used in packaging or cushioning. Although most of the PVOH/clay composites properties have been characterized previously, some important issues like the influence of polymer and clay ratio or the behaviour under impact are still not fully evaluated over a wide range of compositions.

To be mentioned as well, PVOH is a flammable polymer with a low limiting oxygen index value of 19.7 [3] which results in a significant restriction of its fields of application. It was previously studied that flame retardant properties of PVOH can be improved by the incorporation of different types of additives. To the requirement of environmental protection, several halogen-free commercially available flame retardant (FR) additives were adopted. Potassium carbonate and silica gel were selected according to the results of Gilman et al. [4] who demonstrate that the flammability of PVOH can be reduced by the presence of relatively small quantities of these fillers in compression moulded disks. This was mainly attributed to a synergetic ability in the formation of char. In another study [5], phosphorous-nitrogen

compounds and ammonium polyphosphate were combined to form an intumescent flame retardant agent for PVOH. However, there is no report on the flammability of these PVOH based aerogels. Aluminium trihydroxide (ALH) is a commonly FR filler. It undergoes endothermic dehydration by releasing vapour with the in situ formation of thermally stable alumina upon burning [6, 7]. Although the fire retardant effectiveness of ALH is poor and relatively high loading (>60 wt%) is needed for adequate flame retardancy [8], it is looked upon as a 'greener' FR, which does not have negative impacts on the environment.

In the present chapter, the effect of PVOH and clay ratio on the microstructures and mechanical behaviour of the aerogel composites was analysed. At the same time, in an attempt to improve the properties of PVOH/clay composites, different flame retardant agents were added into the clay-polymer colloidal system to produce modified aerogel composites via the freeze-drying method.

4.2 Experimental Section

4.2.1 Materials

Polyvinyl alcohol and sodium montmorillonite were used throughout this chapter. Aluminium trihydroxide, Ammonium polyphosphate compound (APP, budit3079), Silica gel and potassium carbonate were chosen as flame retardant agents to modify the properties of PVOH-clay aerogels. The details of all the materials could be seen in chapter 3. All ingredients were used without further purification.

4.2.2 Aerogels Preparation

PVOH/clay aerogel composites were prepared by combining clay gels and polymer solutions following the method described in section 3.2. PVOH water solutions were prepared by magnetically stirring at 80 ℃ until a transparent solution was observed.

The final polymer-clay sol was frozen followed by liophilizition. The composites were coded *xPyC,* where *x* and *y* correspond to polymer and clay weight concentration in precursor suspension, respectively.

Aerogels modified with flame retardant (FR) fillers were prepared using the same freeze-drying method. Both flame retardant agents and clay were dispersed in the same baker with deionized water and then mixed with polymer solution. All the components in the aerogels were noted by its weight ratio to 100ml of deionised water. For example, sample 5P5C2APP means that the weight ratios of PVOH, clay and APP are 5%, 5% and 2% respectively. The composite 5P5C was set as the control sample.

4.2.3 Characterization

All the characterization methods are described in detail in chapter 3. Composite aerogels were characterized by compression, instrumented impact, scanning electron microscopy, thermogravimetric analysis and cone calorimetry.

4.3 Results and Discussion

4.3.1 Influence of Polymer/Clay Ratio on the Structures and Mechanical Properties of Aerogels

(a) Morphology and Microstructure

The PVOH/clay aerogels exhibited a lamellar morphology in which clay particles were linked edge-to-face much like a "house of cards" owing to opposite surface and edge charges that exist in clays as was reported by Van Olphen [9]. The pocket holes within the aerogels, as seen in Figure 4.1, corresponded to the position previously occupied by the ice that was removed during the freeze-drying process. In the cylinder-shaped aerogel specimens, the orientation of layers was mainly radial and

vertical because ice crystal nucleation initiated mainly on surface and growth towards the centre of the gel. Due to the large temperature gradient at the surface, it is likely that these crystals grow in the shape of dendrites. Although radial alignment was the prevailing orientation, it was not fully continuous because of distortions and collisions that occurred between growing ice paths. Also, the different speed of the growing ice depends on its distance to the cooling bath, being an important parameter determining the final morphology.
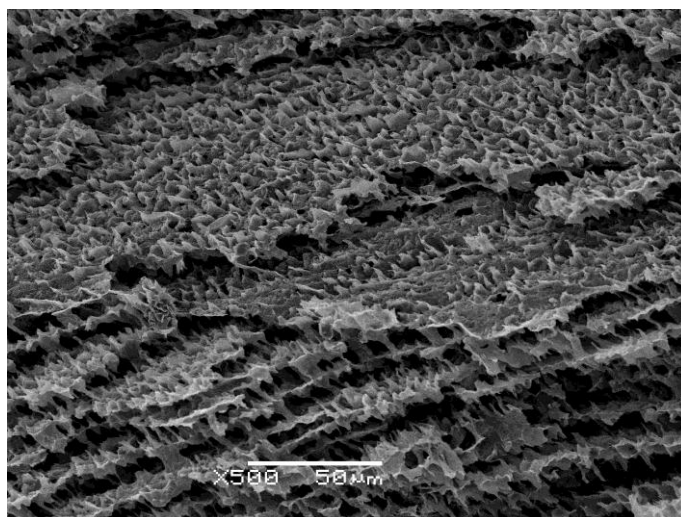
Figure 4.1 Lamellar structure of a PVOH/clay aerogel

Water freezing is a dynamic process relying on the external freezing rate, the solute concentration and solute size [10, 11]. Wang et al have studied the effects of freezing conditions on the morphology and mechanical properties of the PVOH-clay aerogels [12]. Herein, the PVOH/clay ratio is related with the viscosities of suspensions and should affect the ice crystal formation under same freezing rate. Therefore, viscosities of PVOH-clay precursor suspensions were measured and the results are shown in Table 4.1. It can be observed that the viscosities of the precursor suspensions increased more rapidly with clay concentration than with the one of polymer.

To further investigate the effect of polymer/clay ratio on the aerogels structures, solid densities and porosities of the aerogels were measured through a helium

pycnometry. Table 4.1 lists the apparent density (ρ_{app}), theoretic solid density (ρ_{ts}), experimental solid density (ρ_{es}) and porosity of the tested samples. The results displayed in Figure 4.2 indicated that the porosity decreased linearly with the aerogel apparent density.

Table 4.1 Viscosity of precursor suspension and density, porosity of PVOH-clay aerogel

Samples	Viscosity (mpa s)	ρ_{app} (g/cm^3)	ρ_{ts} (g/cm^3)	ρ_{es} (g/cm^3)	Porosity (%)
2.5P2.5C	40±4	0.068±0.001	1.93	1.926±0.004	96.5±0.1
2.5P5C	152±4	0.069±0.001	2.15	2.135±0.005	96.8±0.1
5P2.5C	158±6	0.092±0.002	1.71	1.977±0.003	95.3±0.2
5P5C	222±4	0.105±0.004	1.93	1.890±0.004	94.4±0.2
5P7.5C	585±10	0.116±0.003	2.06	1.885±0.003	93.8±0.2
5P10C	1460±30	0.136±0.002	2.15	1.982±0.003	93.1±0.1
7.5P5C	550±10	0.139±0.003	1.80	1.681±0.002	91.7±0.2
10P5C	800±10	0.180±0.006	1.71	1.604±0.004	88.8±0.1
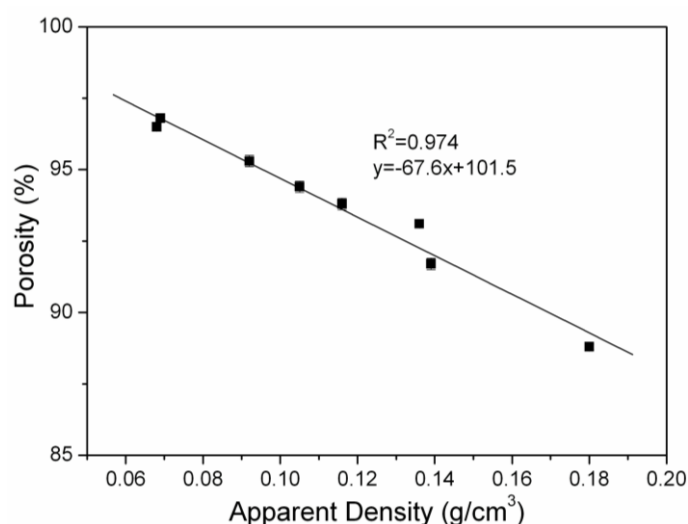
Figure 4.2 Relationship of the porosity and the apparent density of PVOH-clay aerogel

The aerogel density was found to monotonically increase with either the polymer or clay content, as shown in Figure 4.3a. Moreover, clay content had three times lower effect on the apparent density than the one of polymer. This tendency was also valid for the effect of PVOH or clay content on the porosity of the aerogel as shown in Figure 4.3b. This is because the volume stability of resultant aerogels is more affected by clay inorganic fillers than PVOH, of which molecular chains shrinkage

due to internal stresses caused by freeze-drying [13].
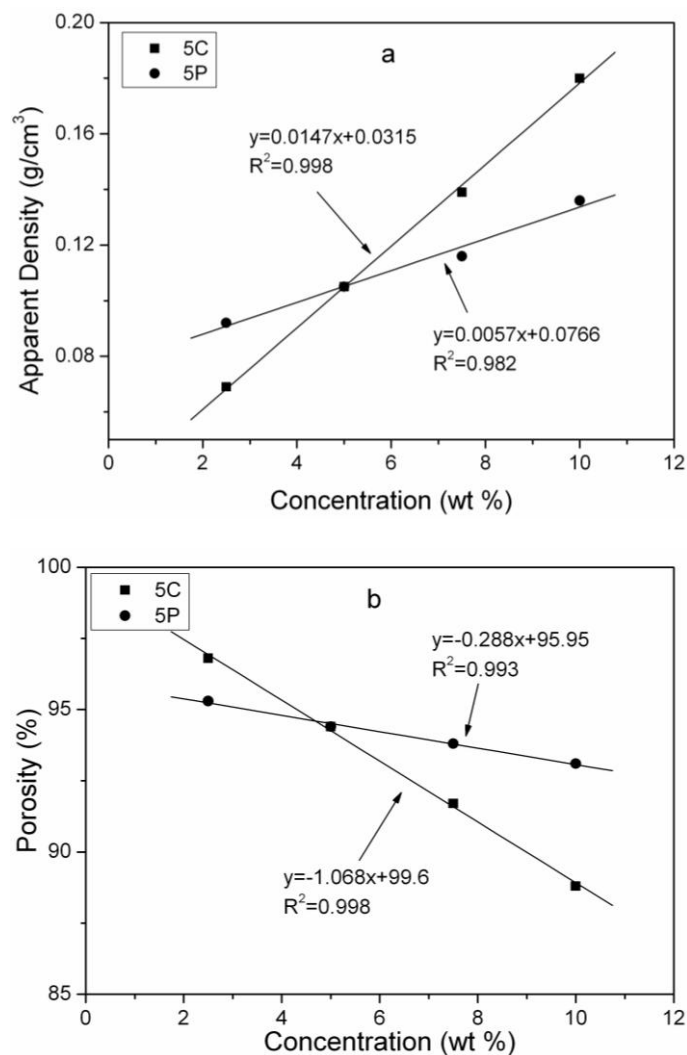
Figure 4.3 Apparent density (a) and Porosity (b) of aerogels versus PVOH or clay concentration. 5P and 5C mean constant PVOH and clay concentration, respectively

Morphologies of the PVOH-clay aerogel composites were studied using SEM. Results are displayed in Figure 4.4. Previous studies [1, 12] indicated that the PVOH molecular chains can strongly interact with the clay platelets by hydrogen bonds, creating a three-dimensional polymer/clay network which was exemplified in all the SEM photos. Polymer phase was mainly located at the interface linking clay layers. When the amount of polymer was raised from 5% to 10%, the fraction that connected adjacent layers increased as observed when Figure 4.4a and Figure 4.4b were compared. On the other hand, the increase of viscosity reduced the rate of crystal

growth by decreasing the rate of water diffusion to the surfaces of growing crystals, thus generating smaller ice crystals [14]. As a result, the layers increased in thickness with the increase of viscosity, while interlayer spacing showed a reversed trend. This tendency can be visually observed in Figure 4.4.
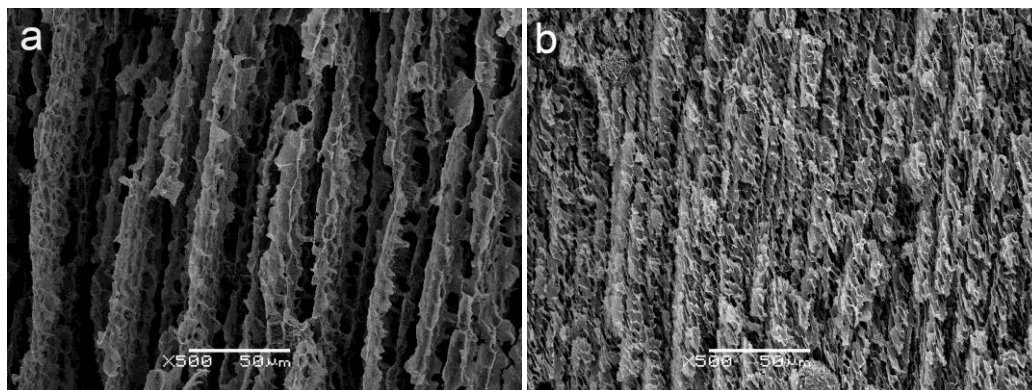
Figure 4.4 SEM image aerogel (a) 5P10C and (b) 10P10C

It should be mentioned that only certain compositions resulted in robust aerogels. When the ratio between polymer and clay was extreme (10P2.5C or 2.5P10C), aerogels were not mechanically stable. In the first case, the shrinkage of the polymer after ice sublimation caused the collapse of layers, whereas in the second case the amount of polymer was not enough to bind clay layers and give adequate mechanical properties.

(b) Mechanical Properties

The compression of aerogels yields the typical behavior of elastic-plastic foams. At very low strains (<5%), an elastic response was observed (see Figure 4.5) followed by a plateau at intermediate strains and a final densification occurred at high strains [15]. For the sake of clarity, only some results are shown in the compressive curves from Figure 4.5. The compressive mechanical performance parameters are listed in Table 4.2, including Young's moduli (E), compressive strength at 10% strain ($\sigma_{10\%}$) and specific moduli (E_s).
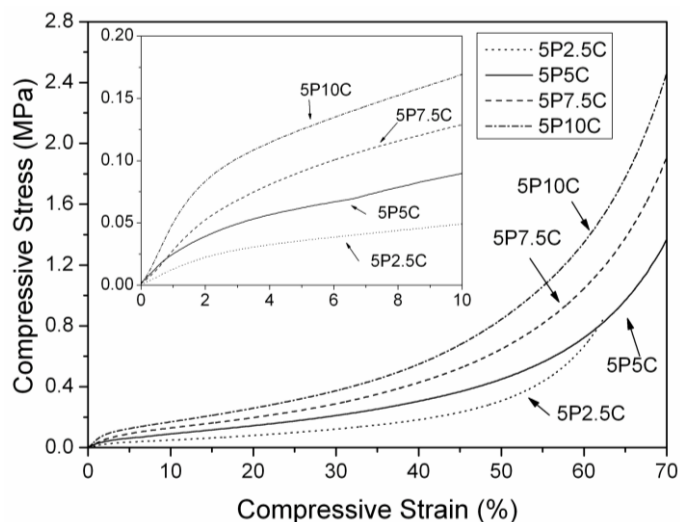
Figure 4.5 Stress-strain compression curves for PVOH-clay aerogels

Table 4.2 Mechanical properties of PVOH-clay aerogels

Samples	Compression			Impact	
	$\sigma_{10\%}$ (kPa)	E (MPa)	E_s (MPa/g cm^{-3})	σ_{max} (MPa)	ε_{max} (%)
2.5P5C	21±2	0.37±0.12	5.36±1.74	0.58±0.07	51±10
5P5C	88±18	2.28±0.51	21.71±4.85	0.66±0.06	46±6
7.5P5C	196±32	4.91±0.27	35.32±1.94	0.72±0.04	27±1
10P5C	430±59	11.97±1.35	66.50±7.50	0.99±0.02	16±<1
5P2.5C	48±3	1.19±0.34	12.93±3.70	0.77±0.03	70±16
5P7.5C	125±12	2.64± 0.41	22.76±3.53	0.57±0.01	39±2
5P10C	167±5	4.78± 0.59	35.15±4.34	0.57±0.03	32±2

The effect of clay or polymer concentration was clearly seen as an increase of both the compression modulus and the maximum compressive stress. To analyze the influence of polymer/clay ratio in the mechanical properties of the PVOH/clay aerogels, the quantity of one of the components was kept constant (5% wt). The compressive strength at 10% of deformation and the modulus were found to present power-law dependence. The exponent defining the polymer dependence was 2.07 for compressive strength at 10% stain and 2.46 for the modulus respectively as shown in Figure 4.6. However, when the amount of clay varied, the exponent remained unchanged at about 0.9 for both strength and modulus. It suggested that polymer has stronger influence than clay on mechanical properties, an effect similarly observed for the density and porosity. This is because PVOH plays the dominant role in

maintaining the integrity of aerogel by encapsulating and bridging clay particles [16]. Therefore, the amount of polymer causes a substantial improvement on the mechanical properties under compression. Moreover, specific moduli of the aerogels linearly increased with the apparent densities of aerogels, as observed in Figure 4.7. This suggested that a good adhesion is created between PVOH and clay nanoparticles.
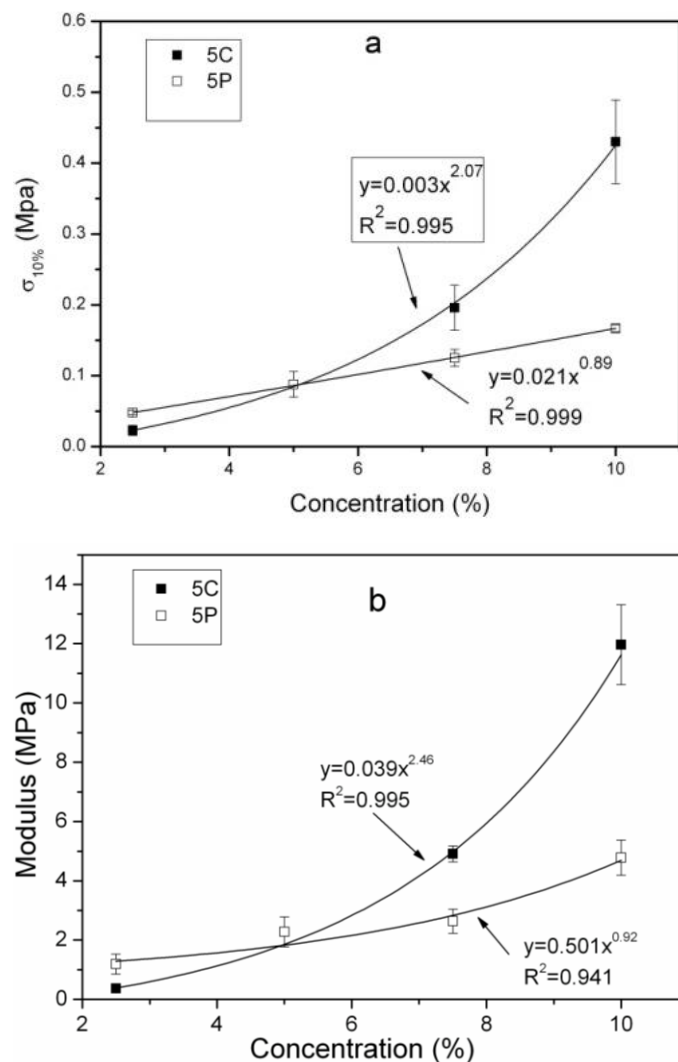
Figure 4.6 Compressive strength (a) and modulus evolution (b) versus PVOH and clay concentration

Impact tests of the aerogels were performed by instrumented falling weight. For the sake of clarity, only some curves are displayed in Figure 4.8. The aerogels were found to behave similar trends as compression tests. The maximum stress (σ_{max}) and the

maximum deformation (ε_{max}) at the impact tests of all PVOH/clay aerogels are recorded and shown in Table 4.2.
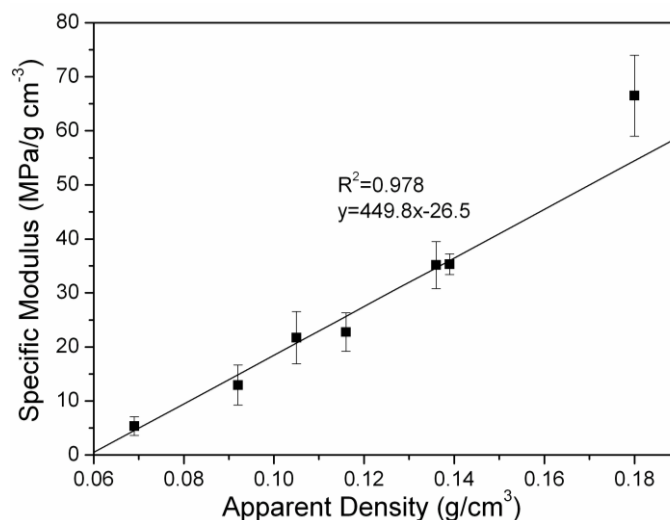
Figure 4.7 Specific modulus variation as a function of apparent density of PVOH-clay aerogels
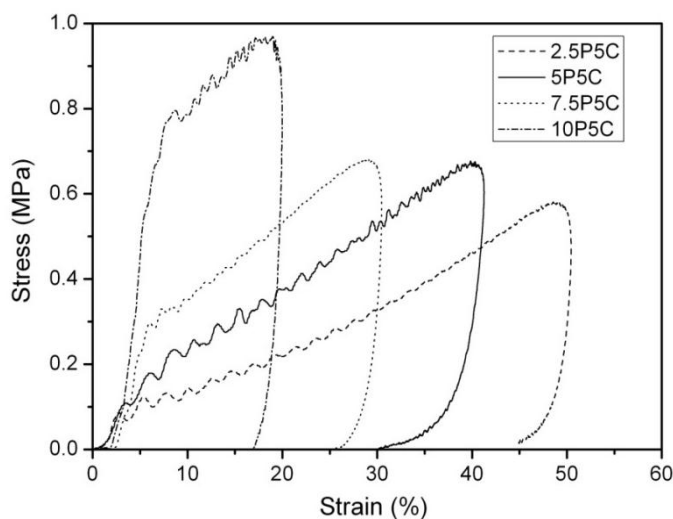
Figure 4.8 Impact stress-strain curves for PVOH-clay aerogels

It could be observed from Figure 4.8 that the structure behaves in a more rigid manner when the amount of polymer is raised in the aerogel. Sample 10P5C exhibited the greatest elasticity region, lowest maximum deformation (16%) and highest strength (0.99 MPa), whereas 2.5P5C presented highest deformation (51%). This is mainly driven by the increase of density and structural integrity of aerogel composites. When the impact tests are conducted, the fraction of polymer connecting adjacent clay

layers by hydrogen bonding prevents them from premature buckling and the clay layers encapsulated by polymer bear the load vertical to the layers. Higher polymer content results in denser polymer binding and a stronger bonding interface. However, increasing the amount of clay at fixed proportion of polymer (5PyC series) did not bring out a remarkable change on the impact response. This can be attributed to the inorganic clay nanoparticles that acted only as reinforced fillers without significant enhancement of the interfacial adhesion between polymer and clay.

4.3.2 Modified PVOH/Clay Aerogels by Different Flame Retardant Fillers

(a) Apparent Density and Morphology

The apparent density of a porous solid is a measure that includes both the volume of the solid as well as the one of the voids of either open or closed type. Table 4.3 shows the results of apparent densities of different aerogel composites. The presence of additives slightly raised the density due to the higher solid content and an increase in precursor solution viscosity. When a solution with a higher viscosity is frozen, the growth rate of ice crystals slows down because of the higher resistance to ice formation. Smaller ice crystals are generated and thus the volumetric expansion of the aerogel is reduced.

ALH particles can be partially hydrolyzed in water and be absorbed on the surface of clay platelets which strengthened the effect of hydrogen bonds and decreased the interlayer spacing (see Figure 4.9(b)). It may have a positive effect on the mechanical properties. Upon incorporating 2%wt of APP, the lamellar architecture was destroyed, as shown in Figure 4.9(c). It should be pointed out that the addition of APP increased the viscosity of the precursor solution when it was prepared. Therefore, the mobility of PVOH molecular chains and clay platelets' ability to rearrange were limited, producing a random or disordered structure instead of a highly ordered lamellar architecture. Aerogels with silica gel and SG/PC kept the similar porous

lamellar structure. However, the amount of polymer fibrils connecting clay platelets was visibly reduced in comparison to the control samples.
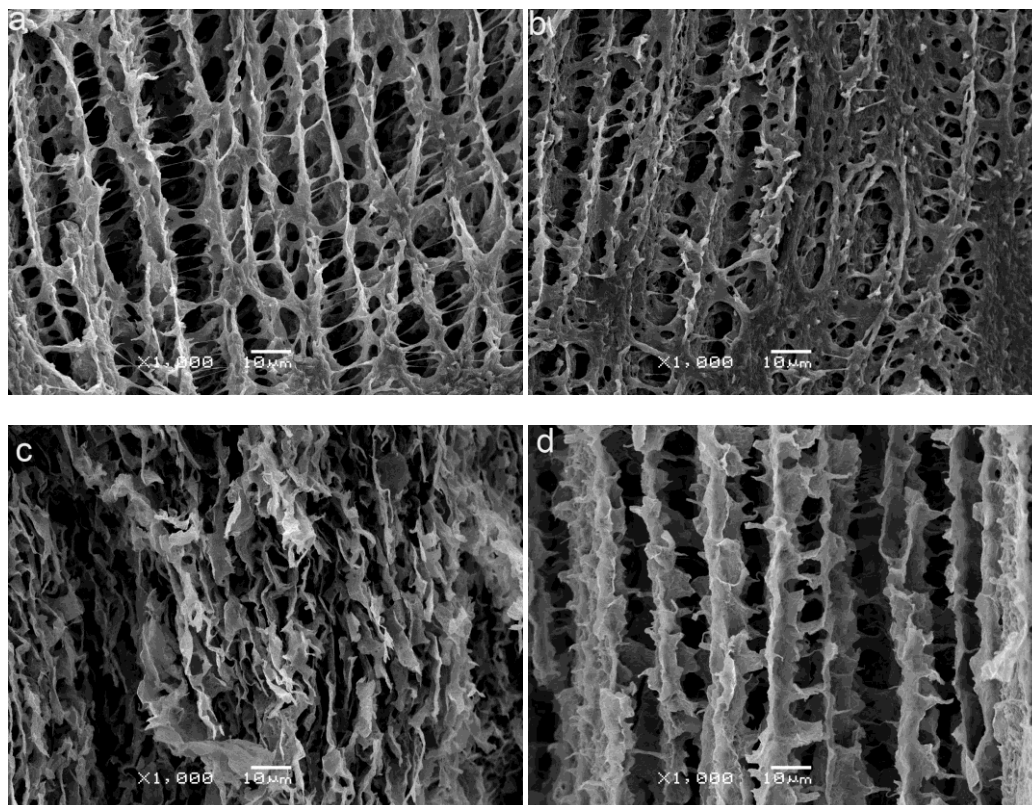
Figure 4.9 SEM micrographs of aerogel composites. (a) 5P5C; (b) 5P5C5Al(OH)$_3$; (c) 5P5C2APP; (d) 5P5C1SG0.6PC

(b) Mechanical Properties

The modified PVOH-clay aerogels still displayed a classic compressive behavior of elastic foam as shown in Figure 4.10. The results showed that the compressive yield stress and compressive modulus of these materials decreased to some extent with addition of different flame retardant particles except for the case containing ALH particles (see Table 4.3).

With the addition of 5% ALH, coherent aerogels exhibited 35% compressive strength (at 10% strain, $\sigma_{10\%}$) but nearly same modulus as control samples. The 5P5C5Al(OH)$_3$ aerogel possessed a layered architecture with the PVOH encapsulating

and bridging the particles. The rigid inorganic ALH particles seemed to accumulate predominantly on the surface of clay platelets, which may be the reason for the compressive stress enhancement.
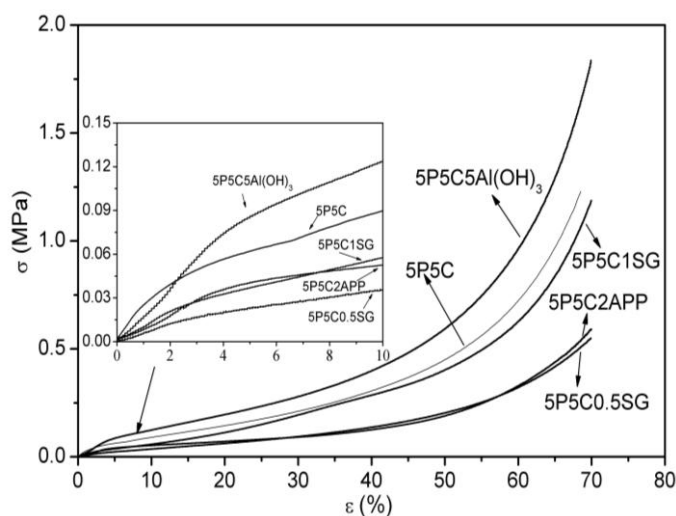
Figure 4.10 Compressive curves of PVOH-clay aerogels with FR fillers

Table 4.3 Apparent densities and mechanical properties of modified PVOH-clay aerogels

Samples	ρ_{app} (g/cm^3)	Compression		Impact	
		$\sigma_{10\%}$ (MPa)	E (MPa)	σ_{max} (MPa)	ε_{max} (%)
5P5C	0.105±0.004	0.088±0.018	2.3±0.5	0.66±0.06	47±3
5P5C5Al(OH)$_3$	0.148±0.003	0.119±0.011	2.1±0.4	0.54±0.01	34±2
5P5C2APP	0.115±0.003	0.048±0.004	0.8±0.2	0.46±0.01	62±3
5P5C0.5SG	0.106±0.004	0.041±0.010	0.8±0.3	0.44±0.01	51±5
5P5C0.5SG0.3PC	0.110±0.003	0.060±0.014	0.9±0.2	0.51±0.01	49±2
5P5C1SG	0.112±0.004	0.065±0.016	1.1±0.2	0.55±0.01	45±3
5P5C1SG0.6PC	0.119±0.005	0.057±0.007	1.0±0.4	0.50±0.03	44±1

APP: Ammonium polyphosphate; PC: Potassium carbonate; SG: Silica gel.

When 2% APP was added to the original solution, the resulting aerogel composites did not show their typical architecture. Instead, the clay layers were found to be distorted and agglomerated, making the material lose its ability to absorb and transfer loads. As a consequence, lower mechanical properties were obtained. The effect of APP on the aerogels mechanical performance was similar to the one of diammonium phosphate on bio-composites made with PLA and PP [17].

Also, the aerogels containing 0.5% SG were found to have a reduction of $\sigma_{10\%}$

and moduli by nearly 50% and 65% respectively in comparison to the control sample. The decrease in the amount of PVOH fibrils connecting adjacent clay layers was thought to be the main reason for this yield strength reduction because the main role of fibrils is to transfer stress and prevent the clay layers from separating or undergo premature buckling. Further increase of SG amount in control sample (1 wt%) did not affect the mechanical properties.
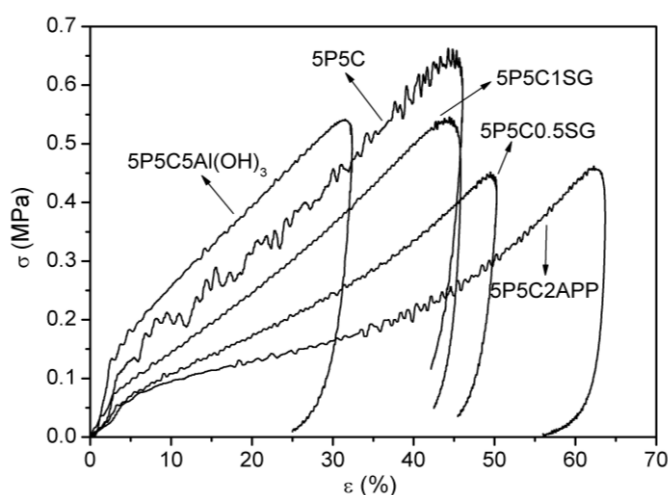
Figure 4.11 Impact tests curves of PVOH-clay aerogels with FR fillers

For the impact tests, in all cases the initial impact energy was fully absorbed by the specimens. In general, similar tendencies to the ones found in compression tests were observed. Although since the strain rate in impact conditions was not a constant value, the results cannot be directly compared [18]. The incorporation of flame retardant agents affected the degree of interfacial bonding between clay particles and polymer matrix. The impact tests results indicated that these interfaces tended to weaken when fillers were incorporated. The exception was the composite with ALH. The addition of ALH particles increased the rigidity of the aerogel as can be seen in the stress-strain plot of Figure 4.11. The sample with 5 wt% of ALH exhibited higher modulus and lower deformation showing the reinforcing effect of the filler.

As it can be also seen in Figure 4.11, the APP had an adverse effect on the impact properties with an average decrease on the maximum stress of about 30% comparing to the 5P5C samples (see Table 4.3). In addition, small cracks were visible in the

surface of the compressed samples, which was an indication of a lower interfacial adhesion between particles and matrix. Lacking of lamellar architecture in these composites (see Figure 4.9c) made the aerogel capable of bearing higher deformations but at the cost of reducing the maximum load they can withstand.

Finally, the effect of silica gel on impact behaviour was evaluated. In the 5P5C0.5SG aerogel, a significant reduction in maximum stress was observed and deep cracks appeared after impact indicating the collapse of the structure. By increasing the concentration of silica gel to 1%, the aerogel became harder and fewer cracks appeared on the surface compared with sample 5P5C0.5SG, as seen in Figure 4.12.
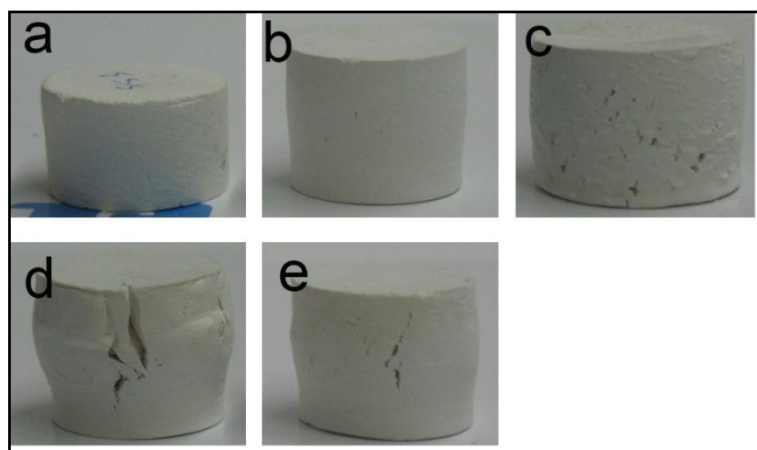
Figure 4.12 Modified PVOH-clay aerogel samples photos after impact tests: (a)5P5C; (b)5P5C5Al(OH)$_3$; (c)5P5C2APP; (d)5P5C0.5SG; (e)5P5C1SG

(c) Thermogravimetric Analysis

Figure 4.13 shows thermogravimetric analysis results of PVOH/clay aerogel with different FR agents and the control sample 5P5C. These aerogels displayed similar decomposition patterns on two main steps of weight loss. The first step, observed from 60 °C, was attributed to the removal of absorbed water. The wide temperature range of moisture lose (60 °C~130 °C) was likely due to the highly tortuous path

created by the layered clay structure. The second step, occurring after the onsets of aerogels degradation (at 5% weight loss after 150 ^{o}C), was related to the decompositions of PVOH or flame retardant agents. Table 4.4 shows the temperature at 5% mass loss after 150 ^{o}C ($T_{d5\%}$), temperature at maximum mass decomposition rate (T_{dmax}), maximum mass decomposition rate (dW/dT_{max}) and residue amount (W_R), respectively.
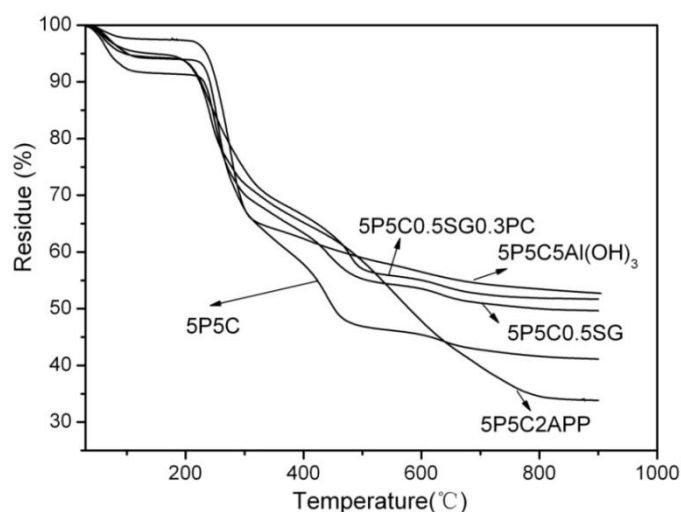
Figure 4.13 TGA curves of PVOH/clay aerogel and PVOH/clay aerogel composites with different FR fillers

Table 4.4 TGA data of FR fillers modified PVOH/clay aerogels

Samples	$T_{d5\%}$ (°C)	T_{dmax} (°C)	dW/dT_{max} (%/°C)	W_R (%)
5P5C	242	254	0.85	41.1
5P5C5Al(OH)$_3$	243	276	0.58	52.7
5P5C2APP	223	235	0.23	33.8
5P5C0.5SG	241	249	0.28	49.7
5P5C1SG	239	252	0.15	45.8
5P5C0.5SG0.3PC	228	239	0.12	51.7
5P5C1SG0.6PC	215	233	0.17	49.5

It was found that the addition of 5 wt% ALH significantly reduced the amount of bonded water in the aerogel. This is because the content of hydrophilic PVOH decreases and aerogel porosity reduces with the addition of ALH. PVOH-clay aerogel was observed to begin to decompose at 242 °C, which was overlapped with the

decomposition of ALH occurring at 240 °C [8]. There was no apparent retardation on $T_{d5\%}$ before 300 °C by incorporating ALH. However, the rate of weight loss of the aerogel reduced and temperature at maximum decomposition rate increased. Both the endothermic dehydration of ALH and the formation of an alumina layer are responsible for this improvement in thermal stability [6].

Sample 5C5P2APP began to decompose at lower temperature (180°C) comparing with the control sample. However, studies carried out on PVOH/APP/clay systems [19] have demonstrated a synergistic effect between APP and clay. The 5C5P2APP aerogel presented a much slower rate of decomposition at temperatures between 250 °C and 650°C than the control sample due to the retardant effect of the APP which is known to react with hydroxyls to form a cellular charred layer on the surface, limiting the heat transfer.

It was reported [4] that silica gel could increase the rate of ash formation which is known to act as insulator between the flame and the burning material. In a similar manner PC can play a synergistic role on the silica gel which improved its effect as a flame retardant agent [4, 20]. At temperatures higher than 270 °C, the addition of 0.5 wt% silica gel reduced the rate of weight loss of the aerogel. However, no significant changes were observed by increasing concentration of silica gel from 0.5% to 1%. Doping with PC, the weight loss rate reduced slightly compared with PVOH/clay/SG samples, which was associated to an increase in the amount of ash generated during the test. However, the presence of K^+ increases the concentration of radicals, accelerating the oxidation reactions of polymer [21]. Therefore, the $T_{d5\%}$ and T_{dmax} decreased with the addition of PC.

In summary, the addition of flame retardant fillers to PVOH aerogels decreased the rate of weight loss at temperatures higher than 250 °C whereas the onset of PVOH decomposition was not affected.

(d) Combustion Behaviour

Cone calorimetry is a testing method which can quantitatively analyze flammability by measuring the heat release rate (HRR) from a sample on bench-scale, and is widely used to predict the burning behavior of materials under real fire conditions. The fire behavior of modified PVOH/clay aerogels was investigated using this method. The flammability data, such as peak of heat release rate (PHRR), total heat release (THR), time to peak of heat release rate (TTPHRR), and fire growth rate (FGR), are summarized in Table 4.5. FGA is defined by the ratio of PHRR to TTPHRR, which is an indicator of flame spreading rate. The FGA of 5P5C5Al(OH)$_3$ and 5P5C2APP decrease to 0.5 and 0.4 respectively, which suggests aerogels modified with ALH and APP exhibit much lower tendency to burn compared with 5P5C and traditional EPS foams of which FGA value are 2.0 and 5.7, respectively [22].
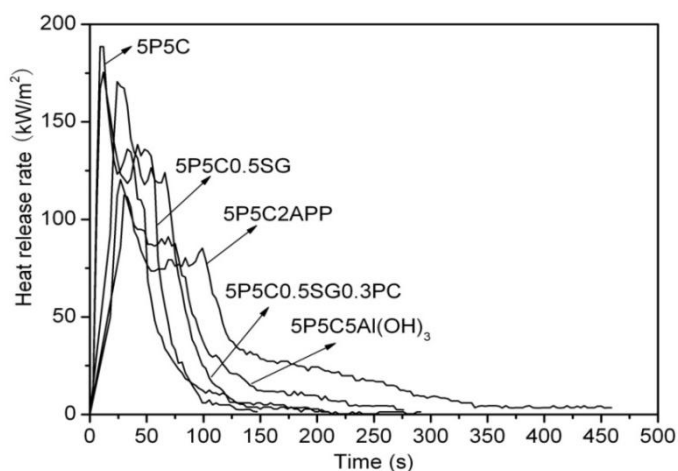
Figure 4.14 Heat Release Rate of PVOH/clay aerogel and PVOH/clay aerogel composites with different FR fillers as a function of burning time

Figure 4.14 shows heat release rate data for the aerogels with flame retardant agents in comparison to the control sample 5P5C. The addition of 5 wt% ALH decreased the peak of heat release rate nearly by 33%, which suggested this aerogel composite had a higher flame resistance compared to the unmodified one. ALH was decomposed into aluminum oxide and water in the temperature range from 200℃ and 300℃ as shown in TGA tests. The evaporation of H$_2$O diluted the combustible gases

and absorbed part of the heat of combustion. Theoretical transformation of ALH to Al_2O_3 made PVOH/clay/ALH samples contain a higher percentage of residue than the control one. The decomposition of ALH into Al_2O_3 improved the thermal conductivity of aerogels and reduced the peak of heat released rate. It was reported that the effectiveness of ALH tended to be limited since relatively large amounts of the filler were needed for adequate flame retardancy (over 60 wt%) [8]. However, in this work, only 33 wt% ALH were used and mixed with 33 wt% inorganic clay. The fire resistance effect seemed to be similar to the ALH/Si_3N_4 compound [23].

The incorporation of 2 wt% APP into aerogel reduced the heat release rate peak by 36% in comparison to control sample. However, more total heat release was produced. This could be explained through the mechanism of intumescence [19]. In this mechanism, ammonium polyphosphate acts as a flame retardant by a chemical effect in the condensed phase. When the aerogel that contains APP is exposed to fire or heat, the APP starts to decompose at 180°C, commonly into polymeric phosphoric acid and ammonia. The polyphosphoric acid reacts with hydroxyl groups of PVOH to form an unstable phosphate ester, which afterwards undergoes the dehydration. A cellular char was built up on the surface exposed to the heat source, which acted as an insulation layer, preventing further decomposition of the material underneath.

There were only 7% and 2% reductions in peak of heat release rate of the 5P5C0.5SG and 5P5C1G samples, respectively. Moreover, in the aerogel with 1% SG, the total heat released decreased as a result of the accumulation of SG ash on the surface of aerogel composite during combustion [19]. Although the TGA tests estimated the synergistic effect of K_2CO_3 on aerogels with silica gel, there was no significant change in the peak of heat release rate and total heat released in the cone calorimeter tests. It was reported that the present of K_2CO_3 increased the ability to generate silica gel ash and protect the polymer from fire or heat [4], which is associated with the changes of TTPHRR values. However, the effects of K_2CO_3 particles on PHRR and THR were shown to be very limited in PVOH/clay aerogel systems.

Table 4.5 Burning parameters of modified PVOH/clay aerogels

Samples	PHRR (kW/m^2)	THR (MJ/m^2)	TTPHRR (s)	FGR (W/s)	W_R (%)
5P5C	182	9.0	9	2.0	61.9
5P5C5Al(OH)$_3$	122	8.6	27	0.5	65.7
5P5C2APP	115	12.3	30	0.4	57.4
5P5C0.5SG	168	9.2	12	1.4	61.1
5P5C0.5SG0.3PC	174	9.3	24	0.7	59.1
5P5C1SG	179	6.8	15	1.2	65.7
5P5C1SG0.6PC	191	6.7	12	1.6	62.8

4.3.3 PVOH-Clay Composite Aerogels Modified With Different Amount of ALH

In light of the previous experiments, it was found that the mechanical properties as well as flame retardant properties of the PVOH-clay composite aerogels could be improved by adding ALH. To further exploit the effect of ALH on the properties of the aerogels, PVOH-clay aerogels with different amounts of ALH were investigated.

With the increase of ALH in PVOH/clay aerogel, the characteristic clay layers increased in thickness and the fracture surfaces became rougher (see Figure 4.15a). This is because ice growth is affected by the partial hydration of ALH. The formation of electrolyte depresses the freezing point and leads to slower ice crystal growth. In addition, ALH particles with large dimensions retard the ice growth [24]. Therefore, both polymer and filler have sufficient time to diffuse out of the icy crystal region and aggregate between grain boundaries [2].

The compressive curve of sample 5P5C7.5ALH is shown in Figure 4.15b. The Young's modulus and compressive strength at 10% strain were 5.7 MPa and 0.124 MPa respectively with an apparent density 0.154 g/cm^3. Compared with sample 5P5C5ALH, the specific modulus became over 2 times higher. This is because the hydrated Al^{3+} affects the freezing process which is responsible for the change of aerogel structure and corresponding improvement in mechanical properties.
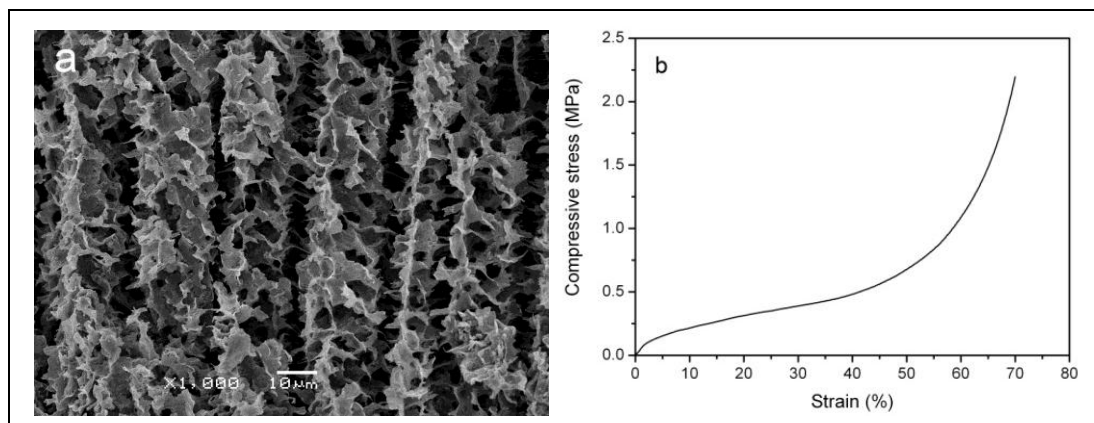
Figure 4.15 SEM photo (a) and compressive curve (b) of sample 5P5C7.5ALH
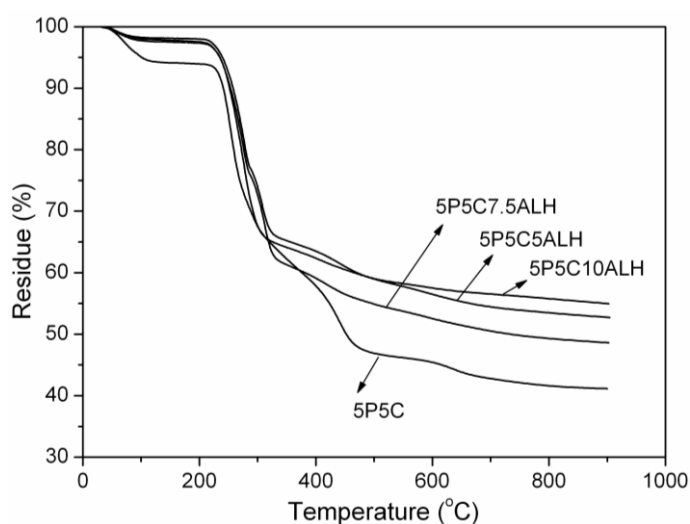
Figure 4.16 TGA curves of PVOH-clay aerogels modified with different amount of ALH

Table 4.6 TGA parameters of PVOH-clay aerogels modified with different amount of ALH

Samples	$T_{d\,5\%}$ after 150 °C (°C)	$T_{d\,max}$ (°C)	dW/dT_{max} (%/°C)	W_R (%)
5P5C	242	254	0.85	41.1
5P5C5ALH	243	276	0.58	52.7
5P5C7.5ALH	243	276	0.53	48.6
5P5C10ALH	247	276	0.54	55.0

The TGA decomposition curves of the aerogels are shown in Figure 4.16 and the detailed parameters of thermal stability are listed in Table 4.6. Samples modified with ALH showed different decomposition patterns in regard to the control sample (5P5C), mainly displaying on the stage of char formation (350-450 °C). This indicated a high loading of ALH increased the char formation of PVOH/clay aerogels.

78

The decomposition of ALH released 35% water of crystallization into the gas phase which can absorb heat and dilute the concentration of combustive gas during the pyrolysis [8]. On the other hand, Al_2O_3 layers obtained from pyrolysis of ALH formed a protective shield for polymer beneath. Lower decomposition rates and T_{dmax} were obtained with addition of higher amounts of ALH. However, the thermal stability of aerogels did not change when the ALH content exceeded 5 wt%. This suggests 5 wt% is the maximum amount for sample 5P5C.

For the cone calorimetry test, the composite aerogels underwent similar pyrolysis process as shown in TGA experiments. The combustive parameters obtained are shown in Table 4.7. The flame retardant properties of aerogels were improved as expected. Increasing the ALH amount into 10 wt%, the peak of HRR decreased from 182 to 72 kW/m^2 and fire growth rate lowered by nearly 9 times comparing to the sample without modification. Also, higher amount of ALH prolonged the TTPHRR. This is mainly due to the diluting effect of the decomposed vapour in the gas phase. In addition, the second peak which appeared in the unmodified sample turned into a plateau stage in the HRR curve when ALH content was over 5 wt% (Figure 4.17). It contributes to the inorganic alumina layers generated during the pyrolysis process increased the density of cellular clay char, protecting the materials beneath [8] [25].
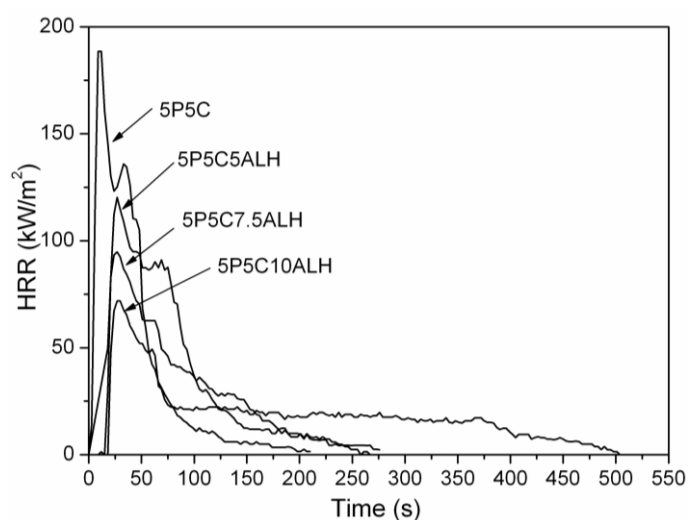
Figure 4.17 Combustive plots of PVOH/clay aerogels modified with ALH

Table 4.7 Burning parameters of PVOH/clay aerogels modified with different amount of ALH

Samples	PHRR (kW/m^2)	THR (MJ/m^2)	TTPHRR (s)	FGR (W/s)	W_R (%)
5P5C	182	9	9	2	61.9
5P5C5ALH	122	8.6	27	0.5	65.7
5P5C7.5ALH	94.8	6.7	27	0.35	54.1
5P5C10ALH	72	8.5	30	0.27	58.4

4.4 Conclusions

Different PVOH/clay aerogels with compositions ranging between 2.5 wt % and 10 wt% with either polymer or clay were prepared using a freeze-drying process. The porosities monotonically decreased with the apparent densities of aerogels. Moreover, polymer concentration was the most important factor affecting the porosities and apparent densities. The mechanical behavior observed under compression and impact tests indicated that the amount of polymer plays the major role on properties while clay content had minor effect. Nevertheless, a minimum clay level (2.5 wt %) was necessary to obtain mechanically robust aerogels. In terms of the microstructure, an increase in the amount of PVOH implied that a greater polymer fraction was linking adjacent clay layers. On the other hand, the increase of clay loading led to a structure with thicker layers.

For the PVOH/clay aerogels modified with flame retardant fillers, the thermal and flame retardant properties were further determined. SEM images showed that all the aerogel composites had a layered structure that was only distorted with the addition of ammonium polyphosphate. The addition of flame retardant agents slightly increased the apparent densities of the aerogels. Compressive properties mainly depended on the interaction of polymer chains with clay platelets. In general, addition of FR fillers made the aerogels weaker because they interfered in the degree of

adhesion with PVOH. The compressive stress at maximum deformation decreased whereas under impact conditions, the same energy was absorbed with higher deformation of the structure. The exception was ALH which made the aerogels behave in a more rigid manner. In terms of thermal stabilization, flame retardant agents decreased the rate of weight loss at temperatures higher than 250 ℃ whereas the onset of PVOH/clay decomposition was not affected. Cone calorimeter results showed that ALH and APP reduced the peak of heat released rate of unmodified PVOH/clay aerogels.

It was proved that ALH can enhance the mechanical properties as well as the flame retardant properties of the PVOH/clay aerogels. The addition of higher amounts of ALH generated a layered structure with thicker layers. Especially when the ALH concentration in the solution was over 5 wt%, the layers significantly increased in thickness due to the ALH particles attached on the clay platelets. On the other hand, large-dimensional ALH particles retarded the ice growth reducing the spacing between the layers. However, the mechanical properties were slightly improved with the addition of high amounts of ALH. When ALH reached 10 wt%, the flame retardant properties were clearly enhanced. This effect is contributed to the decomposition of ALH, which generates vapor, absorbing heat and diluting the concentration of combustive gas. Moreover, inorganic alumina layers formed during the pyrolysis process creates protective barrier, retarding the burning. The TGA test also proved this role.

Generally, this chapter showed the PVOH/clay exhibited excellent mechanical properties when proper polymer/clay ratio was designed. The thermal stability and flame retardant properties were improved by physically addition of flame retardant fillers. In addition, the ALH enhanced the mechanical properties as well as the thermal stability and flame retardant properties. It allows a way to prepare an alternative of traditional petroleum-based foams.

References

[1] Hallensleben ML. Polyvinyl Compounds, Others. Ullmann's Encyclopedia of Industrial Chemistry: Wiley-VCH Verlag GmbH & Co. KGaA; 2000.

[2] Alhassan SM, Qutubuddin S, Schiraldi D. Influence of Electrolyte and Polymer Loadings on Mechanical Properties of Clay Aerogels. Langmuir. 2010;26:12198-202.

[3] Naitana S, Ledda S, Loi P, Leoni G, Bogliolo L, Dattena M, et al. Polyvinyl alcohol as a defined substitute for serum in vitrification and warming solutions to cryopreserve ovine embryos at different stages of development. Animal reproduction science. 1997;48:247-56.

[4] Gilman JW, Ritchie SJ, Kashiwagi T, Lomakin SM. Fire-retardant additives for polymeric materials. I. Char formation from silica gel-potassium carbonate. Fire And Materials. 1997;21:23-32.

[5] Chen G, Wang W. Role of freeze drying in nanotechnology. Drying Technology. 2007;25:29-35.

[6] Bourbigot S, Le Bras M, Leeuwendal R, Shen KK, Schubert D. Recent advances in the use of zinc borates in flame retardancy of EVA. Polymer degradation and stability. 1999;64:419-25.

[7] Castrovinci A, Camino G, Drevelle C, Duquesne S, Magniez C, Vouters M. Ammonium polyphosphate–aluminum trihydroxide antagonism in fire retarded butadiene-styrene block copolymer. European Polymer Journal. 2005;41:2023-33.

[8] Hapuarachchi T, Peijs T. Aluminium trihydroxide in combination with ammonium polyphosphate as flame retardants for unsaturated polyester resin. eXPRESS Polymer Letters. 2009;3:743-51.

[9] H VO. Polyelectrolyte reinforced aerogels of clays-application as chromatographic adsorbents. Clay Miner. 1967:423-35.

[10] Gutiérrez MC, Ferrer ML, del Monte F. Ice-Templated Materials: Sophisticated Structures Exhibiting Enhanced Functionalities Obtained after Unidirectional Freezing and Ice-Segregation-Induced Self-Assembly. Chemistry of Materials. 2008;20:634-48.

[11] Gutiérrez MC, García‑Carvajal ZY, Jobbágy M, Rubio F, Yuste L, Rojo F, et al. Poly (vinyl alcohol) scaffolds with tailored morphologies for drug delivery and controlled release. Advanced Functional Materials. 2007;17:3505-13.

[12] Wang Y, Gawryla MD, Schiraldi DA. Effects of freezing conditions on the morphology and mechanical properties of clay and polymer/clay aerogels. Journal of applied polymer science. 2013;129:1637-41.

[13] Liu D, Ma Z, Wang Z, Tian H, Gu M. Biodegradable Poly (vinyl alcohol) Foams Supported by Cellulose Nanofibrils: Processing, Structure, and Properties. Langmuir. 2014;30:9544-50.

[14] Deville S, Saiz E, Nalla RK, Tomsia AP. Freezing as a path to build complex composites. Science. 2006;311:515-8.

[15] Gibson LJ, Ashby MF. Cellular solids: structure and properties. 2nd ed: Cambridge university press; 1999.

[16] Bandi S, Schiraldi DA. Glass transition behavior of clay aerogel/poly(vinyl alcohol) composites. Macromolecules. 2006;39:6537-45.

[17] Suardana NPG, Ku MS, Lim JK. Effects of diammonium phosphate on the flammability and mechanical properties of bio-composites. Materials & Design. 2011;32:1990-9.

[18] Avalle M, Belingardi G, Montanini R. Characterization of polymeric structural foams under compressive impact loading by means of energy-absorption diagram. International Journal of Impact Engineering. 2001;25:455-72.

[19] Zhao C-X, Liu Y, Wang D-Y, Wang D-L, Wang Y-Z. Synergistic effect of ammonium polyphosphate and layered double hydroxide on flame retardant properties of poly (vinyl alcohol). Polymer degradation and stability. 2008;93:1323-31.

[20] Kashiwagi T, Gilman JW, Butler KM, Harris RH, Shields JR, Asano A. Flame retardant mechanism of silica gel/silica. Fire And Materials. 2000;24:277-89.

[21] Gilman JW, Lomakin S, Kashiwagi T, VanderHart DL, Nagy V. Characterization of Flame-retarded Polymer Combustion Chars by Solid-state ^{13}C and ^{29}Si NMR and EPR. Fire and materials. 1998;22:61-7.

[22] Chen H-B, Wang Y-Z, Sánchez-Soto M, Schiraldi DA. Low flammability, foam-like materials based on ammonium alginate and sodium montmorillonite clay. Polymer. 2012;53:5825-31.

[23] Shi Z, Fu R, Agathopoulos S, Gu X, Zhao W. Thermal conductivity and fire resistance of epoxy molding compounds filled with Si_3N_4 and $Al(OH)_3$. Materials & Design. 2012;34:820-4.

[24] Deville S, Saiz E, Tomsia AP. Ice-templated porous alumina structures. Acta Materialia. 2007;55:1965-74.

[25] Pinto UA, Visconte LLY, Gallo J, Nunes RCR. Flame retardancy in thermoplastic polyurethane elastomers (TPU) with mica and aluminum trihydrate (ATH). Polymer degradation and stability. 2000;69:257-60.

Chapter 5: Green Bio-based Aerogels Prepared from Recycled Cellulose Fiber Suspensions

5.1 Introduction

Aerogels prepared from renewable resources have been subject of considerable recently interest as promising bio-based alternatives for petroleum-derived foams. The potential applications of these bio-aerogels include lightweight construction, separation agents [1, 2], sensors [3] or supercapacitors [4], to mention a few.

However, one of the most important issues that need to be addressed prior to the general use of bio-based aerogels is the improvement of their mechanical performance. Different approaches have been taken to enhance the mechanical properties of these aerogels, such as the addition of clay [5], the creation of chemical crosslinks [6] or the reinforcement with natural fibers [7]. Recently, strong and flexible aerogels based on cellulose nanofibers (CNFs) from wood pulp were prepared via freeze-drying [8, 9]. Robust CNFs aerogels were created thanks to the presence of strong hydrogen bonding between the fibers. Also, it was possible to alter the microstructures and mechanical properties by changing either the freeze-drying condition or the CNFs concentration in the precursor solution [10].

Apart of natural sources like wood or plants, cellulose fibers can be obtained from paper or cardboard wastes. Although their mechanical properties are interior to than the ones of CNFs, this type of fibers could be used to make successful green industrial products. According to the statistics, recycling one ton of paper saves roughly 17 trees, 2.5 cubic metres of landfill space, 1.36 tons of water, 378.5 litres of gasoline, 27.2 kilograms of air pollutants, 10401 kilowatts of electricity [11]. Therefore, aerogels based on recycled cellulose fibers (RCF) could be a new

application for these residues.

The earlier works from CNFs-starch biofoams [12, 13] suggests that it may be possible to obtain high-performance bio-based aerogels by combining cellulose fibers with polymers based on polysaccharides. Sodium carboxymethylcellulose (CMC) is an anionic water-soluble polysaccharide derivative with carboxymethyl groups bound to hydroxyl groups of the glucopyranose monomers that make up the cellulose backbone. Building on the earlier experience of preparing cellulose nanocomposite films [14], CMC addition is also considered a possible way to improve the mechanical properties of RCF aerogels.

Flame resistance is another important parameter for foams. Previous work showed that sodium montmorillonite clay (Na^+-MMT) is an efficient filler to enhance flame retardancy and thermal stability of the aerogels [15]. The presence of clay leads to the formation of a barrier during burning which isolates the underlying materials from the heat radiation. Ammonium polyphosphate (APP), a halogen-free intumescent flame retardant agent, has been studied in polyvinyl alcohol (PVOH)/clay aerogel composites from chapter 4, showing positive effects on the fire retardancy by a chemical reaction in the condensed phase. On the other hand, Zhao's work [16] showed that layered double hydroxide (LDH) played a synergistic role with APP on fire retardancy of PVOH. Clay has a similar structure than LDH, therefore a synergistic effect between clay and APP may be expected.

In this chapter, a fully biodegradable biocomposite based on RCF/CMC was produced through a freeze-drying process. In addition, clay and APP were used to improve the flame retardancy of the prepared bio-based aerogels and to preserve their environmentally friendly character. The microstructures as well as the mechanical, thermal and fire behaviour of the bio-aerogels have been characterized.

5.2 Experimental

5.2.1 Materials

The raw materials for preparing aerogels were mentioned in Section 3.2. Recycled cellulose fibers (RCF) were produced according to the previous literature [17]. A pulp containing 10 wt% solids was finally obtained. The other ingredients like sodium carboxymethylcellulose, sodium montmorillonite and ammonium polyphosphate were used as received.

5.2.2 Aerogel Preparation

10 wt% of RCF pulp was initially diluted to appropriate concentration, followed by addition of the desired amount of CMC powder. The resultant suspensions were mixed under mechanical stirring at 80 ^{o}C until achieving homogenous mixtures (precursor suspensions). Then they were transferred into cylindrical vials of 30 mm diameter or into square-shaped molds (100×100 mm) and frozen over night in a freezer operating at -27 ^{o}C. Final aerogels were obtained using the lyophilization method discussed in chapter 3. The denomination of obtained samples is according to the constituents used followed by its respective concentration percentage in 100 ml of aqueous solution. For instance, F5C2.5 contains 5 wt% RCF and 2.5 wt% CMC; where F and C stand for RCF and CMC respectively. Same solid amounts remained in the aerogels when the ice was removed.

Flame-retardant modified aerogels were prepared in a similar way. Firstly, clay and APP powders were both dispersed in (50 ml of) deionized (DI) water using an IKA Ultra-turrax disperser operated at 8000 rpm for 30 min. Then 50 ml of CMC/RCF suspension which contained 2.5 g of RCF and 2.5 g of CMC was added. The mixture was mechanically stirred until they became homogeneous and then it was freeze-dried. The resultant aerogels were named as *MxAy*, where M and A represent MMT and APP respectively; x and y are their concentration percentage in the final

precursor suspension. For example, M2.5A0.5 aerogel was prepared adding 50 ml water containing 2.5 g of MMT and 0.5 g of APP to 50 ml water containing 2.5g RCF and 2.5 g of CMC. The composition summary of all the prepared samples is shown in Table 5.1.

5.2.3 Characterization

Samples in this chapter were characterized using Helium pycnometry, mercury intrusion, SEM, compression, TGA, cone calorimetry and FTIR, which were discussed in Chapter 3.3 in detailed. The shrinkage degree (SD) of aerogels is calculated by comparing the diameter of the samples diameter before (D_b) and diameter after (D_a) freeze-drying and according to equation 5.1. D_b was equal to the diameter of cylinder mold for preparing aerogels.

$$\text{SD} = \frac{D_b - D_a}{D_b} \times 100\% \qquad\qquad 5.1$$

The moisture uptake of the samples and viscosity of the precursor suspension were also measured according to the method described in chapter 3.

Table 5.1 Composition of the precursor suspension for preparing RCF/CMC/clay aerogels

Samples	RCF (wt%)	CMC (wt%)	Clay (wt%)	APP (wt%)
F2.5C0	2.5	0	0	0
F0C2.5	0	2.5	0	0
F2.5C1.2	2.5	1.25	0	0
F2.5C2.5	2.5	2.5	0	0
F3.7C2.5	3.75	2.5	0	0
F5C2.5	5	2.5	0	0
M2.5A0	2.5	2.5	2.5	0
M2.5A0.2	2.5	2.5	2.5	0.25
M2.5A0.5	2.5	2.5	2.5	0.5
M0A0.5	2.5	2.5	0	0.5

5.3 Results and Discussion

5.3.1 SEM Analysis

The microstructure of pure RCF aerogel is shown in Figure 5.1a. In the micrograph, it can be seen that the fibers are distributed randomly without a defined alignment. Due to their large dimensions, fibers are not pushed aside by the growing ice and therefore no predominant orientation is observed. In contrast, CNF aerogels as previously reported in literature [8] displayed a cellular cross-section in which the cell wall consisted of CNFs, as a result of the much smaller fiber dimensions and faster applied freezing rate.

Interestingly, when 1.25 wt% CMC was introduced into the precursor solution, a lamellar structure appeared in the resultant sample F2.5C1.2, as seen in Figure 5.1b. The molecules of CMC are pushed into interstitial regions of the ice upon the ice crystals growth. After ice sublimation, laminas are remained forming the typical "house of cards" aerogel structure [18]. Some fibers can also be found bridging the channels left by the ice.

As measured by the apparent density, the porosity of aerogels decreased with the increase of CMC content, being more evident when Figure 5.1b and Figure 5.1c are compared. This effect is related to the amount of solids in the precursor suspension. The higher the amount of solids in the suspension, the lower is the ice expansion, thus decreasing the final apparent density. Moreover, aerogels with increasing amount of solids exhibited thicker layers, which was associated with the slow ice crystals growth in viscous suspensions.

As expected, pure CMC aerogels displayed smooth layer surface (Figure 5.1d), which was similar with previous work on aerogels prepared from different types of thickening agents [5]. By adding 5 wt% of RCF (F5C2.5), the lamellar structure was lost due to fiber aggregation (Figure 5.1e). The maximum content of fiber to avoid this phenomenon was found to be 3.75 wt%.

For the case of flame retardancy modified aerogels (Figure 5.1f), the absence of

isolated clay layers suggested that aerogel laminas were formed via CMC encapsulating clay nanoparticles again with intercalated fibers. Further addition of APP did not affect the microstructures of the RCF/CMC/clay aerogels.
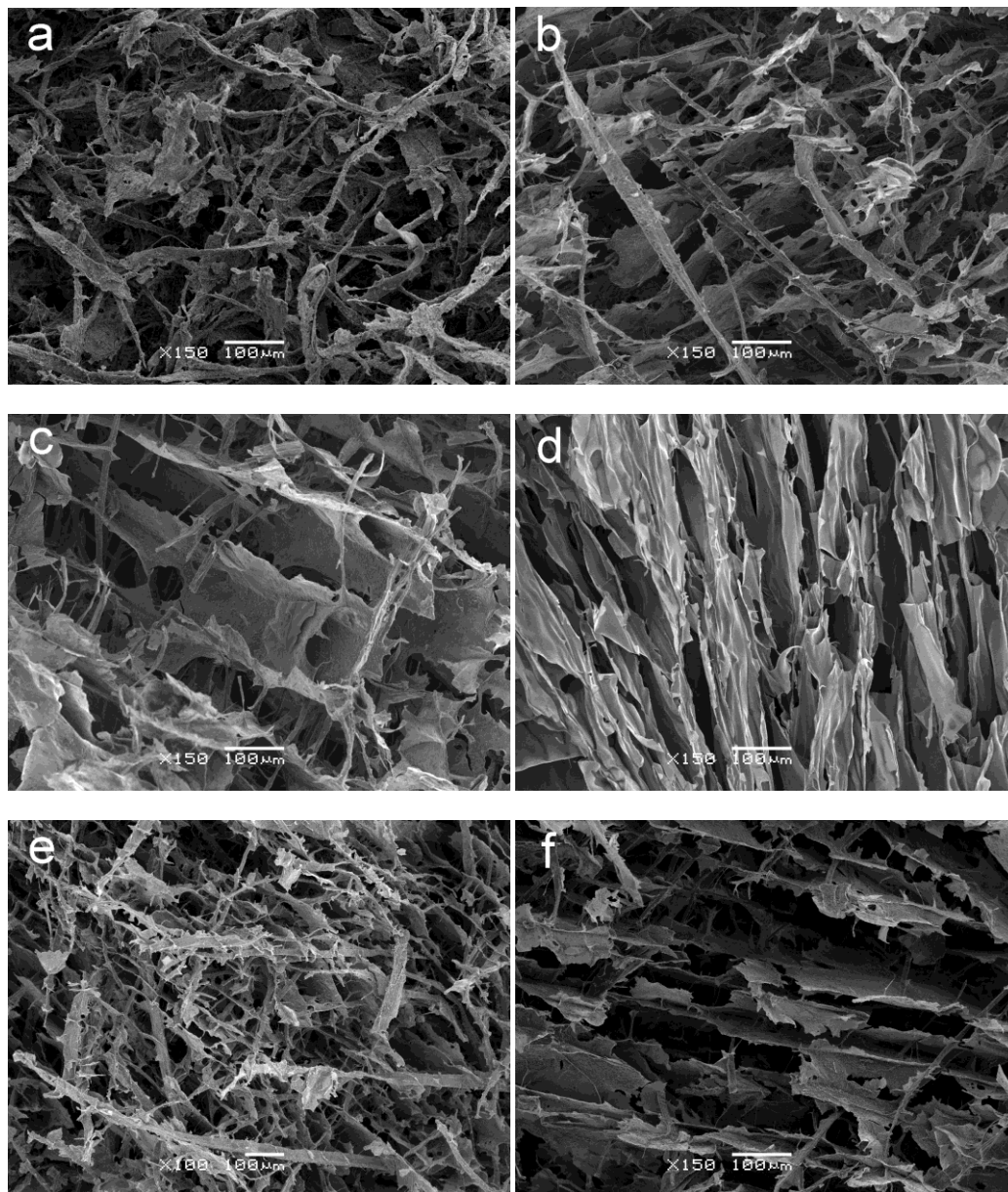
Figure 5.1 SEM micrographs of RCF/CMC aerogels: (a) F2.5C0, (b) F2.5C1.2, (c) F2.5C2.5, (d) F0C2.5, (e) F5C2.5, (f) M2.5A0

5.3.2 Porosity and Pore Distribution

To further investigate the microstructure of aerogels, the porosity and the pore distribution of some of the samples were determined using a helium pycnometry and mercury intrusion respectively. Also the viscosities of precursor suspensions and the shrinkage of aerogels were measured as additional information. The results are represented in Table 5.2, such as shrinkage degree, precursor suspension viscosity, average pore size and porosities.

The pore distributions of the aerogels are shown in Figure 5.2. Mercury pressure applied to the external surface of samples generates compressive stress that may collapse the pore especially when a high pressure is applied. However, the pore distribution curves in this study were smooth suggesting there was no buckling during the mercury penetration.

Table 5.2 The moisture uptake, shrinkage, precursor suspension viscosity, pore size and porosity of the aerogels based on RCF/CMC

Samples	Moisture uptake (%)	SD (%)	Viscosity (m pa s)	Pore size (μm)	Porosity (%)
F0C2.5	10.6±1.5	14.4±0.6	2280±40	40	98.0
F2.5C2.5	6.6±0.9	10.5±1.8	1860±20	130	97.0
F3.7C2.5	5.5±0.4	9.0±0.2	-	-	96.2
F5C2.5	5.4±0.5	7.7±0.2	-	-	95.6
F2.5C0	2.5±0.1	10.9±1.6	-	-	98.6
F2.5C1.2	5.1±0.3	12.1±2.6	330±10	150	98.2
M2.5A0	4.3±0.4	8.1±1.0	1980±40	75	96.1

"-"means not determined; all the error values of porosity are less than 1%.

The sample F0C2.5 showed the highest viscosity in precursor solution and largest shrinkage as well as the smallest pore size. It is considered that CMC has a low crystallinity and is prone to shrink after ice sublimation because of hydrogen bonding between its molecules [19]. The precursor suspension viscosity of aerogels decreased with the increase of fiber content. When RCF are introduced, the cellulose fibers act as "plasticizer", generating molecular interactions with CMC molecules. This will lower the strong intermolecular hydrogen bonding of CMC thus decreasing the

viscosity of precursor suspension. Also because of this plasticization effect of RCF, the RCF/CMC aerogel composites displayed lower shrinkage compared with pure CMC aerogel. Moreover, the shrinkage of the samples was further reduced with the increase of fiber content in the aerogels.
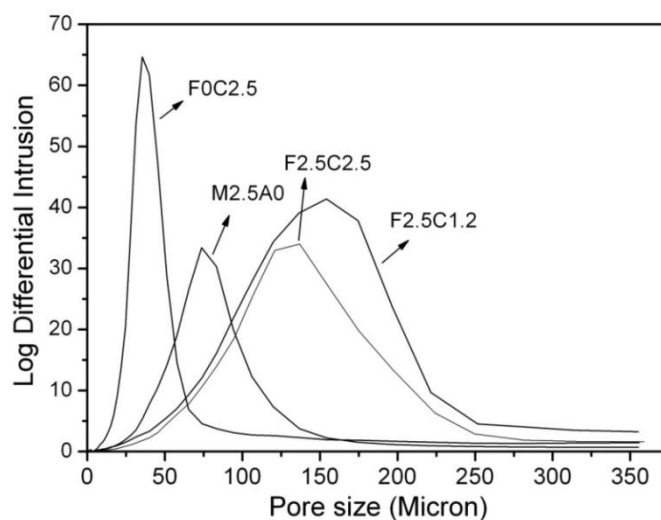
Figure 5.2 Pore distributions of aerogels based on RCF/CMC

Adding 50% fibers to sample F0C2.5 (F2.5C2.5), the pore dimension increased from 40 to 130 μm. This is because the presence of high fiber loading reduces the aerogels shrinkage. On the other hand, the viscosity of precursor suspension plays an important role on the pore size of resultant aerogels. Lower viscosity allows ice crystals to grow faster to final larger size, which leaves larger pore after freeze-drying [20, 21]. Clay addition or usage of more CMC raised the viscosity of the suspension reducing the pore dimensions. Also, this tendency of pore size change was valid in SEM observation.

5.3.3 Moisture Uptake

The moisture uptake of the aerogels is also listed in Table 5.2. As expected, it was reduced at elevated fiber content. This is mainly due to the less hygroscopic nature of cellulose fiber compared to CMC [13]. However, when the RCF content was over 50

wt% in aerogel composites with same CMC amount, moisture uptake tended to be stable because the aerogels porosities do not change substantially.

5.3.4 Compression Tests

The compressive stress-strain curves of samples are presented in Figure 5.3. For most of them, the stress-strain behavior was linear at low strains with the slopes strongly depending on densities. At this stage, the deformation was mainly due to elastic bending of the cell walls. Then a "plateau zone" appeared due to cell collapse. Typical elastic-plastic polymer foams showed a horizontal plateau region after reaching a yield stress [22]. However, the present aerogel composites, especially those with comparatively higher densities, displayed a gradually increasing stress in this stage. At high strains, the densification occurred with the steep rising of the stress which is due to the opposing cell walls touching [22]. The optical microscope photos of sample F2.5C2.5 before and after compression are shown in Figure 5.4. It can be observed that the original layered structure was deformed and the layers touched with each other after compression test. The parameters defining the compressive mechanical behaviour of the aerogels are summarized in Table 5.3.

Table 5.3 Mechanical properties of aerogels based on RCF/CMC

Samples	ρ_{app} (g/cm^3)	E (MPa)	E_s (MPa/g cm^{-3})	σ_y (kPa)	σ_{sy} (kPa/g cm^{-3})	E_a at 70% ε (kJ/m^3)
F2.5C0	0.030	0.13±0.01	4.23±0.33	5.7±0.4	191±16	10.9±1.9
F0C2.5	0.036	1.56±0.17	43.05±5.07	24.7±1.5	679±41	60.0±1.3
F2.5C1.2	0.042	1.15±0.34	23.39±2.26	46.1±5.2	1093±123	55.9±2.3
F2.5C2.5	0.057	2.87±0.78	56.21±8.91	77.6±4.2	1341±76	132.2±3.9
F3.7C2.5	0.075	5.04±0.49	66.59±7.01	133.7±7.4	1767±92	201.6±14.9
F5C2.5	0.087	4.16±1.21	61.31±5.62	164±15.8	1880±180	245.8±12.9
M2.5A0	0.076	3.63±0.52	48.73±6.54	89.1±1.8	1436±478	154.8±4.4
M2.5A0.2	0.082	3.25±0.49	39.31±5.83	109±43.8	1325±518	174.2±10.7
M2.5A0.5	0.083	2.34±0.71	28.25±7.75	63.6±26.1	759±298	155.8±6.6
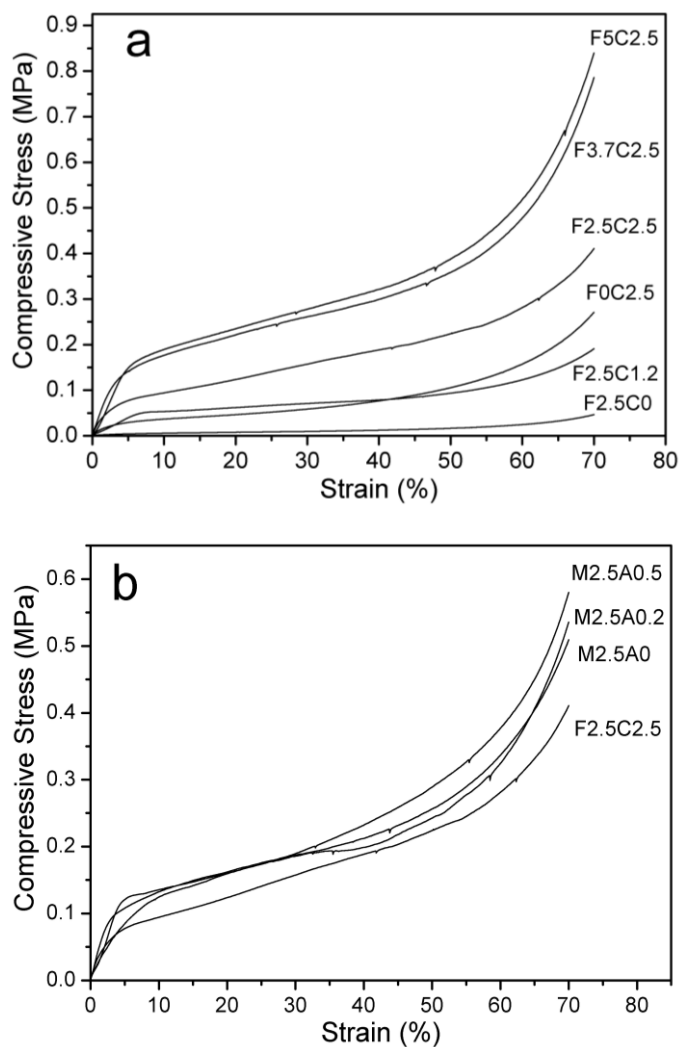
Figure 5.3 Compressive stress-strain curves of (a) RCF/ CMC aerogels and (b) flame retardancy modified aerogels
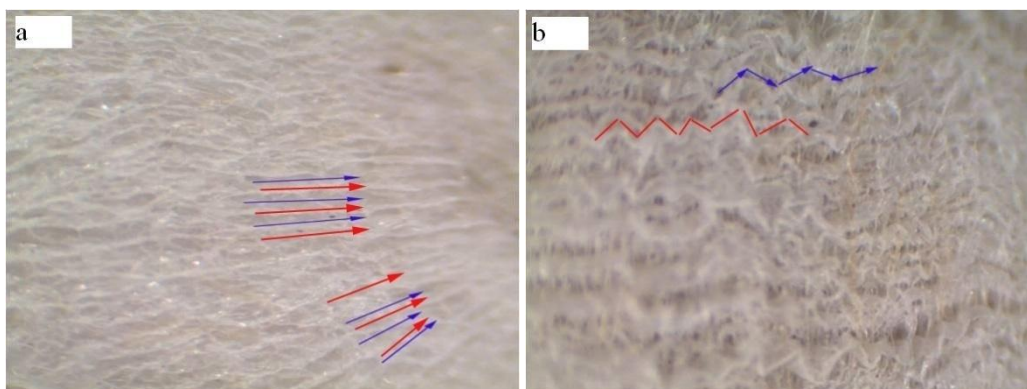
Figure 5.4 Optical microscope photos of sample F2.5C2.5 before (a) and after (b) compression

The sample F2.5C0 showed much lower mechanical properties compared to those found in literature for CNFs aerogels which had a modulus of 1.36 MPa and yield strength of 92.7 KPa with a similar density ($0.035 g/cm^3$) [8]. This is because CNF aerogels have a cellular structure as well as the cell walls consist of nanofibers with much higher specific surface and mechanical properties than the ones used in this work.

Pure CMC aerogel, F0C2.5, had a similar apparent density than F2.5C0 but behaved in a more rigid way. Also, the mechanical properties of F2.5C0 were enhanced through adding 1.25 wt% of CMC into its precursor suspension. Both the specific modulus (E_s) and absorbed energy (E_a) were increased by nearly 4 times. The specific yield stress (σ_{sy}) became 5.7 times higher. Two factors contribute to this effect. Firstly, CMC can form stable structures due to the inherent self-association of the molecules via hydrogen bonding [23]. In second term, CMC and fibers have similar chemical structures and polarities which lead to the development of a good adhesion between them.

A monotonic increase in the specific modulus and yield strength (σ_y) with the increase of CMC concentration is observed in Table 5.3. When more CMC is added to the aerogels, the density of links between fibers becomes higher, improving the integrity of the materials. The composite F2.5C2.5 had a modulus (E) of 2.87 MPa which was much higher than the modulus of cellulose whisker aerogel (778 kPa) with a density of 0.11 g/cm^3 [24]. F2.5C2.5 presented a layered architecture connected with fibers (Figure 5.1c) as well as the strong molecular affinity between CMC and RCF as previously discussed. This makes the resultant aerogels behave in a much more rigid manner.

In order to further investigate the effect of fiber content on the mechanical properties of RCF/CMC aerogel composites, aerogels with constant CMC concentration (2.5 wt%) were prepared. Table 5.3 shows that the modulus of the aerogels increased with the RCF content up to 3.75 wt% where a maximum was reached. F3.7C2.5 presented mechanical properties comparable to the ones of the CNF aerogel [8]. However, when the RCF amount was further increased, there was no

significant change in mechanical properties. This could be due to fiber aggregation in the precursor solution when its concentration reached a critical value. When fibers were in excess, they remained isolated in the obtained aerogel, having a lack of adhesion with CMC (Figure 5.1e).

In the case of flame retardant modified aerogels, there was no significant improvement in the mechanical properties by the clay presence. Both CMC and clay possess negative charges on their surface and a weak interaction between them may be expected. This phenomenon was likewise found when testing clay-CMC films [14]. However, in the present case, clay was added to improve thermal and fire properties rather than the mechanical ones. APP incorporation reduced the mechanical properties of the RCF/CMC/clay aerogels in a similar way as described in previous chapter on PVA-clay-APP systems, which showed that the addition of APP had a side effect on the mechanical properties. The slight hydrolysis of APP decreased the pH value of the suspension, which had a negative impact on the interaction between fibers and CMC.

5.3.5 Thermal Stability

Generally, the TGA patterns of RCF/CMC aerogels can be divided into three steps (Figure 5.5). The first step below 150 ^{o}C is due to the evaporation of moisture absorbed by the aerogels. In the second stage, a rapid mass loss occurred above 250 ^{o}C, which involves the oxidative decomposition of the cellulosic molecular chains. A further increase in temperature leads to a slow thermal degradation, followed by a carbonization process in the final stage [25]. With the addition of APP or clay, the corresponding TGA curves changed, showing a new degradation step around 400 ^{o}C. This step may be due to the formation of char which delays the decomposition rate. The parameters for the thermal stability of each sample, such as the onset of decomposition temperature $T_{d5\%}$, the temperature at maximum weight loss rate T_{dmax}, the maximum weight loss rate dW/dT_{max}, and the residue amount at 600 ^{o}C are listed in Table 5.4. $T_{d5\%}$ is defined as the temperature at which 5% weight loss beyond total

water evaporation, which occurs at 150 ^{o}C.
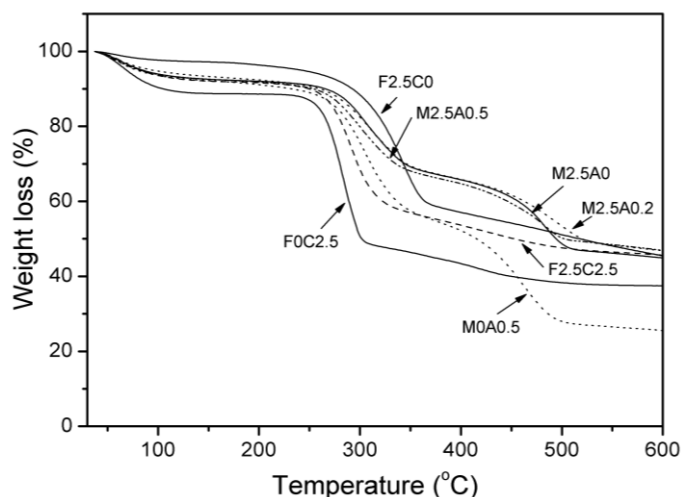
Figure 5.5 TGA weight loss curves of aerogels based on RCF/CMC

Table 5.4 TGA data of aerogels based on RCF/CMC

Samples	$T_{d5\%}$ (^{o}C)	T_{dmax} (^{o}C)	dW/dT_{max} (%/^{o}C)	W_R (%)
F0C2.5	260.7	282.6	1.12	37.5
F2.5C0	276.6	342.2	0.60	45.2
F2.5C2.5	265.8	290.7	0.72	45.6
M2.5A0	281.6	304.3	0.35	44.9
M2.5A0.2	270.9	301.1	0.33	46.8
M2.5A0.5	272.2	311.3	0.31	46.9
M0A0.5	262.8	304.3	0.53	25.5

Sample F2.5C2.5 showed a decomposition behaviour which was intermediate between the pure components. RCF showed a lower rate of degradation and a higher stability than CMC due to its higher crystallinity degree [19].

With the addition of clay, the thermal stability of the aerogel was enhanced. Both $T_{d5\%}$ and T_{dmax} increased by nearly 15 ^{o}C, and the maximum weight loss rate dropped by about 50%. Inorganic clay nanoparticles played a role of thermal insulator, protecting the polymer of being decomposed rapidly as has been reported in previous works [5]. The incorporation of 0.5 wt% of APP into F2.5C2.5 did not markedly affect the $T_{d5\%}$. However, the T_{dmax} increased by nearly 15 ^{o}C and dW/dT_{max} decreased from 0.72 to 0.53. This suggests that the kinetic thermal stability was enhanced due to

the retardant effect of the APP. APP is able to react with the hydroxyl groups of the cellulose pyranose ring to yield a cellular compact char, limiting the heat transfer [16]. M2.5A0.2 showed slightly higher char residue and lower decomposition rate as compared to M2.5A0. Increasing the amount of APP to 0.5 wt%, T_{dmax} increased by 7 ^{o}C, indicating a certain synergistic effect on the thermal stability. However, the addition of APP lowered $T_{d5\%}$ of M2.5A0 because the APP decomposition started at a lower temperature (about 200 ^{o}C).

5.3.6 Cone Calorimetry

The relevant flammability data of modified RCF/CMC aerogels samples from cone calorimetry tests are summarized in Table 5.5, which includes time to flame extinguish (t_e) and the other parameters that were defined in chapter 4. The combustion patterns in terms of heat release rate as a function of their burning time are illustrated in Figure 5.6. In addition, photos of the char of flame retardant-modified aerogels after cone calorimetry tests are shown in Figure 5.7.
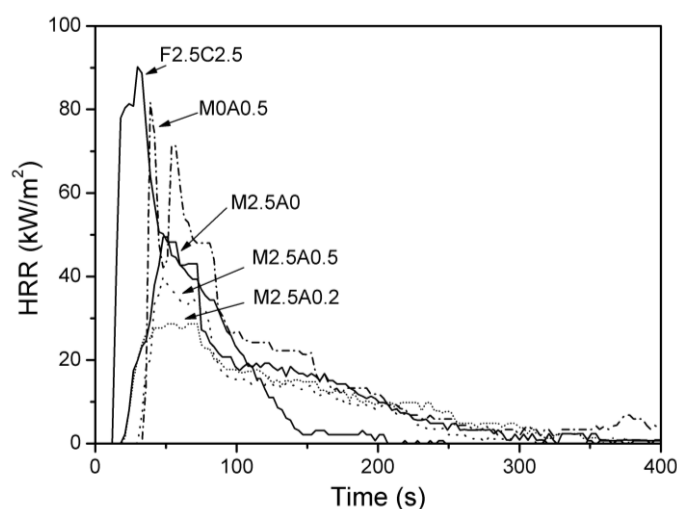
Figure 5.6 Heat release rate of flame retardancy modified RCF/CMC aerogels

Unmodified sample displayed a typical combustion behaviour described in previous works on bio-based aerogels [26]. Its HRR pattern started with a vigorous burning

episode followed by a long fire disappearing region with low HRR values. With the addition of APP or clay, the initial combustion step was delayed and HRR plots decreased in height and flattened out prior to completing the test. Sample M0A0.5 should show a continuous HRR plot, however it displayed a combustive pattern with a valley in the initial stage. This is because the sample was cracked upon burning (see Figure 5.7b) and protective layer was broken, which transiently allows the fire transmission from the top to the bottom of the samples.
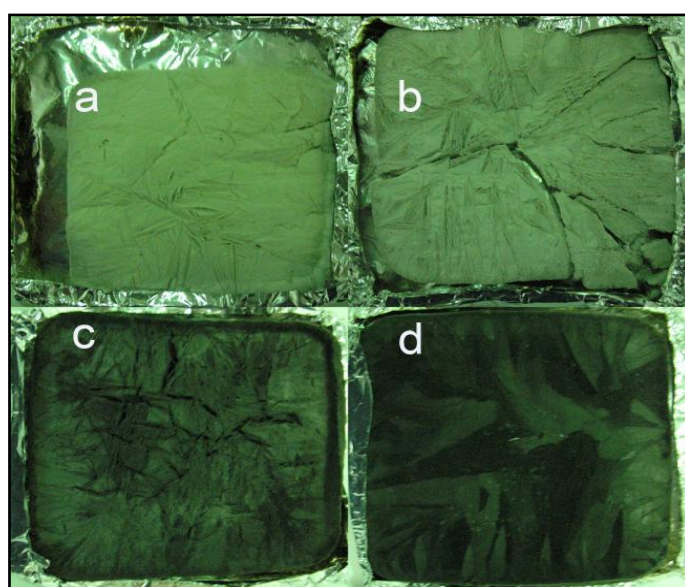
Figure 5.7 Photos of the chars of flame retardancy modified aerogel samples after cone colorimetry tests: (a)F2.5C2.5, (b)M0A0.5, (c)M2.5A0, (d)M2.5A0.5

Table 5.5 Combustive parameters of flame retardancy modified RCF/CMC aerogels

Samples	Mass (g)	t_e (s)	TTPHRR (s)	PHRR (kW/m^2)	FGR (kW/m^2 s)	THR (MJ/m^2)	W_R (%)
F2.5C2.5	4.0	106	30	90.2	3.01	5.03	23.1
M2.5A0	5.1	28	48	49.5	1.03	4.64	41.2
M2.5A0.2	5.4	36	51	28.7	0.56	4.05	43.6
M2.5A0.5	5.5	15	48	39.8	0.83	3.5	42.9
M0A0.5	4.8	45	39	81.6	2.10	5.58	24.0

When 10% APP was added to F2.5C2.5 (sample M0A0.5), the PHRR decreased by 9.5% and the FGR also reduced by nearly 30%. Moreover, the time to peak heat released rate (TTPHRR) became 9 seconds longer. This is mainly attributed to the

formation of an intumescent char network as discussed in the thermal stability section. On the other hand, APP decomposition produced inert gas (NH_3), which also dilutes the combustive fuel in the gas phase.

It has been widely accepted that clay served as a flame retardant in biopolymer aerogels [15]. A similar effect was observed in the present work with RCF/CMC aerogels. The PHRR, FGR and time to flame extinguish (t_e) decreased significantly with the addition of clay. Furthermore, self-ignition of the samples by the heat radiation was retarded. This is due to the presence of high quantity of clay (33 wt%). As discussed previously, sample M2.5A0 had a layered structure (Figure 1f) consist of CMC encapsulated clay platelets. When it was burned, CMC was decomposed into combustive gas and a porous ceramic clay layers was left. Gradually, clay layers enriched on the top of the sample and a cellular inorganic char was created, protecting the material beneath the surface being burned rapidly and limiting the oxygen content in the flame zone. Moreover, this cellular clay char formed a complex labyrinth through which combustion gases diffuse out of the material. On the other hand, MMT as a layered double hydroxide (LDH) may crosslink with CMC and RCF through hydration reaction, which was studied in PVOH-LDH system [16].

The best flame retardant performance was observed for the samples containing both clay and APP. M2.5A0.2 displayed approximately 1/3 of PHRR and 1/5 of FGR compared to the unmodified one. This indicates that APP and clay have a synergistic effect.

The photos of the char after burning are given in Figure 5.7. F2.5C2.5 showed a white residue (Figure 5.7a). The incorporation of APP turned the color of char into grey (Figure 5.7b). With the addition of clay, the initial sample shapes were preserved in their black chars (Figure 5.7c). This is due to the formation of a dense ceramic skeleton generated by clay assembling when the samples are burned.

In comparison to other bio-based aerogels prepared by the same freeze-drying process, such as wheat gluten [26], the RCF/CMC aerogels showed lower PHRR and much higher residue amount. This is maybe partially due to the presence of some inorganic compounds in the RCF suspension, such as $Al_2(SO_4)_3$ and $CaCO_3$, which

are commonly used as fillers in the paper industry.

5.3.7 FTIR Analysis

FTIR spectroscopy was used to investigate the aerogel and their char residues which were collected after cone calorimetry tests. The IR patterns are shown in Figure 5.8 and Figure 5.9, respectively.
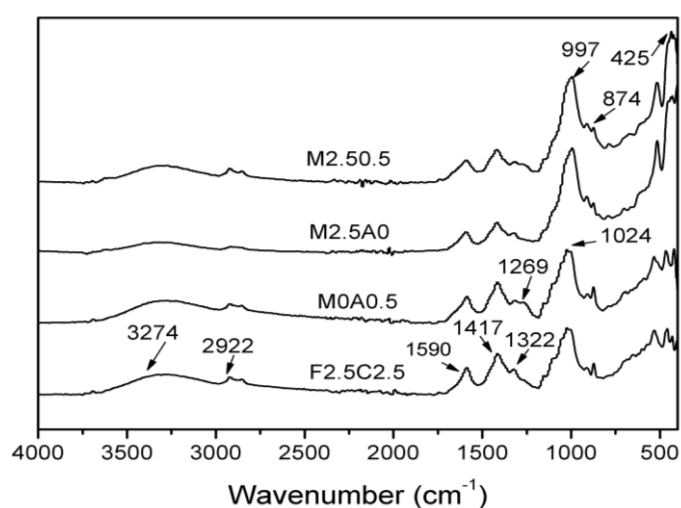
Figure 5.8 FTIR patterns of flame retardant modified RCF/CMC aerogels
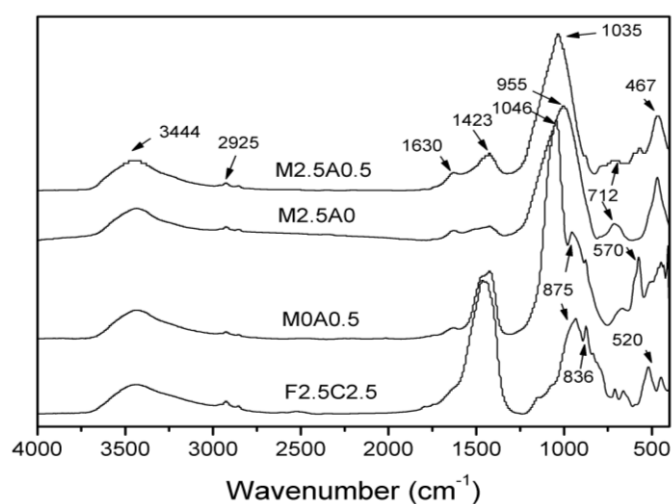
Figure 5.9 FTIR spectra of RCF/CMC aerogel chars

In the IR pattern of sample F2.5C2.5, the band at 3274 cm^{-1} is due to OH stretching, and ones at 1590 cm^{-1} and 1322 cm^{-1} are attributed to carboxyl from CMC. At the same time, it can be observed that CH_2 stretching and bending characteristic bands were shown at 2922 cm^{-1} and 1417 cm^{-1}, respectively. Moreover, peak at 1024 cm^{-1} is associated with C-O-C asymmetry stretching which connects pyrane rings, in which CH vibration was displayed on 874 cm^{-1} [27].

In comparison to F2.5C2.5, The appearance of the band at 1269 cm^{-1} in sample M0A0.5 is attributed to P=O stretching [28], indicating the incorporation of APP. With the addition of MMT, the band C-O-C at 1024 cm-1 shifted to 997 cm^{-1}, which is because it is overlapped by Si-O-Si stretching characteristic peak [29, 30].

For the char of sample F2.5C2.5, bands at 3444 cm^{-1} were related to free OH stretch. The characteristic peaks at 2925 cm^{-1} and 1423 cm^{-1} were associated to CH_2 asymmetry stretch and CH_2 scissoring vibration, respectively [27]. This indicated that aliphatic compounds existed in the char of cellulose based aerogels. When APP was incorporated, a new band at 1046 cm^{-1} was observed in the char of M0A0.5, which is attributed to P-O-C stretching [31, 32]. During the burning process, APP is firstly decomposed into poly(phosphoric acid) and then it reacts with the hydroxyl group on cellulose through esterification. For the char of M2.5A0, the peaks at 955 cm^{-1} and 467 cm^{-1} were associated to Si-O-Si and Al-O group respectively. The new band at 712 cm^{-1} was related to the CH stretching in ring compound [33]. The CH_2 characteristic band at 1423 cm^{-1} of sample M2.5A0 decreased significantly in intensity as compared to F2.5C2.5 char, indicating that the amount of aliphatic groups was significantly reduced. This is possible because clay can catalyze the formation of a stable ring char structure during the polymer pyrolysis in the presence of hydroxyl groups [16]. By adding APP to M2.5A0, the P-O-C band at 1035 cm^{-1} appeared and overlapped with the Si-O band. The poly(phosphoric acid) obtained from APP pyrolysis may have reacted with the hydroxyl groups on the clay surface, releasing water and producing covalent bonds. The resultant char is complex and distinctly different from the chars with APP or clay alone [16]. The band at 1630 cm^{-1} was due to the C=C stretch which only appeared when APP or clay was added, suggesting that

samples were not totally oxidized during pyrolysis because of the insulating effect of the formed protective char.

On the basis of the FTIR analysis, four possible char formation mechanism in cellulose/clay/APP composite aerogels during burning were proposed, which are shown in Figure 5.10. As discussed previously in cone calorimetry part, the improvement in flame retardant properties of modified aerogels is due to condensed phase flame retardant mechanism. Clay addition can promote the formation of compact layered char in condensed phase during burning in cellulose matrix.
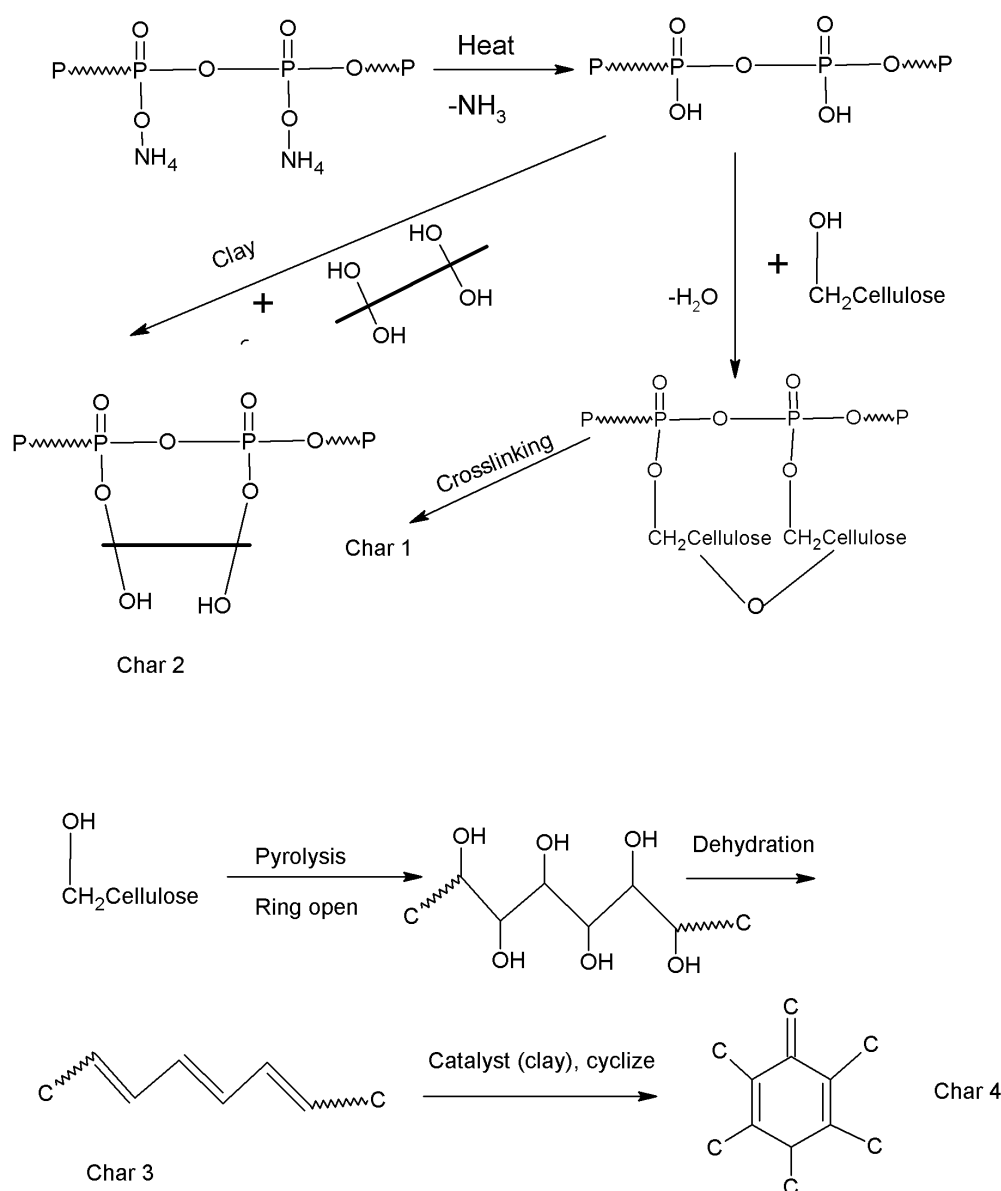
Figure 5.10 Scheme of possible flame retardancy mechanism in cellulose/clay/APP aerogels

5.4 Conclusions

Recycled cellulose fiber (RCF) from waste paper pulp and a food thickening agent carboxymethylcellulose (CMC), were used to prepare green bio-aerogels. By changing the amount of RCF or CMC, samples showed different microstructures, varying from random to a "house of card" structure. RCF played a role of "plasticizer" reducing the viscosity of precursor suspension of aerogels. Pore dimension of the aerogels decreased with the increase of RCF content. On the other hand, CMC acted as binding agent for the fibers, effectively improving the mechanical properties of aerogels which were also increased with the fiber amount up to 3.75 wt%. However, a high loading RCF not only promotes moisture resistance but also improves the dimensional stability of composite aerogels during freeze-drying process. The addition of clay did not significantly change the mechanical properties, but greatly enhanced the thermal stability and flame retardant behaviour. Clay platelets played a role of protective thermal barrier and also limited shrinkage of the aerogels during the burning process. Ammonium polyphosphate (APP) and clay played a synergetic effect on the flame retardancy and thermal stability of cellulosic aerogels. This work showed a possible way to produce green foam-like materials as potential candidates for substituting traditional petroleum-based foams.

References

[1] Cervin NT, Aulin C, Larsson PT, Wågberg L. Ultra porous nanocellulose aerogels as separation medium for mixtures of oil/water liquids. Cellulose. 2012;19:401-10.

[2] Korhonen JT, Kettunen M, Ras RHA, Ikkala O. Hydrophobic Nanocellulose Aerogels as Floating, Sustainable, Reusable, and Recyclable Oil Absorbents. ACS applied materials & interfaces. 2011;3:1813-6.

[3] Wang M, Anoshkin IV, Nasibulin AG, Korhonen JT, Seitsonen J, Pere J, et al. Modifying native nanocellulose aerogels with carbon nanotubes for mechanoresponsive conductivity and pressure sensing. Advanced Materials. 2013;25:2428-32.

[4] Gao K, Shao Z, Wang X, Zhang Y, Wang W, Wang F. Cellulose nanofibers/multi-walled carbon nanotube nanohybrid aerogel for all-solid-state flexible supercapacitors. RSC Advances. 2013;3:15058-64.

[5] Chen H-B, Chiou B-S, Wang Y-Z, Schiraldi DA. Biodegradable Pectin/Clay Aerogels. ACS applied materials & interfaces. 2013;5:1715-21.

[6] Pojanavaraphan T, Magaraphan R, Chiou B-S, Schiraldi DA. Development of biodegradable foamlike materials based on casein and sodium montmorillonite clay. Biomacromolecules. 2010;11:2640-6.

[7] Blomfeldt TO, Kuktaite R, Johansson E, Hedenqvist MS. Mechanical properties and network structure of wheat gluten foams. Biomacromolecules. 2011;12:1707-15.

[8] Sehaqui H, Salajkova M, Zhou Q, Berglund LA. Mechanical performance tailoring of tough ultra-high porosity foams prepared from cellulose I nanofiber suspensions. Soft Matter. 2010;6:1824-32.

[9] Klemm D, Kramer F, Moritz S, Lindstrom T, Ankerfors M, Gray D, et al. Nanocelluloses: A New Family of Nature-Based Materials. Angewandte Chemie-International Edition. 2011;50:5438-66.

[10] Svagan AJ, Jensen P, Dvinskikh SV, Furo I, Berglund LA. Towards tailored hierarchical structures in cellulose nanocomposite biofoams prepared by freezing/freeze-drying. Journal of Materials Chemistry. 2010;20:6646-54.

[11] Rahman MO, Hannan M, Scavino E, Hussain A, Basri H. An efficient paper grade identification method for automatic recyclable waste paper sorting. European Journal of Scientific Research. 2009;25:96-103.

[12] Svagan AJ, Samir MA, Berglund LA. Biomimetic foams of high mechanical performance based on nanostructured cell walls reinforced by native cellulose nanofibrils. Advanced Materials. 2008;20:1263-9.

[13] Svagan AJ, Berglund LA, Jensen P. Cellulose Nanocomposite Biopolymer

Foam-Hierarchical Structure Effects on Energy Absorption. ACS applied materials & interfaces. 2011;3:1411-7.

[14] Liu A, Berglund LA. Fire-retardant and ductile clay nanopaper biocomposites based on montmorrilonite in matrix of cellulose nanofibers and carboxymethyl cellulose. European Polymer Journal. 2013;49:940-9.

[15] Chen H-B, Wang Y-Z, Sánchez-Soto M, Schiraldi DA. Low flammability, foam-like materials based on ammonium alginate and sodium montmorillonite clay. Polymer. 2012;53:5825-31.

[16] Zhao C-X, Liu Y, Wang D-Y, Wang D-L, Wang Y-Z. Synergistic effect of ammonium polyphosphate and layered double hydroxide on flame retardant properties of poly (vinyl alcohol). Polymer degradation and stability. 2008;93:1323-31.

[17] Monfort MC. Process for recycling waste paper, product obtained therefrom and its uses. US Patents; 2011.

[18] Bandi S, Schiraldi DA. Glass transition behavior of clay aerogel/poly(vinyl alcohol) composites. Macromolecules. 2006;39:6537-45.

[19] Liu D, Ma Z, Wang Z, Tian H, Gu M. Biodegradable Poly (vinyl alcohol) Foams Supported by Cellulose Nanofibrils: Processing, Structure, and Properties. Langmuir. 2014;30:9544-50.

[20] Gutiérrez MC, Ferrer ML, del Monte F. Ice-Templated Materials: Sophisticated Structures Exhibiting Enhanced Functionalities Obtained after Unidirectional Freezing and Ice-Segregation-Induced Self-Assembly. Chemistry of Materials. 2008;20:634-48.

[21] Gutiérrez MC, García-Carvajal ZY, Jobbágy M, Rubio F, Yuste L, Rojo F, et al. Poly (vinyl alcohol) scaffolds with tailored morphologies for drug delivery and controlled release. Advanced Functional Materials. 2007;17:3505-13.

[22] Gibson LJ, Ashby MF. Cellular solids: structure and properties. 2nd ed: Cambridge university press; 1999.

[23] Surapolchai W, Schiraldi DA. The effects of physical and chemical interactions in the formation of cellulose aerogels. Polymer Bulletin. 2010;65:951-60.

[24] Gawryla MD, van den Berg O, Weder C, Schiraldi DA. Clay aerogel/cellulose whisker nanocomposites: a nanoscale wattle and daub. Journal of Materials Chemistry. 2009;19:2118-24.

[25] Donius AE, Liu A, Berglund LA, Wegst UG. Superior mechanical performance of highly porous, anisotropic nanocellulose-montmorillonite aerogels prepared by freeze casting. Journal of the Mechanical Behavior of Biomedical Materials. 2014;37:88-99.

[26] Blomfeldt TOJ, Nilsson F, Holgate T, Xu J, Johansson E, Hedenqvist MS. Thermal Conductivity and Combustion Properties of Wheat Gluten Foams. ACS applied materials & interfaces. 2012;4:1629-35.

[27] Socrates G, Socrates G. Infrared and Raman characteristic group frequencies: tables and charts. Third ed: Wiley Chichester; 2001.

[28] Zheltikov A. Course notes on the interpretation of infrared and Raman spectra. Dana W. Mayo, Foil A. Miller and Robert W. Hannah. John Wiley & Sons, Hoboken, NJ, 2004, pp. 567. Wiley Online Library; 2005.

[29] Pandey JK, Singh RP. Green Nanocomposites from Renewable Resources: Effect of Plasticizer on the Structure and Material Properties of Clay-filled Starch. Starch-Stärke. 2005;57:8-15.

[30] Socrates G. Infrared and Raman characteristic group frequencies: tables and charts. 3rd ed: John Wiley & Sons; 2004.

[31] Hu XP, Li YL, Wang YZ. Synergistic effect of the charring agent on the thermal and flame retardant properties of polyethylene. Macromolecular materials and Engineering. 2004;289:208-12.

[32] Li Y, Li B, Dai J, Jia H, Gao S. Synergistic effects of lanthanum oxide on a novel intumescent flame retardant polypropylene system. Polymer Degradation and Stability. 2008;93:9-16.

[33] Setnescu R, Jipa S, Setnescu T, Kappel W, Kobayashi S, Osawa Z. IR and X-ray characterization of the ferromagnetic phase of pyrolysed polyacrylonitrile. Carbon. 1999;37:1-6.

Chapter 6: Foam-like Clay Aerogel Composites Prepared from Agar and Xanthan Gum

6.1 Introduction

Robust, foam-like and biodegradable polymer/clay aerogels have been successfully created by blending brittle clay aerogels with biopolymers, such as casein [1], alginate [2], pectin [3], to name a few.

Xanthan gum (XG) is a water soluble heteropolysaccharide produced by *Xanthomonas campestris*. It is used in a broad range of industries for applications such as emulsion stabilizer [4], rheological control agent [5] and controlled drug delivery purposes [6] among many others. The main-chain has analogies with the cellulose ((1→4)-β-glucan) with trisaccharide side-chains consisting of β-D-(1→2)-mannose attached to alternate glucose units in the main-chain [7, 8].

Agar consists of a mixture of agarose and agaropectin, whereby the former is the predominant component consisting of a linear polymer made up of D-galactose and 3,6-anhydro-L-galactopyranose, and the latter is a heterogeneous mixture of smaller molecules [9]; it has been used extensively as a gelling agent in the food industry due to its excellent ability to form hard gels at low concentrations.

Synergic effects between different polysaccharides have been reported, such as the improvements in viscosity in the agar-locust bean gum (LBG) mixtures [10]. Cases of tailored strength and texture of agar-LBG gels have also been studied based on changing the ratio of agar and LBG [11]. Xanthan gum solutions at low temperature (< 40 $^{\circ}$C) have been reported to show an ordered conformation and a tenuous gel strength [12]; the viscosity of xanthan gum/agar mixtures can be

adequately varied by changing their relative proportions [13]. Taking these facts into consideration, it is believed the xanthan gum gel strength can be improved by blending it with agar. Moreover, the presence of hydroxyl units along the backbone and branches can provide xanthan gum and agar the capability of forming hydrogel networks, which are necessary to achieve the desired robust foam-like aerogels.

In this chapter, foam-like aerogel composites based on xanthan gum and Na^+-MMT were produced. Additionally, a route to modify different properties by the addition of agar is investigated. The structure, mechanical properties, thermal stability, flammability and the ability to take up moisture of the different biopolymer/clay aerogels are herewith studied and discussed.

6.2 Experimental Section

6.2.1 Materials

All the information of materials used (xanthan gum, agar, glycerol and clay) are introduced in Chapter 3 (Section 3.1). All ingredients were used without further purification

6.2.2 Sample Preparation

The aerogels preparation has been proposed in section 3.2. In this chapter, glycerol, kept at 20% relative to the weight of polymers, was added to the polymer solution as a plasticizer. Biopolymers firstly were mixed with glycerol and then dissolved in water at 75 ^{o}C under mechanically stirring for 2 hours. The final polymer-clay precursor suspension were frozen in a solid CO_2/ethanol bath (-78 ^{o}C). The composition summary of the different prepared samples is shown in Table 6.1. Sample identification consists of the constituents used followed by its respective concentration percentage in aqueous solution, where X, A, and C stand for xanthan

gum, agar, and clay, respectively.

Table 6.1 Composition of aqueous suspensions for preparing the XG/agar/clay aerogels

Samples	Composition			
	Xanthan gum (wt %)	Agar (wt %)	Glycerol (w/w)	Na^+-MMT (wt %)
A2.5	0	2.5	20	0
A1.7C2.5	0	1.75	20	2.5
A5C2.5	0	5	20	2.5
A2.5C2.5	0	2.5	20	2.5
X2.5	2.5	0	20	0
X5	5	0	20	0
X2.5C2.5	2.5	0	20	2.5
X2.5A2.5C2.5	2.5	2.5	20	2.5
X2A0.5C2.5	2	0.5	20	2.5
X1.5A1C2.5	1.5	1	20	2.5
X1A1.5C2.5	1	1.5	20	2.5
X0.5A2C2.5	0.5	2	20	2.5

6.2.3 Characterization

The characterization details of aerogels such as SEM, compression test, moisture content, FTIR, TGA and cone calorimetry were presented in Chapter 3.

6.3 Results and Discussion

6.3.1 Microstructures and Mechanical Properties.

Agar/Clay Aerogels

Agar aqueous solution showed super high viscosity even though when a low content was used to prepare aerogels, which resulted in a difficult operation during the samples preparation process. Therefore, glycerol as a plasticizer was adopted to

improve the processing. The maximum concentration of agar used in this study was 5 wt%, as higher values made the solution too viscous to be adequately blended.

The compressive behavior of agar-clay aerogels are shown in Figure 6.1. All the results of compression tests are represented in Table 6.2.
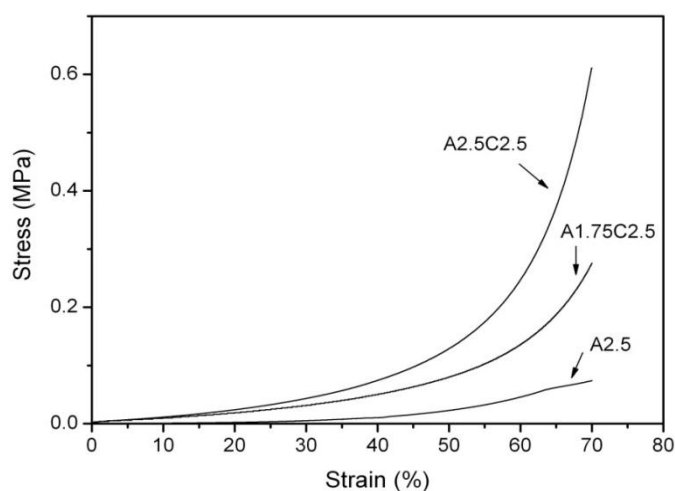
Figure 6.1 Compressive curves of agar-clay aerogels

Table 6.2 Compressive properties parameters of agar/clay aerogels

Samples	ρ_{app} (g/cm^3)	E (MPa)	E_s (MPa /(g cm^3))	$\sigma_{30\%}$ (kPa)	E_a at 30% ε (kJ m^{-3})
A2.5	0.046±0.001	0.01±<0.01	0.15±0.02	6±1	12.0±0.9
A1.75C2.5	0.046±0.001	0.49±0.10	10.53±2.26	28±2	37.6±6.1
A2.5C2.5	0.061±0.001	0.75±0.09	12.30±1.50	43±10	86.6±11.7
A5C2.5	0.120±0.004	5.21±1.75	44.45±9.45	442±62	354.9±60.4

By addition of 50% clay, the resultant aerogels (A2.5C2.5) exhibited much better mechanical performance than sample A2.5. This is due to the strong interaction between the agar molecules and clay surface. Clay played a role of reinforcement in the composites as has been shown in prior works [3, 14]. Fixing the amount of clay and changing the agar concentration, the mechanical properties of the resultant aerogels increased with their apparent densities. Sample A5C2.5 showed mechanical properties parameters with high standard deviation values due to the uneven polymer/clay distribution in the aerogel samples. High viscosity is initiated by high

agar loading (5 wt%) leading to an inhomogeneous precursor suspension.
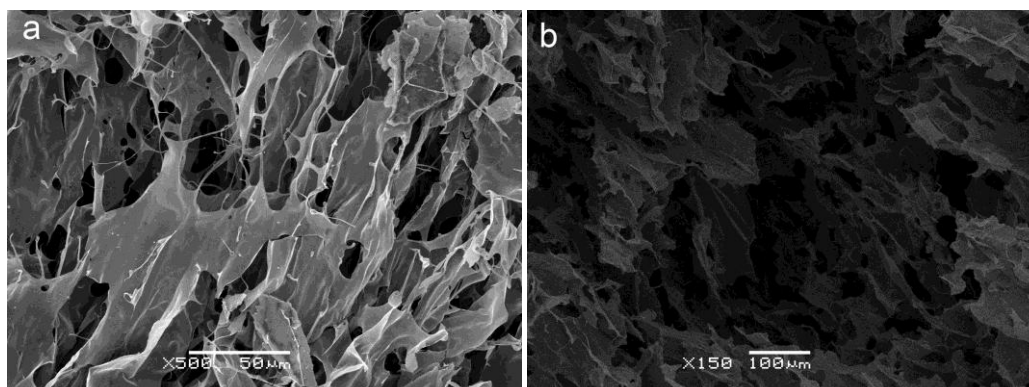
Figure 6.2 SEM photos of (a) A2.5 and (b) A2.5C2.5

In regard to the microstructure, clay addition did not bring in the expected layered architectures. Sheets composed of clay and agar were randomly distributed (Figure 6.2b). This is not only because agar has a super high viscosity, but also due to the fast gelation ability of agar. Strong agar gel is formed quickly at approximate 35 $^{\circ}$C [15] when its aqueous solution is being frozen. Both factors retard the growth of ice crystals, resulting in a random structure with much fewer layered patterns, as seen in sample A2.5C2.5.

Xanthan gum/Clay Aerogels

Aqueous solutions containing low quantity of xanthan gum also show high viscosities. However, XG aerogels displayed layered structure as seen in Figure 6.3. With the same polymer concentration, XG solution is much less viscous than the one of agar [13], making their structures distinct.

Neat XG aerogels exhibited different architectures depending on the amount of polymer. This can be seen with samples at 2.5 wt% concentration forming a layered structure aligned with the direction of the ice crystal growth (Figure 6.3a), and those at 5 wt% concentration resulting in a network-like structure with polymer fibrils connecting the holes (Figure 6.3b). This behavior is consistent with previous studies

[1, 2, 14], pointing at an obstruction of ice crystal growth rate caused by an increase of solution viscosity. In fact, aerogels prepared by freeze-drying can be considered as open channel foams with the holes being the space left by ice after sublimation.

The introduction of clay yielded a more regular layered structure due to the orientation of clay platelets along the ice boundaries. In comparison to pristine XG aerogels, the fractured surface of X2.5C2.5 (Figure 6.3c) was coarser, which was expected due the brittle nature of the clay layers.
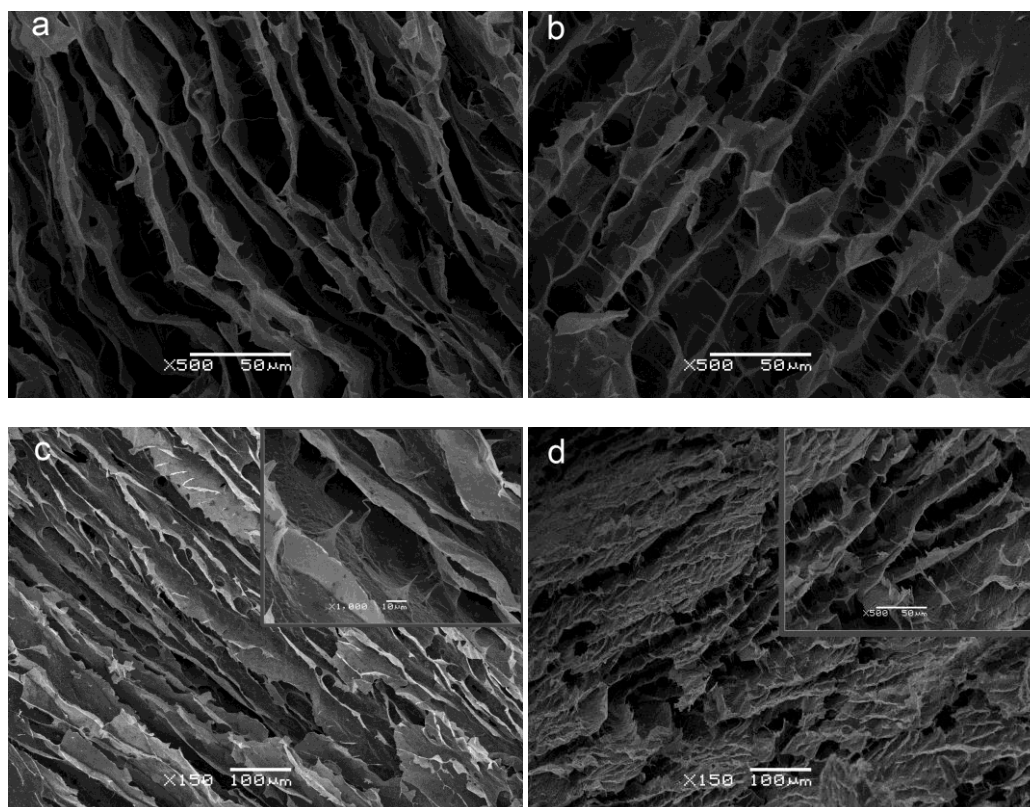
Figure 6.3 SEM micrographs of XG based aerogels. (a) X2.5; (b) X5; (c) X2.5C2.5; (d) X2.5A2.5C2.5. The details of structures are included in the inserts

The aerogels were afterward conducted with compression tests and the results are shown in Figure 6.4. Table 6.3 lists the densities and several relevant mechanical properties corresponding to the aerogels produced. With a low density of 0.044 g cm^{-3}, sample X2.5 had a Young's modulus (E) of 0.6 MPa, exhibiting comparably higher mechanical properties than other non-crosslinked bio-based aerogels of similar densities, such as casein [16] and pectin [3]. By incrementing the XG amount to 5%,

the modulus was significantly increased to 2.51 MPa and the yield stress (σ_y) dramatically improved 8-fold on the original strength of X2.5; but the density only slightly increased to 0.063 g cm^{-3}. This improvement in mechanical properties is possibly attributed to the polymer network structure presented in X5, in comparison to the one of X2.5. It provides a more efficient stress distribution, hence preventing the aerogel structure to undergo early failure.
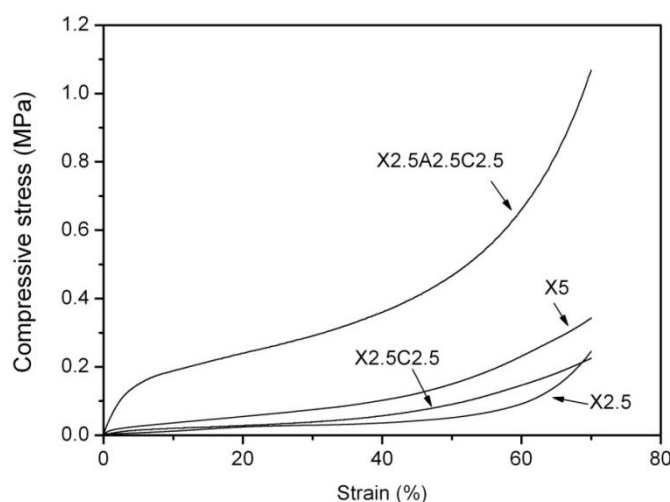
Figure 6.4 Compressive curves of XG based aerogels

Table 6.3 Compressive properties parameters of XG/clay aerogels

Samples	ρ_{app} (g cm^{-3})	E (MPa)	E_s (MPa/(g/cm^3))	σ_y (kPa)	$\sigma_{70\%}$ (MPa)	E_a at 70% ε (kJ m^{-3})
X2.5	0.044±0.003	0.60±0.11	13.5±1.9	2.5±0.5	0.26±0.13	33.7±8.4
X5	0.063±0.001	2.51±0.29	40.1±4.1	19.5±4.4	0.34±0.05	79.5±14.4
X2.5C2.5	0.056±0.001	0.94± 0.11	16.8±2.1	10.5±3.7	0.24±0.02	51.7±2.5
X2.5A2.5C2.5	0.101±0.001	4.77±0.66	47.3±6.3	83.4±10.6	1.0±0.01	236.3±33.9

Although clay has been widely used as reinforcement in polymer composites [17, 18], the incorporation of 2.5% clay into 2.5% XG solution did not provide any remarkable benefits in mechanical properties, or at least not as much as those achieved with X5 with similar density. This fact is attributed to the lack of polymer fibrils connecting clay layers in X2.5C2.5 composite, as seen in Figure 6.3c.

It has been widely studied that blending two different hydrocolloids may result in

a deep change in both the physical and the rheological properties of mixed solutions or gels [19]. XG was thought to be very compatible with agar due to their similar macromolecular chemical structures. Agar displays a linear macromolecular conformation, making its gel strength higher than the one of XG which exhibits a molecular structure with long branches [12]. Blending agar into XG/clay precursor suspension may be a way to improve the mechanical properties of XG based aerogels. When 2.5 wt% agar was added to X2.5C2.5 aerogel, the layered structure was maintained, however it showed a coarser fractured surface and more polymer interconnections appeared between clay layers (Figure 6.3d) due to the higher viscosity of precursor suspension in comparison to the initial X2.5C2.5. On the other hand, gelling chains of agar are interfered into ungelling ones of XG by hydrogen bonding in the aqueous solution. Thus, a synergistic effect between them brings well dispersed coupled networks for this binary system [19], which will influence the structures and properties of resultant aerogels.

Sample X2.5A2.5C2.5 exhibited superior mechanical properties as expected with a modulus of 4.77 MPa and apparent density of 0.101 g/cm^3. This result is comparable to cellulose nanofiber foams (0.103 g cm^{-3}, 5.31MPa) produced by the same freeze-drying way [20], and higher, for instance, than rigid polyurethane foams (0.19 g cm^{-3}, 4.7 MPa) [21], although the energy absorption and yield stress are lower. Moreover, compressive modulus values with very low standard deviations suggested that homogeneous structures were obtained within this composite. It also can be observed that there is no evidence of phase separation for agar and XG from SEM photos (Figure 6.3d). Therefore, blending agar into XG is a feasible way to improve the XG based aerogel properties.

Xanthan gum-agar/Clay Aerogels

The above findings demonstrate the important role of solution viscosity in the final aerogel structure. By keeping the amount of polymer constant, it is possible to tailor

the viscosity, the final structure and, ultimately, the mechanical properties of the aerogel by adjusting the ratio between XG and agar. To understand the effect of XG/agar ratio on the aerogel structure and mechanical performance, samples based on constant content of biopolymers and clay were investigated.

When the XG/agar ratio reached 60/40, polymer fibrils connecting clay layers became visible, as shown in the detail of Figure 6.5a. However, the typical layered structure of the clay aerogel became a honeycomb-like pattern (Figure 6.5c) when the ratio of agar in the mixture was increased further to 40/60. This phenomenon suggests that the microstructures of aerogels not only depend on the percentage of biopolymers, but also on their ratio in the mixture.
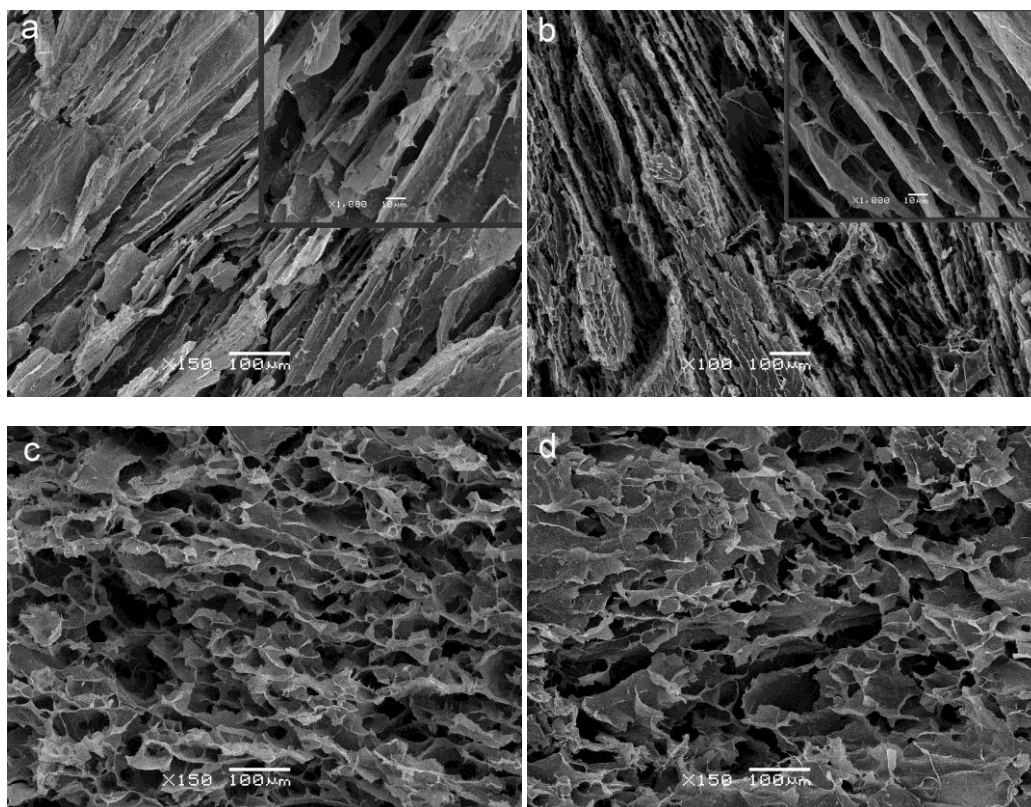
Figure 6.5 SEM micrographs of XG-agar/clay aerogels. (a) X2A0.5C2.5; (b) X1.5A1C2.5; (c) X1A1.5C2.5; (d) X0.5A2C2.5. The details of structures are included in the inserts

The compression curves are represented in Figure 6.6a. All the samples exhibited an elastic-plastic behavior of polymeric foams. The compressive parameters are summarized in the Table 6.4. Different XG/agar ratios resulted in similar densities,

but contrasting values of yield stress and specific modulus, which are represented in
Figure 6.6b and Figure 6.6c, respectively.
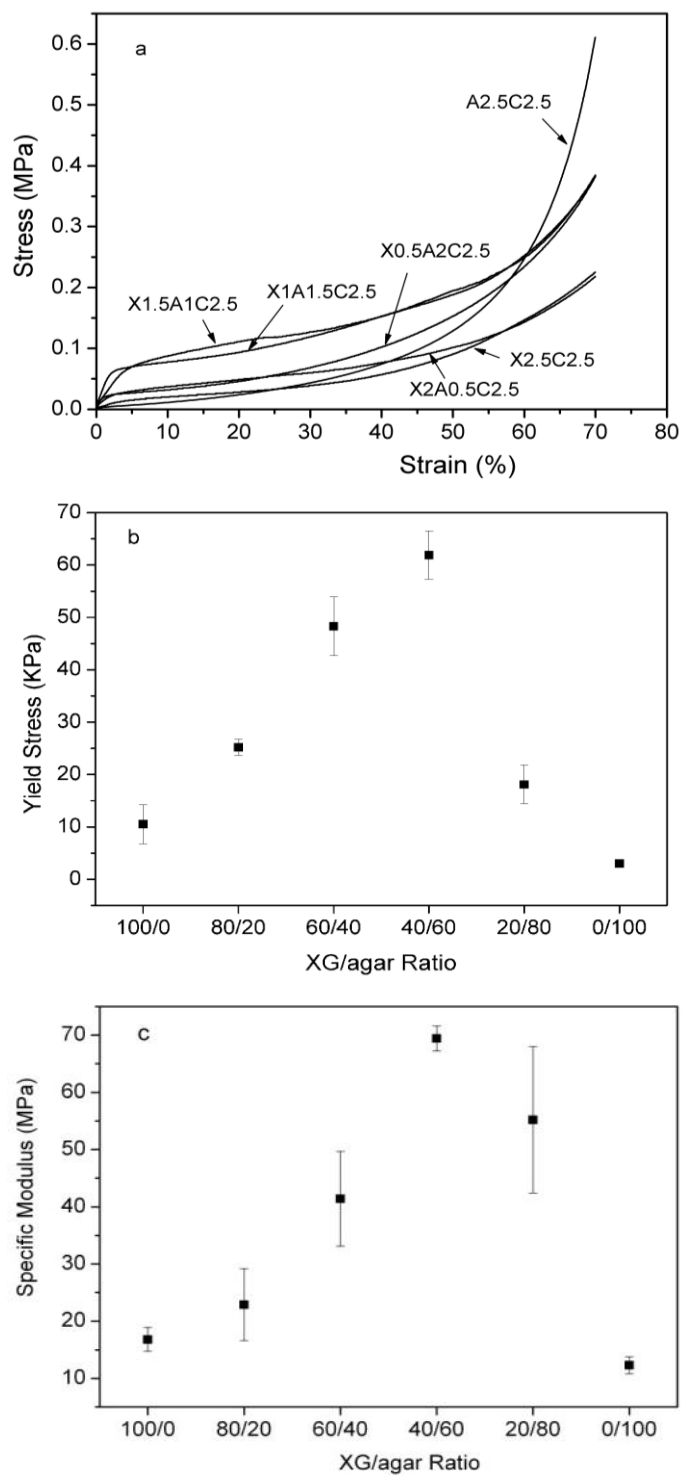
Figure 6.6 (a) Compressive stress-strain curves, (b) yield stress and (c) specific modulus of
XG/agar/clay aerogel composites based on constant polymer/clay ratio

117

In comparison to those containing only a single type of polymer, XG/agar aerogel composites displayed a significant improvement in mechanical properties, indicating a synergistic effect between both biopolymers. When the weight ratio of XG/agar was 40/60, the aerogel exhibited the highest specific modulus (E_s) and yield stress (σ_y). Moreover, this composition, along with the one with 60/40, absorbed the highest level of energy during the compression process. This behavior appears to be closely related to the microstructure changes within the aerogels, which shifted from a layered structure to a honeycomb-like network.

Having insufficient links in layered polymer/clay structures inevitably makes the aerogel brittle and susceptible of premature failure, which usually starts as localized fractures prior to propagating to a catastrophic collapse [22, 23], for this reason, a high density of interconnections is required to obtain a tough material. Accordingly, mechanical loads in honeycomb structures are borne by the cell walls, and in the case of compression forces, these undergo bending as the load increases [24]. These benefits can be seen on sample with 40/60 of XG/agar, which exhibits a higher load-bearing capacity when compared to clay lamellar structures without sufficient polymer linking such as the composition prepared by 60/40 of XG/agar. This behavior was also expected for composites with a higher XG/agar ratio, however at high proportions of agar (e.g. 20/80), a less regular structure and large voids appeared, which inevitably diminished the mechanical properties. Similar behaviour occurred in the agar-clay aerogels.

Table 6.4 Mechanical properties of XG/agar/clay aerogels

Samples	ρ_{app} (g cm^{-3})	E (MPa)	E_s (MPa cm^3/g)	σ_y (kPa)	$\sigma_{70\%}$ (MPa)	E_a at 70% ε (kJ m^{-3})
X2.5C2.5	0.056±0.001	0.94± 0.11	16.8±2.1	10.5±3.7	0.24±0.02	51.7±2.5
X2A0.5C2.5	0.061±0.002	1.39±0.34	22.9±6.3	25.2±1.5	0.20±0.02	55.3±7.9
X1.5A1C2.5	0.066±0.001	2.72±0.58	41.4±8.3	48.3±5.6	0.41±0.06	112.2±12.4
X1A1.5C2.5	0.059±0.001	4.12±0.13	69.4±2.2	61.9±4.6	0.36±0.03	97.9±14.7
X0.5A2C2.5	0.059±0.001	3.23±0.70	55.2±12.8	18.1±3.7	0.39±0.01	80.4±1.3
A2.5C2.5	0.061±0.001	0.75±0.09	12.3±1.5	3.0±0.5	0.75±0.19	86.6±11.7

6.3.2 Moisture Uptake
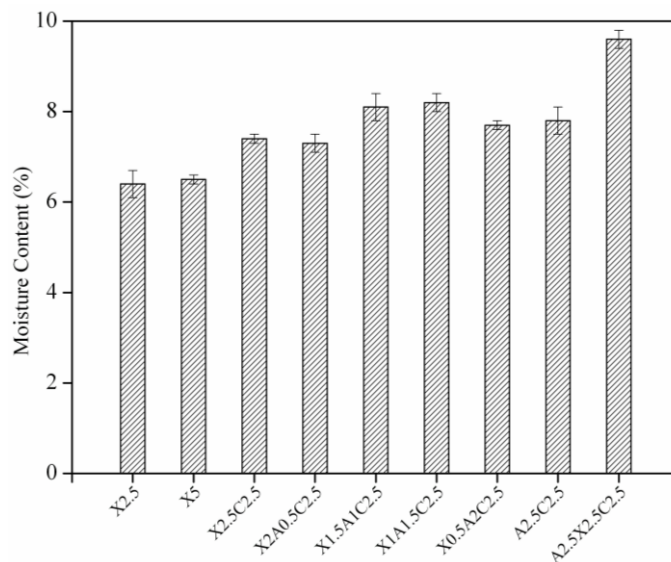
Figure 6.7 Moisture uptake of XG/agar/clay aerogels

The moisture content of aerogels is presented in Figure 6.7. As a general trend, lower moisture absorptions were observed in neat XG aerogels and higher water uptakes occurred in the aerogel composites. Due to its hydrophilic nature, the addition of clay increased the moisture uptake. The sample X2.5A2.5C2.5 had the highest resulting content, possibly due to the combined effect of XG/agar blending and the clay introduction. XG/agar/clay aerogel composites with constant polymer concentration maintained stable and similar levels of moisture regardless of the XG/agar ratio.

6.3.3 FTIR-ATR Spectra and Analysis

The FTIR-ATR spectra of neat XG aerogels and XG/agar/clay aerogel composites are showed in Figure 6.8. The broad band ranging from 3279 to 3346 cm^{-1} corresponded to the bonded O-H stretching and the one at ~1601 cm^{-1} is attributed to O-H bending vibrations, which is related to water crystallization [25]. This indicates that the moisture absorbed in the aerogels appears as a formation of bonded water. The bands at 2918 cm^{-1}, 1406 cm^{-1} and 1018 cm^{-1} were assigned to -CH$_2$ asymmetric stretch,

119

-CH$_2$ scissoring vibration and C-O-C symmetry stretch in the pyranose ring respectively [26]. The band at ~1719 cm^{-1} was regarded as acetyl C=O stretch vibration in the side-chain of XG [27], which was consistent with its absence in the agar spectra and its appearance in the XG/agar mixture. For the sample X2.5, the peak of C-O-C asymmetry stretch was shifted to lower wavenumbers with the addition of clay and a new peak appeared at 515 cm^{-1}, which was associated with Al-O bending in the clay. This suggests that the hydrogen bonding was formed between hydroxyl on the XG's pyranose ring and silanol on the clay surface. The carbonyl band at 1719 cm^{-1} also was displaced to lower wavelengths at 1714 cm^{-1} when the clay was added. However, this band was very weak and partially overlapped with the OH band appearing at ~1601 cm^{-1}. Overall, the shift of characteristic bands and changes in peak intensity reveal the presence of molecular interactions between biopolymers and clay as well as between agar and XG.
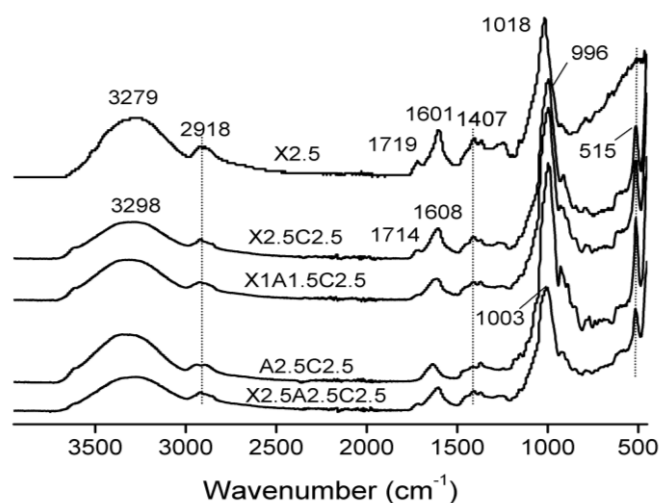
Figure 6.8 FTIR-ATR spectra for neat XG aerogel, XG/clay aerogel, XG/agar/clay aerogels and agar/clay aerogel

6.3.4 Thermal Stability

The thermal stability of aerogels was investigated by TGA analysis. For the sake of clarity, only some results are shown in the thermograms depicted in Figure 6.9. For

each sample, the corresponding onset decomposition temperature ($T_{d5\%}$), highest weight decomposition temperature (T_{dmax}), maximum weight loss rate (dW/dT_{max}) and percentage of residue (W_R) are listed in Table 6.5. $T_{d5\%}$ was given as the temperature at which 5% weight beyond total loss of water occurred. The trends of $T_{d\ 5\%}$ were used to evaluate the thermal stability of bio-based aerogels.
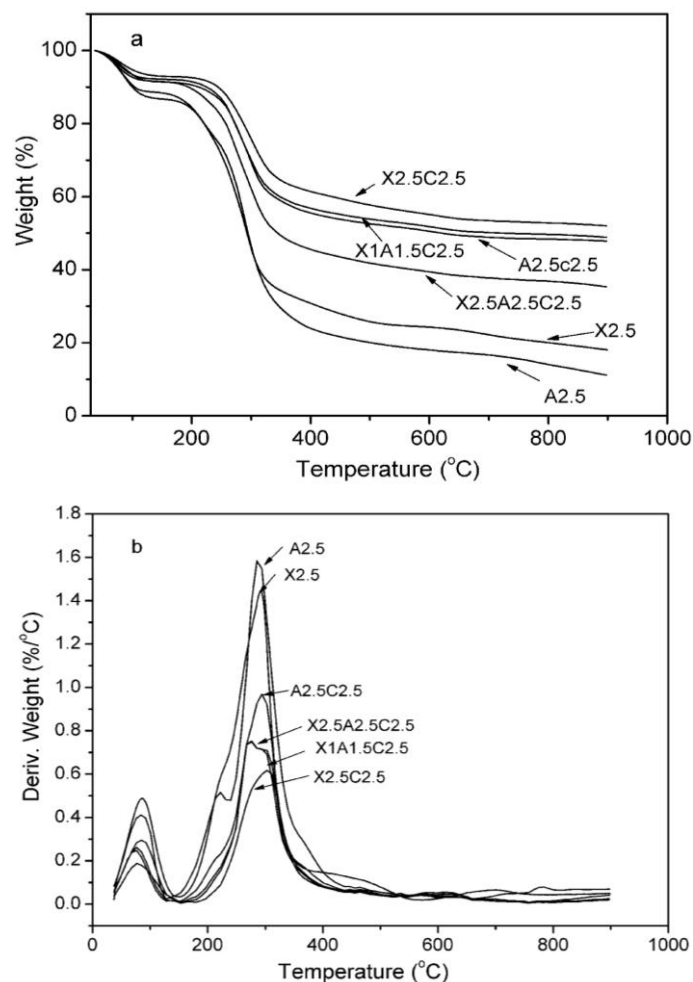
Figure 6.9 TGA (a) and DTG (b) curves of XG/agar/clay aerogel composites

These bio-based aerogels showed similar decomposition patterns with two main stages: bound water loss and aerogels matrix decomposition (Figure 6.9a). From the derivative weight loss rate (Figure 6.9b), it could be observed that adsorbed water was totally removed at 150 ^{o}C, which was coincident with previous observations performed on other bio-based aerogels [28]. The comparison of TGA curves corresponding to the raw materials allowed to determine that added glycerol was

eliminated between 180 and 250 ^{o}C, which overlaps with the onset decomposition temperatures of XG and agar occurring at ~235 ^{o}C and ~240 ^{o}C respectively.

The addition of 50 % clay increased $T_{d5\%}$ by almost 50 ^{o}C and T_{dmax} by nearly 10 ^{o}C. This effect is attributed to the thermal insulation and mass transport barrier created by the clay. On the contrary, the addition of 1/3 agar to X2.5C2.5 had a negative effect on the thermal stability, possibly related to the resulting denser and more compact structure of the aerogel, considering that a reduced porosity implies an increase in the thermal conductivity. These morphological differences are patent in the SEM analysis discussed earlier, whereby X2.5C2.5 (Fig. 3b) and A2.5C2.5 (Fig. 2b) exhibit a looser structure while XG/agar/clay composites have a denser architecture.

The maximum weight loss rate is closely related to the thermal characteristics of the polymer used. A2.5 gave the highest maximum weight loss rate and this value steeply decreased from 1.58 to 0.97 %/^{o}C when clay was added; a similar effect was observed on X2.5. This improvement is supported by the formation of an inorganic layer on the sample surface during the increasing thermal load inflicted by the TGA test. The maximum weight loss rates of samples blended with agar were in the range of 0.62 to 0.97 %/^{o}C. These results are consistent with the XG/agar ratios, and sit on the average range of XG/clay and agar/clay samples; they also indicate that there is no chemical reaction occurring when blending XG with agar, as corroborated with the FTIR results discussed earlier.

Table 6.5 Thermal characteristics of XG/agar/clay aerogel composites

Samples	$T_{d5\%}$ ($^{\circ}$C)	T_{dmax} (^{o}C)	dW/dT_{max} (%/^{o}C)	W_R (%)
X2.5	209.8	292.5	1.44	18.1
X5	204.8	294	1.26	17
X2.5C2.5	255.1	302.9	0.62	52
X2A0.5C2.5	244	301.9	0.64	48.3
X1A1.5C2.5	245.4	276.3	0.75	48.9
X0.5A2C2.5	242.3	268	0.84	47.3
A2.5C2.5	245.7	294.1	0.97	47.9
A2.5	201.2	285.3	1.58	11.2
X2.5A2.5C2.5	222.4	276.3	0.75	35.3

6.3.5 Combustion Behaviour

The combustion behaviour of the different XG/clay aerogels was evaluated in a cone calorimeter. As the TGA tests proved that blending agar into XG diminishes the thermal stability, XG/agar/clay aerogels were not included in this section.
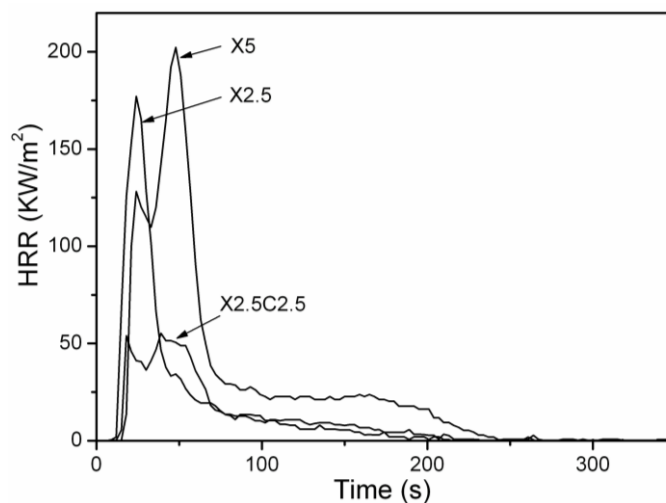
Figure 6.10 Heat release rate of XG aerogels and XG/clay aerogels
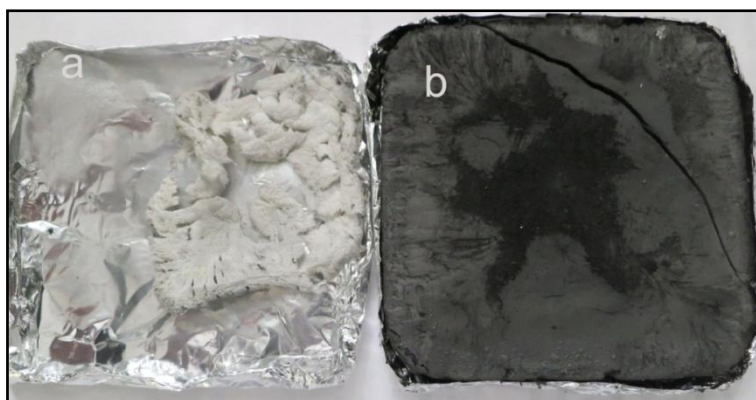
Figure 6.11 Char photos after cone calorimetry tests (a) X2.5; (b) X2.5C2.5

The detailed flammability data of XG/clay aerogels are presented in Table 6.6. The heat released from the materials undergoing burning was considered as the most important parameter that characterizes its fire hazard [29]; accordingly this was analyzed quantitatively on a bench scale [30] and is illustrated in Figure 6.10 in terms of heat released rate (HRR) of XG/clay aerogels as a function of burning time. Also, the sample char obtained after tests were shown in Figure 6.11.

All samples displayed different behavioral patterns, being the one of XG/clay aerogels of particular interest due to its three well defined combustion stages [31]: first a vigorous initiation burning episode followed by a relatively constant HRR phase and a final long flame region gradually disappearing. In comparison with solid polymers, foams burn more quickly, which is explained by the lower thermal conductivity but much higher specific surface area of foams, promoting higher PHRR and lower ignition time [32]. The sample X2.5 began to burn quickly and vigorously, resulting in a low TTPHRR (24s) and high PHRR (177.1 kW/m^2). Increasing polymer amount in XG aerogels generally prolonged the TTPHRR and decreased FGR, however X5, which had higher density and mass, burned more intensively and for a longer period of time with PHRR and THR values increasing to 202.1 kW/m^2 and 7.8 MJ/m^2 respectively. Indeed the effects of density and mass experienced with the above experiment strongly suggests to introduce the terms 'normalized PHRR' (NPHRR) and 'normalized THR' (NTHR) as relevant parameters in the overall combustion behavior, which refer to the ratio of PHRR and THR to the polymer mass in the samples, respectively. Once taken this into consideration, it was observed that both agreed well with the tendency of TTPHRR and FGR (see Table 6.6), whereby flame retardancy is improved due to the microstructure changes referred to in the previous section. Sample X5, which had a continuous network structure and by that a higher thermal conductivity, showed a two-peak signal (Figure 6.10). These findings are consistent with a previous study on flammability of wheat gluten foams and which concluded to be caused by a temporary char layer formed on the specimen surface [31].

The addition of clay decreased all the flammability parameters expressed in terms of heat release. Particularly, the normalized PHRR was reduced to 26.4 kW/m^{2}g, which was lower than those found in neat XG aerogels. This indicates unambiguously that clay plays an important role in reducing the flammability of the systems. It is worth noting that the combustion plot corresponding to X2.5C2.5 flattens out prior to completing the test due to the enrichment of inorganic clay layers on the surface during combustion, which protects the bio-polymer beneath the surface.

Overall, it should be pointed out that the XG aerogels showed lower PHRR and THR than EPS foams [2], PU foams [33] and wheat gluten foams [31] prepared by the same freeze-drying process.

Table 6.6 Burning parameters of XG aerogels and XG/clay aerogel composites

Samples	Mass (g)	TTPHRR (s)	PHRR (kW/m^2)	FGR (kW/m^2 s)	THR (MJ/m^2)	W_R (%)	NPHRR (kW/m^2 g)	NTHR (MJ/m^2 g)
XG2.5	2.8	24	177.1	7.4	4.8	5.7	63.2	1.7
XG5	6.5	48	202.3	4.5	7.8	5.1	31.1	1.2
XG2.5C2.5	4.2	39	55.2	1.4	3.3	45.2	26.4	1.6

6.4 Conclusions

The preparation of foam-like aerogels based on bio-based, renewable xanthan gum and clay were demonstrated using an environmentally friendly freeze-drying process. A novel approach consisting in adding the bio-based polysaccharide agar into the preparation mixture was used to improve the aerogel properties. FTIR characterization showed that xanthan gum and agar were very miscible and that intermolecular interaction was achieved. Different microstructure patterns were visible in the SEM analysis, and these were found to be closely related to the viscosity of the precursor solution. The samples containing a higher concentration of agar relative to XG underwent a significant structural change going from typical layered to a honeycomb-like architecture. The synergistic effect between the two polysaccharides made the XG/agar/clay aerogels display a significant improvement in mechanical properties compared with those containing a single biopolymer. Changing the XG/agar ratio allowed to modify the mechanical properties with only minor repercussions in the density. The highest specific modulus and yield stress were obtained with the 40/60 XG/agar blend, and the highest level of energy absorbed was achieved with the 60/40 of XG/agar sample. The addition of 2.5% agar into X2.5C2.5 increased the modulus to 4.77MPa, a value similar to those of cellulose nanofiber

foams and rigid polyurethane of similar densities. Thermogravimetric analysis (TGA) revealed that clay enhanced the thermal stability of aerogels, being in contrast with the blends of two biopolymers, which exhibited poor results. The cone calorimeter test showed the xanthan gum/clay aerogels possessed lower flammability than EPS foams, PU foams, wheat gluten foams and PVOH/clay aerogels. Clay served as heat and mass transport barriers and significantly improved the flame retardancy.

References

[1] Pojanavaraphan T, Magaraphan R, Chiou B-S, Schiraldi DA. Development of biodegradable foamlike materials based on casein and sodium montmorillonite clay. Biomacromolecules. 2010;11:2640-6.

[2] Chen H-B, Wang Y-Z, Sánchez-Soto M, Schiraldi DA. Low flammability, foam-like materials based on ammonium alginate and sodium montmorillonite clay. Polymer. 2012;53:5825-31.

[3] Chen H-B, Chiou B-S, Wang Y-Z, Schiraldi DA. Biodegradable Pectin/Clay Aerogels. ACS applied materials & interfaces. 2013;5:1715-21.

[4] Garti N. Hydrocolloids as emulsifying agents for oil-in-water emulsions. Journal of Dispersion Science and Technology. 1999;20:327-55.

[5] Rosalam S, England R. Review of xanthan gum production from unmodified starches by Xanthomonas comprestris. Enzyme and Microbial Technology. 2006;39:197-207.

[6] Santos H, Veiga F, Pina ME, Sousa JJ. Compaction, compression and drug release properties of diclofenac sodium and ibuprofen pellets comprising xanthan gum as a sustained release agent. International journal of pharmaceutics. 2005;295:15-27.

[7] Jansson P-e, Kenne L, Lindberg B. Structure of the extracellular polysaccharide from Xanthomonas campestris. Carbohydrate Research. 1975;45:275-82.

[8] Melton LD, Mindt L, Rees DA. Covalent structure of the extracellular polysaccharide from Xanthomonas campestris: evidence from partial hydrolysis studies. Carbohydrate Research. 1976;46:245-57.

[9] Armisen R. Agar. Thickening and gelling agents for food: Springer; 1997. p. 1-21.

[10] Garcia-Ochoa F, Santos V, Casas J, Gomez E. Xanthan gum: production, recovery, and properties. Biotechnology advances. 2000;18:549-79.

[11] Armisen R, Galatas F. Production, properties and uses of agar. FAO Fisheries Technical Paper. 1987:pp. 1-57.

[12] Fishman ML, Qi PX, Wicker L. Advances in biopolymers: ACS Publications; 2006.

[13] Jain-Raina R, Babbar S. Evaluation of blends of alternative gelling agents with agar and development of xanthagar, a gelling mix, suitable for plant tissue culture media. Asian J Biotechnol. 2011;3:153-64.

[14] Pojanavaraphan T, Liu L, Ceylan D, Okay O, Magaraphan R, Schiraldi DA. Solution Cross-Linked Natural Rubber (NR)/Clay Aerogel Composites. Macromolecules. 2011;44:923-31.

[15] Labropoulos KC, Rangarajan S, Niesz DE, Danforth SC. Dynamic rheology of agar gel based aqueous binders. Journal of the American Ceramic Society. 2001;84:1217-24.

[16] MD Gawryla M Nezamzadeh, DA Schiraldi. Foam-like materials produced from abundant natural resources. Green Chemistry. 2008;10:1078-81.

[17] Lan T, Pinnavaia TJ. Clay-reinforced epoxy nanocomposites. Chemistry of Materials. 1994;6:2216-9.

[18] Gopakumar T, Lee J, Kontopoulou M, Parent J. Influence of clay exfoliation on the physical properties of montmorillonite/polyethylene composites. Polymer. 2002;43:5483-91.

[19] The DP, Debeaufort F, Voilley A, Luu D. Biopolymer interactions affect the functional properties of edible films based on agar, cassava starch and arabinoxylan blends. Journal of Food Engineering. 2009;90:548-58.

[20] Sehaqui H, Salajkova M, Zhou Q, Berglund LA. Mechanical performance tailoring of tough ultra-high porosity foams prepared from cellulose I nanofiber suspensions. Soft Matter. 2010;6:1824-32.

[21] Calvert KL, Trumble KP, Webster TJ, Kirkpatrick LA. Characterization of commercial rigid polyurethane foams used as bone analogs for implant testing. Journal of Materials Science: Materials in Medicine. 2010;21:1453-61.

[22] Johnson JR, III, Spikowski J, Schiraldi DA. Mineralization of Clay/Polymer Aerogels: A Bioinspired Approach to Composite Reinforcement. Acs Applied Materials & Interfaces. 2009;1:1305-9.

[23] Finlay K, Gawryla MD, Schiraldi DA. Biologically based fiber-reinforced/clay aerogel composites. Industrial & Engineering Chemistry Research. 2008;47:615-9.

[24] Gibson LJ, Ashby MF. Cellular solids: structure and properties. 2nd ed: Cambridge university press; 1999.

[25] Mayo DW, Miller FA, Hannah RW. Course notes on the interpretation of infrared and Raman spectra: John Wiley & Sons; 2004.

[26] Pandey JK, Singh RP. Green Nanocomposites from Renewable Resources: Effect of Plasticizer on the Structure and Material Properties of Clay-filled Starch. Starch-Stärke. 2005;57:8-15.

[27] Socrates G, Socrates G. Infrared and Raman characteristic group frequencies: tables and charts. Third ed: Wiley Chichester; 2001.

[28] Heath L, Zhu L, Thielemans W. Chitin Nanowhisker Aerogels. Chemsuschem. 2013;6:537-44.

[29] Janssens ML. Measuring rate of heat release by oxygen consumption. Fire Technology. 1991;27:234-49.

[30] Morgan AB, Bundy M. Cone calorimeter analysis of UL-94 V-rated plastics. Fire and materials. 2007;31:257-83.

[31] Blomfeldt TOJ, Nilsson F, Holgate T, Xu J, Johansson E, Hedenqvist MS. Thermal Conductivity and Combustion Properties of Wheat Gluten Foams. ACS applied materials & interfaces. 2012;4:1629-35.

[32] Realinho V, Haurie L, Antunes M, Velasco JI. Thermal stability and fire

behaviour of flame retardant high density rigid foams based on hydromagnesite-filled polypropylene composites. Composites Part B: Engineering. 2014;58:553-8.

[33] Checchin M, Cecchini C, Cellarosi B, Sam F. Use of cone calorimeter for evaluating fire performances of polyurethane foams. Polymer Degradation and Stability. 1999;64:573-6.

Chapter 7: Bio-aerogels based on Arabic Gum and Clay

7.1 Introduction

Increasing concern on environmental protecting requires expanding the usage of biopolymers derived from natural sources that may replace petroleum-based polymers in future. Foam-like aerogels based on biopolymers allow a way to explore the application of abundant biopolymers that can be widely obtained from plants, animals or waste products [1].

Arabic gum (AG) is exuded from the gum tree, consisting of a mixture of high molecular weight polysaccharide (major component) and hydroxyproline rich glycoprotein (minor component) [2]. The main structural feature of the major component is a backbone of β-galactopyranose units with 1,3 bonds and side chains of 1,6-linked galactopyranose units terminating in β-D-glucuronopyranose and 4-O-methyl-β-D glucuronopyranose [3]. Due to its unique emulsification, film-forming, and encapsulation properties, AG is extensively used in industry, such as food [4], paper [5] and pharmacy [6].

In this chapter, bio-based AG was used to prepared light-weight aerogels using a freeze-drying way. Sodium montmorillonite (Na^+-MMT) was added to improve the properties of bio-based aerogels.

7.2 Experimental Section

All the information of raw materials (AG and Na^+-MMT) was included in Chapter 3.1.

Aerogels preparation just followed the method introduced in chapter 3.2 and the definition of samples was AG or clay used followed by their respective concentration in precursor suspensions. The microstructures, porosities, mechanical properties, thermal stability and fire behaviour have been investigated according to the description in chapter 3.3.

7.3 Results and Discussion

7.3.1 Density and Porosity

Theoretic solid densities (ρ_{ts}) of the AG-clay composite aerogels were calculated according to equation 7.1:

$$\rho_{ts} = \frac{1}{w_{AG}/\rho_{AG} + w_C/\rho_C} \tag{7.1}$$

Where, w_{AG} and w_C are the mass fractions of AG and clay in the dry aerogels, respectively. ρ_{AG} and ρ_C are the densities of AG and clay, respectively. Clay density (2.6 g/cm^3) was taken from the supplier. The experimental solid densities of pure AG aerogels were equal to the one of AG solid powder, which was measured using Helium Pycnometry (1.302 g/cm^3). Porosity, defined as the volume fraction of voids, was calculated according to method discussed in chapter 3.3. The results are summarized in Table 7.1.

Slight differences were observed between experimental and theoretical apparent densities of AG-clay aerogels, indicating that the pores in the aerogel were mainly open. All the tested samples exhibited high porosities of around 90%. For neat AG aerogels, increasing AG content from 7.5 to 15 wt%, the porosity reduced by 5.7%. Similar tendency were found in AG-clay aerogel composites. Generally, the higher the solid content resulted in a lower porosity.

Table 7.1 Density and porosity of AG/clay aerogels

Samples	ρ_{app} (g/cm^3)	ρ_{es} (g/cm^3)	ρ_{ts} (g/cm^3)	Porosity (%)
AG5C5	0.088±0.001	1.799±0.003	1.652	95.1±<0.1
AG7.5C5	0.115±0.001	2.079±0.004	2.065	94.4±<0.1
AG10C5	0.149±0.013	2.196±0.001	2.476	93.2±0.1
AG7.5	0.085±0.001	1.302±0.002	1.302	93.5±<0.1
AG10	0.109±0.018	1.302±0.002	1.302	91.6±1.4
AG15	0.154±0.009	1.302±0.003	1.302	88.2±0.1

7.3.2 Morphology

The morphological microstructures of AG/clay aerogels are shown in Figure 7.1. Sample AG7.5 exhibited a layered structure without polymer connection between layers (Figure 7.1a). When the content of AG was increased to 15 wt%, the layers increased in thickness. But there was no obvious change in the density of links between the layers (Figure 7.1b). Comparing with other biopolymer aerogels, for example, pectin aerogel [7] or the one based on xanthan gum studied in chapter 6, AG aerogels did not display network structures. One of reason is that AG solution keeps a low value of viscosity even when a high concentration is adopted. For instance, 30% AG solutions have a lower viscosity than 1% xanthan gum and sodium carboxymethylcellulose at low shear rates [8]. The second factor is that both AG and clay are negatively charged on the surfaces, causing repulsion between them.

When 5 wt% clay was added into AG7.5, viscosity of corresponding precursor suspension increased. The ice front growth was retarded by the fluid viscosity and secondary crystallization occurred [9], resulting in a rough fracture surface (Figure 7.1c). Increasing the AG concentration in the precursor suspensions of AG-clay aerogels to 15 wt%, a continuous "house of cards" structure appeared due to the further increment of viscosity.

These varieties of microstructures within aerogels are responsible of the mechanical properties changes discussed in the following section.
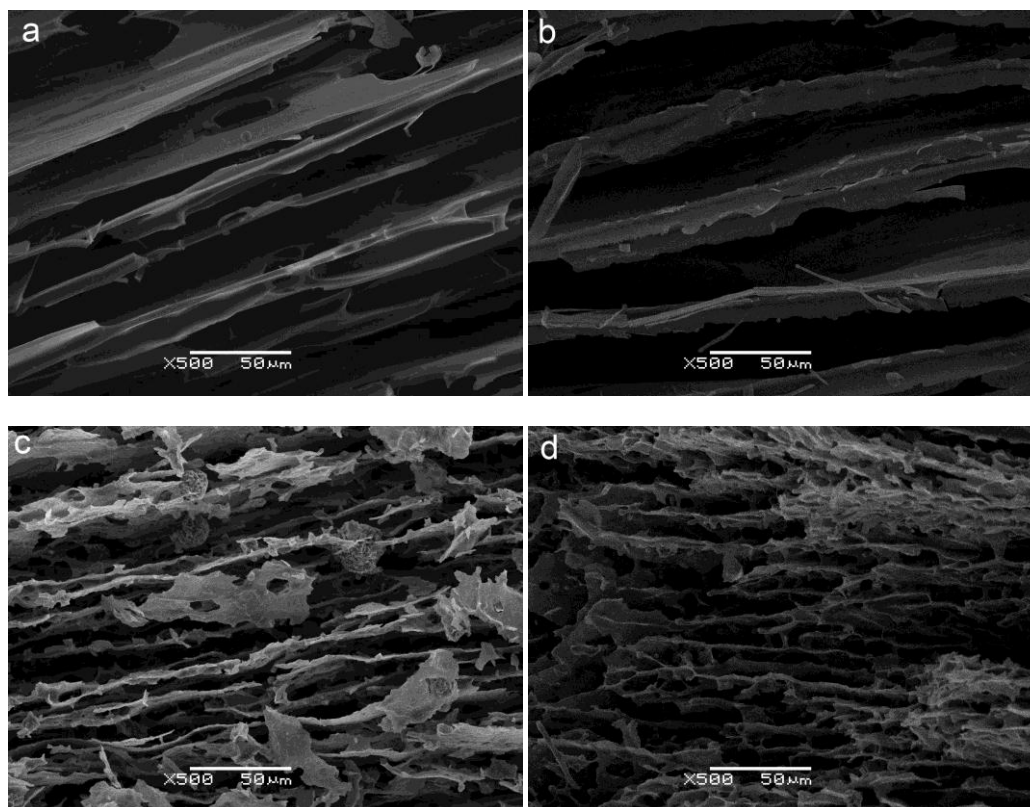
Figure 7.1 SEM photos of AG/clay aerogels: (a) AG7.5; (b) AG15; (c) AG7.5C5; (d) AG15C5

7.3.3 Mechanical Properties

The compressive stress-strain curves of the AG and AG/clay aerogels are shown in Figure 7.2a. Generally, these samples showed the similar compressive behavior than the biopolymers/clay aerogels discussed in previous chapters. Compressive mechanical properties parameters, such as compressive modulus (E), specific compressive modulus (E_s), compressive stress at 70% strain (σ_{max}), and energy absorbed (E_a) are listed in Table 7.2. Several finding should be mentioned for AG/clay aerogels. Firstly, sample AG5 was too brittle to be tested. Secondly, the plateau stage of stress was not observed in sample AG15. This is due to the high AG concentration used and resultant high apparent density. Thirdly, rough trace in the compressive curve of sample AG15C5 indicated structure defects within the aerogel.
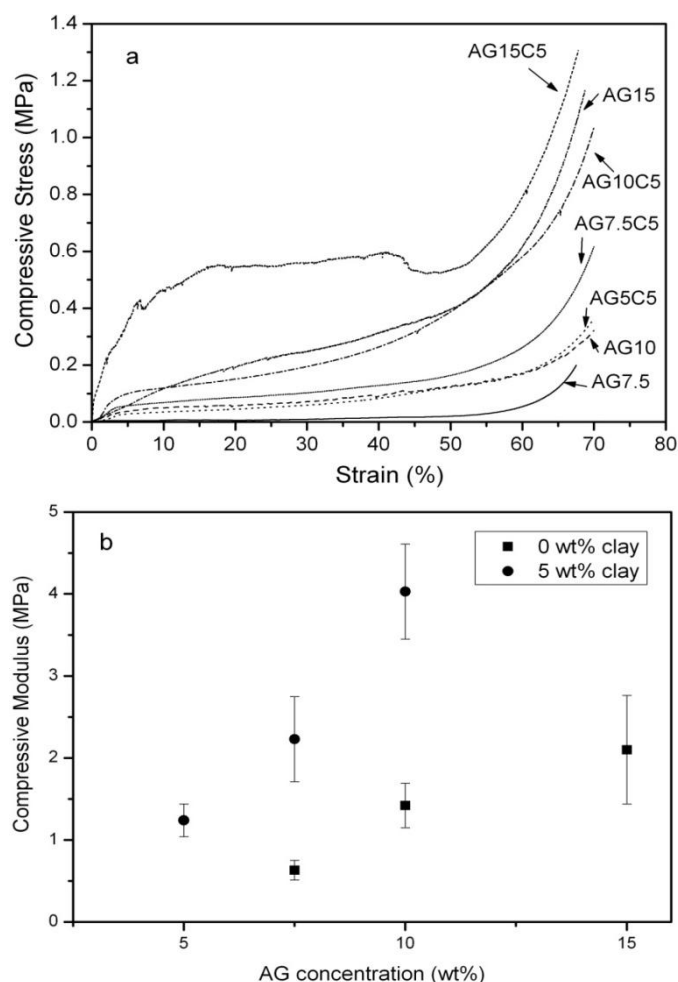
Figure 7.2 (a) Compressive curves of AG/clay aerogels; (b) The AG concentration effect on compressive modulus of aerogels

Table 7.2 Compressive mechanical properties of AG/clay aerogels

Samples	ρ_{app} (g/cm^3)	E (Mpa)	$\sigma_{70\%}$ (Mpa)	E_s (Mpa/g cm^{-3})	E_a at 70% ε (kJ cm^{-3})
AG7.5	0.085±0.001	0.63±0.11	0.11±0.06	7.47±2.11	11.9±2.2
AG10	0.109±0.018	1.42±0.27	0.26±0.08	10.59±2.13	48.8±11.9
AG15	0.154±0.009	2.10±0.66	1.08±0.14	10.86±2.86	240.3±44.9
AG5C5	0.088±0.001	1.24±0.19	0.35±0.01	13.91±1.99	44.1±3.3
AG7.5C5	0.115±0.001	2.26±0.12	0.40±0.05	19.43±1.12	62.3±14.9
AG10C5	0.149±0.013	4.03±0.57	0.60±0.19	29.93±3.44	70.5±1.1
AG15C5	0.180±0.002	25.76±4.20	1.29±0.03	142.71±22.94	314.8±20.6

The compressive modulus of aerogels increased with the AG or clay content, as observed in Figure 7.2b. Sample AG15 had a modulus of 2.10 MPa, which was much higher than the one of AG7.5 (0.63 MPa). However, the specific compressive

modulus of pure AG aerogels did not significantly increase with the AG content. This suggested that the neat AG aerogels properties were only dependent on their apparent densities.

When 5 wt% clay was added, the specific modulus of AG7.5C5 significantly increased by 1.6 times compared with AG7.5 (see Table 7.2). This result was consistent with the finding of prior works on biopolymer-clay aerogel composites [7, 10]. Compared with AG7.5C5, sample AG15C5 showed a layered structure with denser polymer links (Figure 7.1d), thus it exhibited much higher mechanical performance. However, catastrophic fracture occurred in sample AG15C5 when it was compressed. The reason is that both AG and clay platelets surface are negatively charged, which causes a weak adhesion between them.

Increasing the AG content increased the apparent density and hereby reinforced the mechanical properties of the aerogels. The power-law developed by Gibson and Ashby [11] for cellular solids was used to analyze mechanical properties, as shown in equation 7.2.

$$K/K_S \propto C\left(\rho/\rho_s\right)^n \qquad\qquad 7.2$$

Where K means a mechanical property of foams, K_S is the property of the corresponding fully solid material. ρ and ρ_s are the apparent density and solid density, respectively; ρ_s herein are thought to be equal to theoretical solid density. C and n are structural parameters [11, 12]. In present work, exponent values for modulus and ultimate strength of pure AG aerogels were 1.95 and 3.84, respectively. However, for AG/clay aerogels composites of which the relative density changed, the values of n were 3.28 and 1.46 for modulus and ultimate strength, respectively.

The exponent values changed with the material structures. For open-cell foams, the exponent is expected to be 2 [11]. Wood has exponent of 3 in the radial direction due to anisotropy of the structure [11] and silica aerogels show a value in the range of 2.6-3.8 because of different samples preparation methods [13]. For pure AG aerogels,

the exponent for modulus was 1.95 (Figure 7.3), which was consistant with the open structure generated in the aerogels. This value increased to 3.28 with the addition of clay, similar to the value found in PVOH-clay aerogels (3.74) [14]. It is attributed to the reinforcing effect of clay and the more anisotropic structures induced by clay aggregation in the composites.
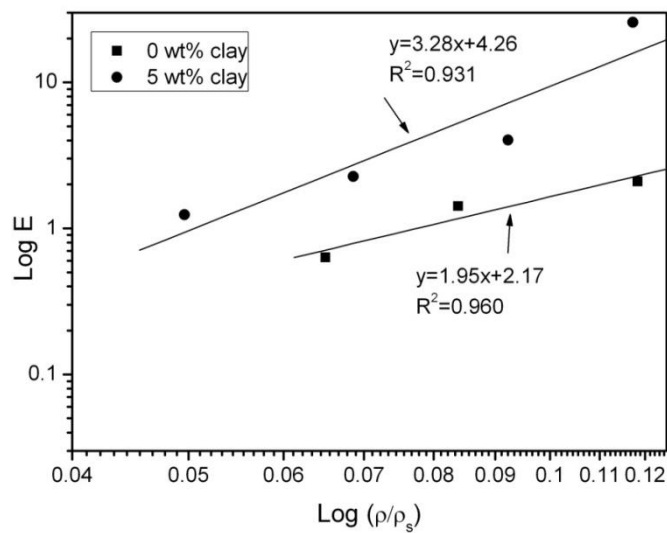
Figure 7.3 Compressive modulus of the AG/clay aerogels as function of relative density

7.3.3 Thermal Stability

Thermal stability of AG/clay aerogels were studied by thermogravimetric analysis under dry nitrogen atmosphere. The weight loss curves are shown in Figure 7.4. The decomposition of aerogels can be divided in three stages. Firstly, the moisture in AG aerogels was evaporated under the thermal loading up to 150 ^{o}C. Then dehydration and decarboxylation reaction of AG occurred when the temperature was over 250°C [15]. AG was quickly decomposed during this step. Finally, the char left after the second stage was oxidized (>330 ^{o}C) with the increased temperature and the aromatic components were formed. $T_{d5\%}$ is defined as the temperature at which 5% weight after 150 ^{o}C (dW/dT≈0) was recorded to investigate the thermal stability of the bio-based aerogels. Table 7.3 summarizes decomposition temperature at 5% weight loss ($T_{d\,5\%}$),

temperature at maximum weight loss rate ($T_{d\ max}$), maximum mass decomposition rate (dW/dT_{max}) and residue amount (W_R).
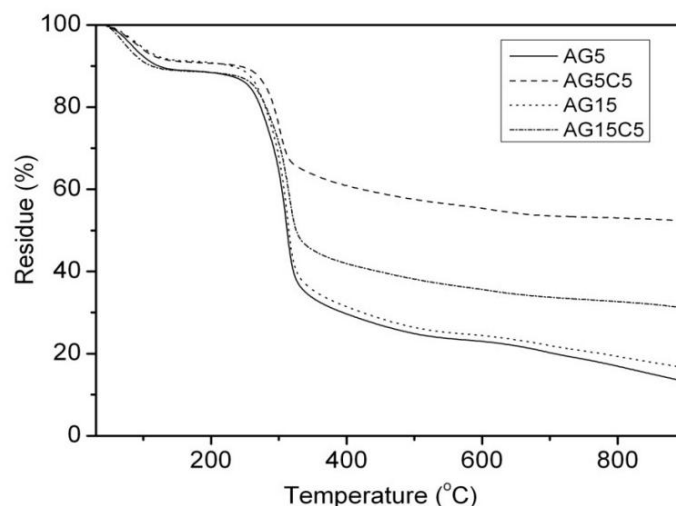
Figure 7.4 TGA weight loss curves of AG/clay aerogels

Table 7.3 Parameters for thermal stability of AG/clay aerogels

Samples	$T_{d\ 5\%}$ (^{o}C)	$T_{d\ max}$ (^{o}C)	dW/dT_{max} (%/^{o}C)	W_R (%)
AG5	258.6	310.4	1.41	13.2
AG5C5	274.5	299.0	0.69	52.3
AG15	261.2	311.7	1.47	16.5
AG15C5	267.7	308.3	1.09	38.2

In comparison to sample AG5, it can be observed that AG5C5 presented higher $T_{d\ 5\%}$ (275 ^{o}C) and much lower maximum mass decomposition rate (0.7 %/^{o}C). The residue amount was obviously increased by adding inorganic clay. For sample AG15C5, $T_{d\ 5\%}$ increased by nearly 7 ^{o}C and maximum mass decomposition rate decreased 0.4 %/^{o}C respectively comparing to AG15. The differences in thermal stability of samples AG5C5 and AG15C5 were attributed to the relative content of clay in the composites. Higher clay content led to lower degradation rate and higher initial decomposition temperature. These findings were consistent with the previous works in which clay was used to improve the thermal stability of bio-based aerogels. However, clay addition caused a lower $T_{d\ max}$, possibly related to the higher thermal conductivity resulting from denser and more compact structure of the aerogel.

7.3.4 Combustion Behaviour

The combustion behaviour of the aerogels was investigated using a cone calorimeter. The detailed flammability parameters are given in Table 7.4 and the heat released undergoing burning is illustrated in terms of heat released rate (HRR) as a function of burning time (Figure 7.5). The definition of all the parameters is given in chapter 4. A two-peak signal appeared in the HRR curves of the sample loaded with clay. It seemed to be due to the transient protective effect of the clay layers during the combustion [16]. The following combustion of the material occurred when the layer was broken.

Table 7.4 Combustive parameters of AG/clay aerogels

Samples	t_i (s)	t_e (s)	TTHRR (s)	PHRR (kW/m^2)	FGR (kW/m^2 s)	THR (MJ m^{-2})	W_R (%)
AG15	10	386	36	232.9	6.5	19	2.9
AG15C5	11	146	27	121.1	4.5	17.2	23.6
AG5C5	15	91	24	56.4	2.4	4.9	45.4

t_i: time to ignite

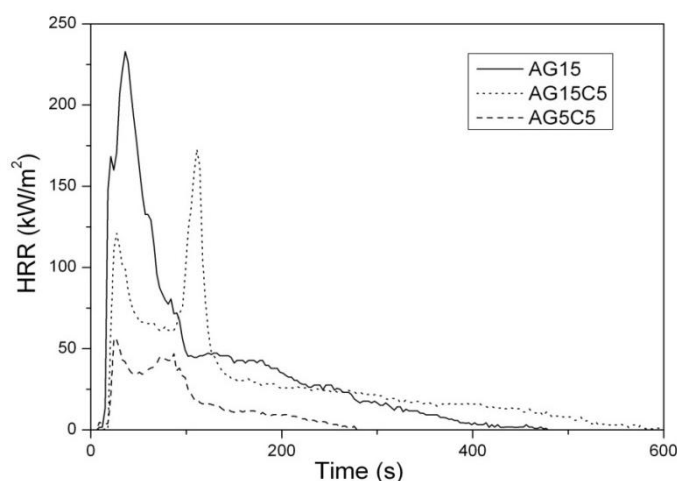

Figure 7.5 HRR as a function of time during cone calorimetry tests

Sample AG15 had a PHRR value of 233 kW/m^2 and time to PHRR of 36 s. Adding 33 % clay, PHRR decreased to 121 kW/m^2 and the FGR values reduced from 6.5 to 4.5 kWm^{-2} s. This tendency was also found in the other bio-based aerogels

when clay was adopted to improve the flame retardant properties. This is because of the formation of an inorganic clay layer by phase enrichment on the sample surface during the increasing thermal load [17], which brings a decomposition rate decline for the underlying polymer fraction. Decreasing the ratio of AG/clay, the flame retardant effect of clay was more remarkable, as displayed in sample AG5C5.

7.4. Conclusion

Arabic gum, a type of polysaccharide from African plant, was used to prepared green aerogels. Clay was added to improve the properties of Arabic gum aerogels. In comparison with the other biopolymers/clay aerogels, AG/clay aerogels behaved in a brittle manner due to weak interaction between AG and clay. This is because both components are negatively charged. Also, the AG solution showed a low viscosity even upon a high content (15%) was adopted, leading a layered structure without sufficient connection between them. For thermal stability and combustive behavior, clay layers within the aerogels acted as physical barrier, retarding the oxidation of AG underneath.

References

[1] Kaplan DL. Biopolymers from renewable resources: Springer Verlag; 1998.

[2] Randall R, Phillips G, Williams P. The role of the proteinaceous component on the emulsifying properties of gum arabic. Food Hydrocolloids. 1988;2:131-40.

[3] Sanchez C, Renard D, Robert P, Schmitt C, Lefebvre J. Structure and rheological properties of acacia gum dispersions. Food Hydrocolloids. 2002;16:257-67.

[4] Krishnan S, Kshirsagar AC, Singhal RS. The use of gum arabic and modified starch in the microencapsulation of a food flavoring agent. Carbohydrate Polymers.

2005;62:309-15.

[5] Verbeken D, Dierckx S, Dewettinck K. Exudate gums: occurrence, production, and applications. Applied Microbiology and Biotechnology. 2003;63:10-21.

[6] Ward FM. Uses of gum arabic (Acacia sp.) in the food and pharmaceutical industries. Cell and Developmental Biology of Arabinogalactan-Proteins: Springer; 2000. p. 231-9.

[7] Chen H-B, Chiou B-S, Wang Y-Z, Schiraldi DA. Biodegradable Pectin/Clay Aerogels. ACS applied materials & interfaces. 2013;5:1715-21.

[8] Phillips GO, Williams PA. Handbook of hydrocolloids: Elsevier; 2009.

[9] Deville S, Saiz E, Nalla RK, Tomsia AP. Freezing as a path to build complex composites. Science. 2006;311:515-8.

[10] Chen H-B, Wang Y-Z, Schiraldi DA. Foam-like materials based on whey protein isolate. European polymer journal. 2013;49:3387-91.

[11] Gibson LJ, Ashby MF. Cellular solids: structure and properties. 2nd ed: Cambridge university press; 1999.

[12] Hilyard N. Mechanics of cellular plastics. England: Applied Science; 1982.

[13] Ma H-S, Roberts AP, Prévost J-H, Jullien R, Scherer GW. Mechanical structure-property relationship of aerogels. Journal of Non-Crystalline Solids. 2000;277:127-41.

[14] Alhassan SM, Qutubuddin S, Schiraldi D. Influence of Electrolyte and Polymer Loadings on Mechanical Properties of Clay Aerogels. Langmuir. 2010;26:12198-202.

[15] Cozic C, Picton L, Garda M-R, Marlhoux F, Le Cerf D. Analysis of arabic gum: Study of degradation and water desorption processes. Food Hydrocolloids. 2009;23:1930-4.

[16] Alexandre M, Dubois P. Polymer-layered silicate nanocomposites: preparation, properties and uses of a new class of materials. Materials Science and Engineering: R: Reports. 2000;28:1-63.

[17] Kashiwagi T, Harris Jr RH, Zhang X, Briber R, Cipriano BH, Raghavan SR, et al. Flame retardant mechanism of polyamide 6-clay nanocomposites. Polymer. 2004;45:881-91.

Chapter 8: Glutaraldehyde Cross-linked Starch/Clay Aerogel

8.1 Introduction

Starch is one of most abundant plant polysaccharides with numerous applications in different industries due to its cheap price. Those include functions as energy nutrient in food products as well as additive in non-food products like textile and paper [1]. It mainly consists of amylose and amylopectin, of which the relative proportion depends on the starch source (e.g., potato, corn, wheat, tapioca) [2]. Amylose is linearly comprised of α-(1→4)-linked D-glucopyranosyl units with an average M_w of 500 kg/mol while amylopectin is composed by a backbone of 1,4-α-D-glucose with 1,6-branched glucopyranosyl units, forming the amorphous part and the crystalline parts, respectively [3]. Although several studies about starch aerogels have been published [4-8], starch has not been commonly used as a material for aerogel matrix.

Gleen reported the structures and properties of pure starch aerogels that were prepared using different drying process [9]. However, the mechanical properties of starch aerogel have been not systematically investigated. Also, there are no studies performed on how to improve the mechanical performance of starch aerogels. Sodium montmorillonite (Na$^+$-MMT) has been widely used to successfully enhance mechanical properties as well as the thermal stability and flame resistance of bio-based polymer aerogels [10, 11]. Therefore, it is expected that starch/clay composite aerogels will show superior properties than pure starch aerogels. On the other hand, chemical cross-linking can improve the properties of aerogels. Glutaraldehyde (GL) can react with hydroxyl groups on the starch molecules [12, 13]. It has been utilized to crosslink starch foam particles [14] and starch-polyvinyl

alcohol films [15]. This chemical process is related with a hydrated etherization reaction which is time-costly and needs drastic reactive conditions [16]. Recently, microwave-induced synthesis was considered with great interest due to its high efficiency [17]. Graft copolymerizations of polysaccharides have been reported without radical initiators or with very low initiator concentration on the effort of microwave irradiation [18-21]. It is feasible to take advantage of this approach to realize the cross-linked reaction of GL and starch.

In this chapter, bio-based starch aerogels were prepared using a freeze-drying process. Na^+-MMT was added to starch aerogel, forming an organic-inorganic hybrid aerogel. GL was designed to react with starch with the assistance of microwave irradiation. The effect of clay addition and GL cross-linking on structures and mechanical properties of starch aerogels were investigated.

8.2 Experimental

All the information of raw materials for preparing the aerogels was presented in Chapter 3.1.

Pure starch aerogels were prepared following the method presented in chapter 3.2. Desired amount of starch powder was dissolved in deionized water, and then mechanically stirred at 80 ^{o}C for 2 hours. The obtained homogenous solutions were frozen at -30 ^{o}C in a fridge over night, and then ice was sublimated using a lyophilizer under 0.001 mbar and -80 ^{o}C, as described in previous chapters.

To produce cross-linked starch aerogels, glutaraldehyde solution was dropped into the prepared homogeneous starch solution. Hydrochloric acid was then added to adjust the PH value of the solution to PH=3. The mixed solutions were irradiated using a domestic microwave oven under 800 watt for 30 seconds. Then the same freeze-drying process was conducted.

The starch/clay aerogel composites were prepared through the same process

reported in previous chapters. The prepared starch solution and clay suspension were mixed to get a homogenous mixture prior to be frozen and lyophilized. GL was also incorporated to crosslink the starch/clay aerogel composites. The dispersed starch-clay mixture with GL was operated in microwave oven for 30 seconds before being frozen.

The identification of samples is according to the containing components followed by their corresponding mass fraction in the precursor suspension, as shown in Table 8.1.

Table 8.1 Composition of the aqueous suspensions for preparing starch based aerogels

Samples	Starch (wt%)	Na^+-MMT (wt%)	GL (w/w %) [a]
S5	5	0	0
S7.5	7.5	0	0
S10	10	0	0
S12.5	12.5	0	0
S5G2.5	5	0	2.5
S5G5	5	0	5
S5G10	5	0	10
S5C2.5	5	2.5	0
S5C5	5	5	0
S2.5C5	2.5	5	0
S7.5C5	7.5	5	0
S5C5G5	5	5	5

[a] (w/w %) indicates the weight percentage of GL relative to the weight of starch in solution.

Samples were subjected to characterization including SEM, compression, FTIR-ATR, and thermal conductivity. All the testing methods were according to the description done in chapter 3.3.

8.3 Results and Discussion
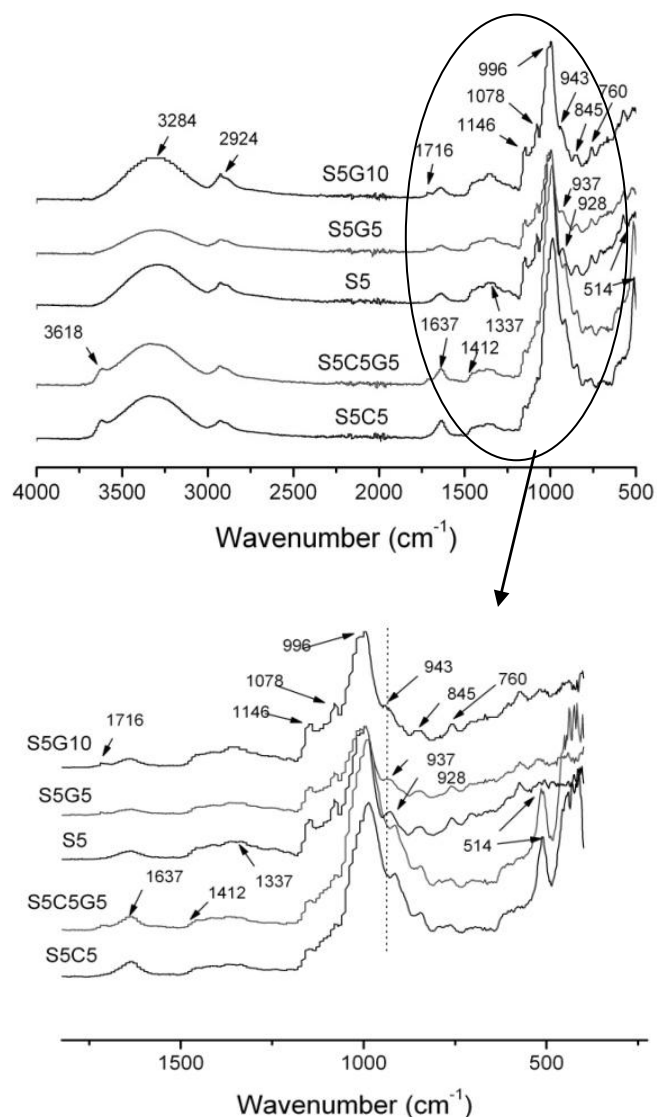
8.3.1 FTIR Spectrum

Figure 8.1 FTIR spectra of starch based aerogels

FTIR analyses were conducted to confirm the cross-linking reaction. Figure 8.1 shows the obtained spectra. The characteristic peaks of pure starch aerogel are located at 3284 cm^{-1}, 2924 cm^{-1} and 1637 cm^{-1}, which corresponds to bonded OH stretching, CH$_2$ asymmetry stretching and OH bending, respectively [22]. For the band of CH$_2$ bending vibration, two peaks appear at 1412 cm^{-1} and 1337 cm^{-1}, which are associated with CH$_2$ scissoring and CH$_2$ twist vibration, respectively [23]. In the region between

144

900 cm^{-1} and 1200 cm^{-1}, the bands at 1146 cm^{-1} and 1078 cm^{-1} contribute to the stretching vibration of C-O-C which bridges the glucoses units; the other two bands at 996 cm^{-1} and 928 cm^{-1} are related to the C-O stretching in anhydrous glucose ring of starch molecules [24]. In addition, the peaks at 845 cm^{-1} and 760 cm^{-1} are assigned to the bending of CH in the glucose ring [22]. With the addition of clay, new peaks appear at 3618 cm^{-1} and 514 cm^{-1}, which are attributed to the free water in the interlayer of pristine MMT and Al-O bending, respectively [25].
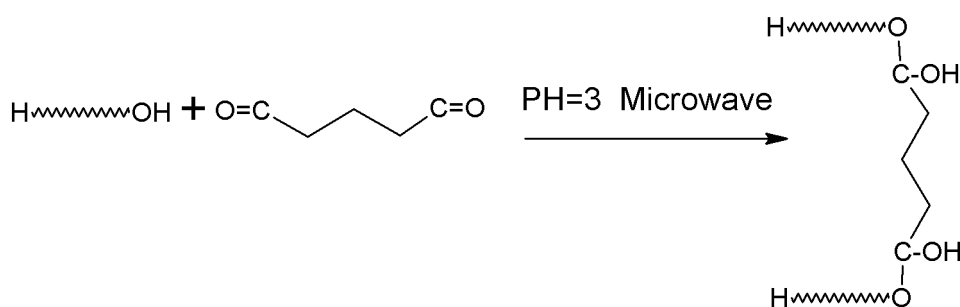

Figure 8.2 The scheme of chemical reaction of starch and GL

When 5 % GL was incorporated, the band at 928 cm^{-1} in pure starch aerogel was shifted to 937 cm^{-1}. This is because -OH in the starch molecules reacted with GL, as depicted in Figure 8.2, affecting the vibration of C-O in glucose ring. Moreover, a new band appeared in 1716 cm^{-1} due to the unreacted C=O groups of GL and the C-O stretching band at 928 cm^{-1} was moved to higher wavenumber (943 cm^{-1}).

8.3.2 Solubility and Swelling

Aerogels crosslinked with different amount of GL and neat starch sample S5 were firstly cut to equal dimensions, and then placed in three different beakers containing 200 ml of DI water at room temperature. It was observed that the unmodified sample was quickly dissolved into the cold water. GL-crosslinked samples were not dissolved; instead, they swelled in water and were transformed into stable hydrogels, as shown

in Figure 8.3.

After staying in DI water at room temperature for 2 weeks, these hydrogels did not show any tendency to dissolve. This suggested that the GL effectively crosslinked the starch molecules. The networks that were formed between the starch molecules created blocked aerogel skeletons. Increasing the temperature to 80 ^{o}C at which starch should be dissolved, sample S5G2.5 was just partly dissolved while the samples containing a higher amount of GL did not show any change.
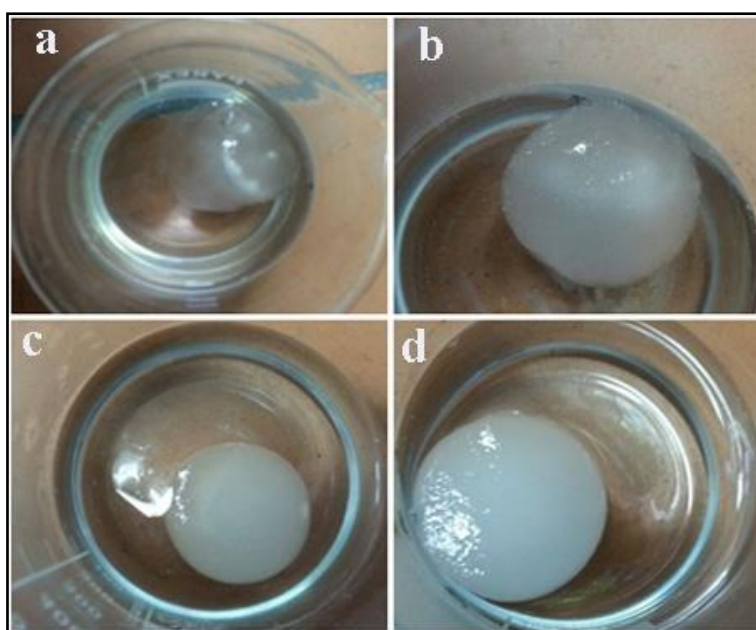

Figure 8.3 Configurations of GL-modified starch in water: (a)S5; (b)S5G2.5; (c)S5G5; (d)S5G10

8.3.3 Morphology

Pure starch aerogels exhibited the layered structures (Figure 8.4a and 8.4b) previously reported in the other biopolymer aerogels prepared through the same freeze-drying process. Increasing starch concentration in precursor solution, the porous laminas in sample S5 (Figure 8.4a) changed to solid layers appeared in sample S10 as can be observed in Figure 8.4b. This is because aerogels containing higher fraction of starch have higher apparent density as well as higher cell wall density.
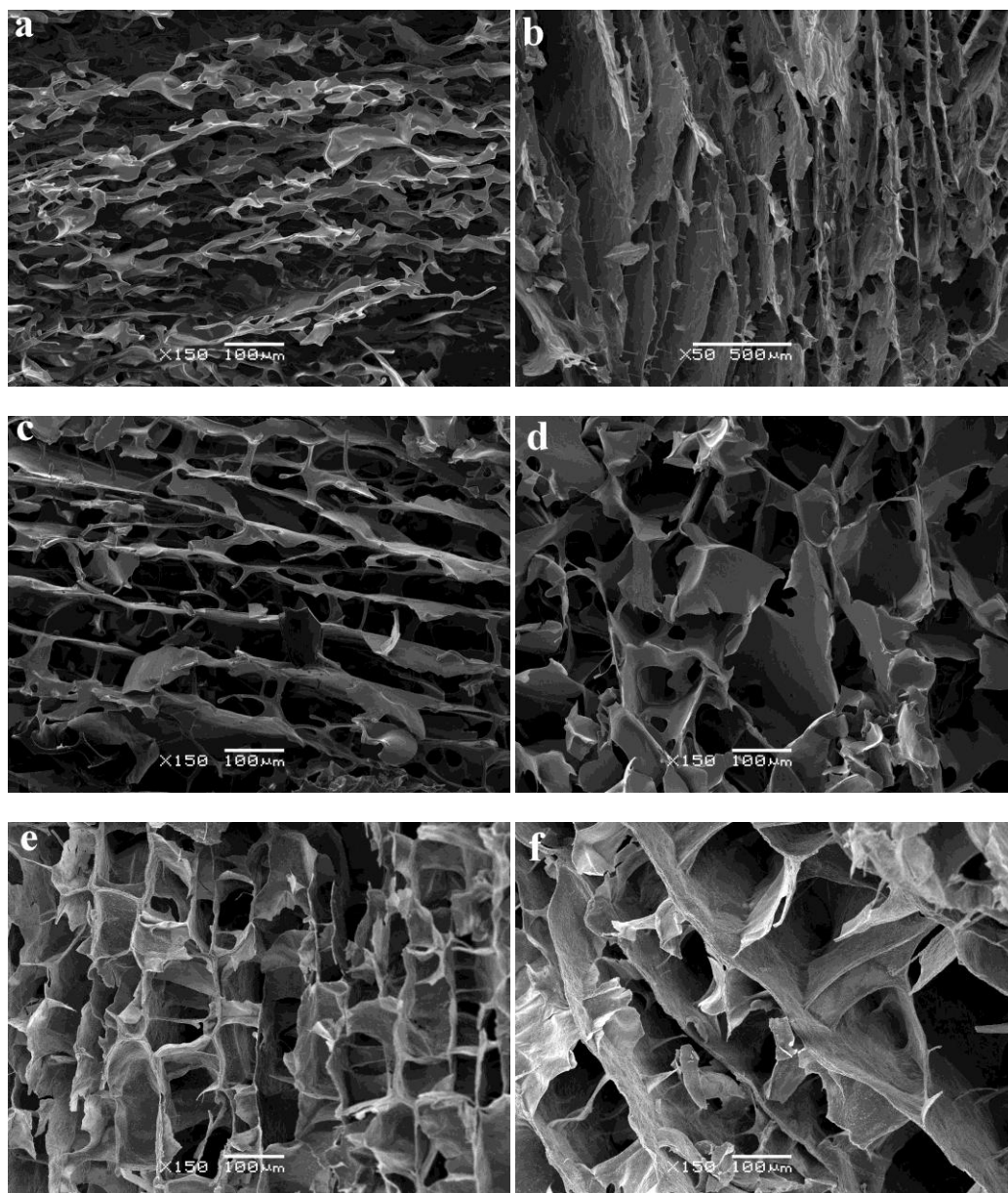
Figure 8.4 SEM micrographs of starch based aerogels: (a)S5; (b)S10; (c)S5G2.5; (d)S5G5; (e)S5C5; (f)S5C5G5

The structures of cross-linked aerogels varied with the content of GL. When 2.5 w/w% of GL was added to crosslink 5 wt% starch solution, the resultant sample (S5G2.5) displayed a lamellar structure composed of solid layers connected with struts (Fig. 8.4c). Starch molecules are assembled into large blocks after the cross-linking reaction, limiting the mass mobility and hence affecting their rearrangement at the grain boundaries between the growing ice crystals [26]. With the quantity of GL increased to 5 w/w%, the lamellar structure was substituted by a honeycomb-like

architecture (Fig. 8.4d) due to the further increment in solution viscosity and decrease in mass mobility of precursor solutions. However, further increase of GL amount to 10 w/w% did not change the aerogel microstructure. This indicates that a GL level of 5 w/w% is the optimum concentration. It kept consistent with FTIR investigation, which showed that unreacted GL was presented when 5 w/w% was added.

When inorganic clay was introduced to the precursor solution, clay nanoparticles were encapsulated by starch and reoriented by the growing ice front upon solution freezing, ultimately resulting in the "house of cards" structure in which the layers were linked by the polymeric phase (Fig. 8.4e). The incorporation of GL did not alter the overall structure of sample S5C5 (Fig. 8.4f).

These structural features are consistent with the observed differences in mechanical properties discussed in the following section.

8.3.4 Compressive Properties

The aerogel samples were subjected to compression test and the compressive stress-strain curves are shown in Figure 8.5. All the samples displayed typical elastic-plastic foam behaviour, which was similar with the other bio-based aerogels. The parameters defining the compressive mechanical behaviour are summarized in Table 8.2.

The mechanical properties of neat starch aerogels were strongly dependent on their densities. Increasing the starch content from 5 wt% to 12.5 wt%, the specific compressive modulus and energy absorption increased by 40 and 16 times, respectively. With the addition of clay, the mechanical performance of S5 was significantly improved. Our previous study and many other works analyzed the effect of clay on the structures and properties of biopolymer-clay aerogels [11, 26, 27]. Clay interacts with the biopolymers, reinforcing the strength of the sheet-like cell wall. Therefore, it enhances the mechanical properties of aerogels. In present work, clay strongly adhered to starch molecules, causing sample S5C5 to exhibit a much higher

structural integrity than S5. Sample S5C5 with a density of only 0.092 g/cm^3 possessed modulus of 7.39 MPa and yield strength of 212 kPa.

Increasing the starch fraction in the starch/clay composites (SxC5 series), the mechanical properties of aerogels were monotonically increased up to 50% even though the apparent density still increased. It may be attributed to the uneven distribution of clay nanoparticles in a highly viscous precursor suspension like the one containing 7.5 wt% of starch.
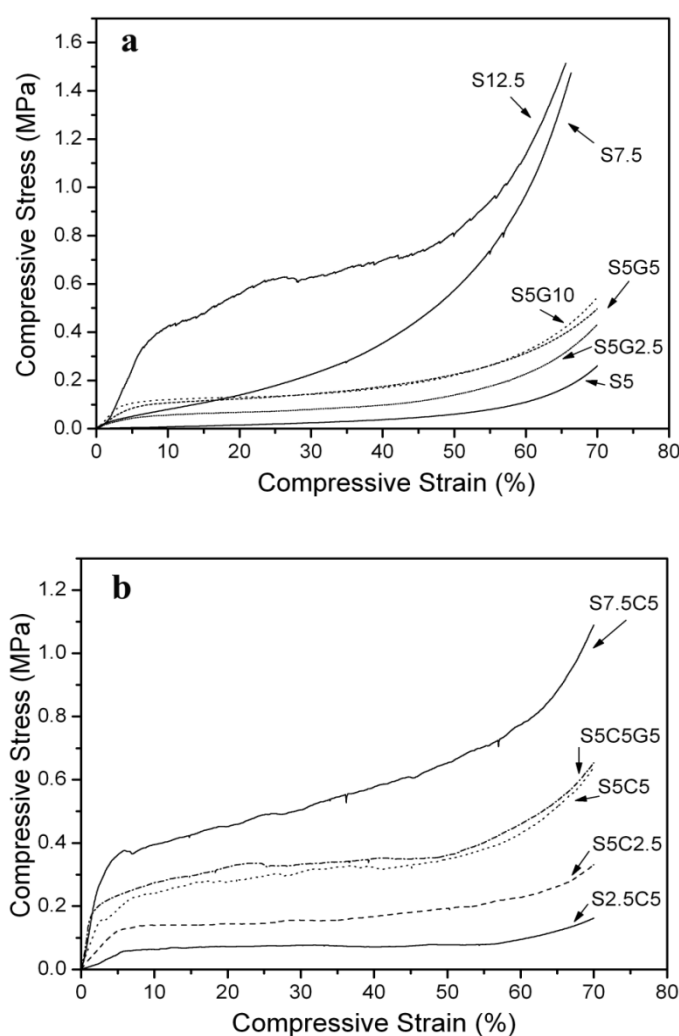

Figure 8.5 Compressive curves of (a) pure starch aerogels and GL cross-linked starch aerogels; (b) starch-clay composite aerogels

Incorporation of GL had a minimal effect on apparent densities of starch aerogels. However, both the compressive modulus and strength values were monotonically

increased with the GL concentration as shown in Table 8.2. Higher GL concentrations result in structures with greater cross-linking density that can support deformation more effectively under applied stress. Nevertheless, there were no significant changes on the specific compressive modulus and absorbed energy when the GL content was increased from 5 w/w% to 10 w/w%. This is because of the marginal effect of GL over 5 w/w% of concentration.

The best composition in the present study is the sample S5C5G5 with a specific modulus of 118 MPa, which is higher than the value of sample S5C5 (80 MPa). It indicates that the cross-linking effect also works within pure starch aerogels as well as the starch-clay aerogel composite.

Table 8.2 Compressive properties of starch based aerogels

Samples	ρ_{app} (g/cm^3)	E (Mpa)	E_s (MPa/g cm^{-3})	$\sigma_{60\%}$ (Mpa)	E_a at 60% ε (kJ/m^3)
S5	0.073±0.003	0.06±0.01	0.82±0.10	0.12±0.01	20.36±0.86
S7.5	0.116±0.008	1.25±0.48	10.79±3.77	0.82±0.18	155.07±26.73
S12.5	0.136±0.008	5.75±1.03	41.11±7.79	1.05±0.11	323.62±61.76
S5G2.5	0.071±0.002	1.6±0.28	22.07±3.34	0.21±0.02	52.65±4.22
S5G5	0.063±0.001	2.05±0.29	32.63±4.42	0.29±0.02	87.76±5.94
S5G10	0.068±0.001	2.42±0.47	35.79±6.96	0.30±0.03	84.74±17.87
S2.5C5	0.082±0.002	1.34±0.11	16.38±1.86	0.11±0.02	37.34±8.09
S5C5	0.092±0.01	7.39±1.64	80.25±18.32	0.44±0.04	189.27±14.38
S5C2.5	0.086±0.003	2.98±0.11	35.27±1.86	0.21±0.02	88.06±8.09
S7.5C5	0.113±0.002	8.85±1.87	78.12±15.10	0.73±0.05	285.77±15.66
S5C5G5	0.101±0.002	11.93±2.27	118.86±22.00	0.43±0.03	170.33±26.33

8.3.5 Thermal Conductivity

The increase of thermal conductivity with aerogel density is a known phenomenon and has been reported, for instance, for silica aerogel [28]. It is attributed to the increase of solid mass and pore wall thickness leading to the increased in solid phase conduction. However, in this research, introducing 50 % clay, the thermal conductivity slightly decreased from 0.059 to 0.053 W/(m K) with the apparent

density increased. This is possibly because the starch-clay hybrid aerogel exhibited a more porous structure than the pure starch aerogel. A tortuous path was created for gas phase transferring. This trend was similar to the one of polyvinyl alcohol-clay aerogels thermal conductivity [29].

In addition, the thermal conductivity of starch/clay aerogels is comparable to those of glass fiber and rock wool (0.04-0.05 W/(m K)) [30] and is lower than that of wood wool (0.09 W/(m K)) [31]. However, it is higher than those of some close-cell foams, such as polystyrene (0.02–0.04 W/(m K)) [32].

8.4 Conclusion

In this chapter, starch aerogels and starch-clay composite aerogels were prepared using the same freeze-drying process. Glutaraldehyde cross-linked aerogels displayed much higher mechanical properties than the unmodified ones. FTIR analysis indicated that glutaraldehyde effectively reacted with starch. The SEM results showed the cross-linking significantly changed the structures of aerogels. GL level of 5 w/w% was the optimum concentration. Thermal conductivity of some samples was investigated. Clay addition reduced the thermal conductivity of starch aerogel due to the tortuous path in starch-clay aerogel.

References

[1] Glenn GM, Imam SH, Orts WJ. Starch-based foam composite materials: Processing and bioproducts. MRS bulletin. 2011;36:696-702.

[2] Ellis RP, Cochrane MP, Dale MFB, Duffus CM, Lynn A, Morrison IM, et al. Starch production and industrial use. Journal of the Science of Food and Agriculture. 1998;77:289-311.

[3] Phillips GO, Williams PA. Handbook of hydrocolloids. In: 2rd, editor. England: Cambridge; 2009. p. 108-41.

[4] Chang X, Chen D, Jiao X. Starch-derived carbon aerogels with high-performance for sorption of cationic dyes. Polymer. 2010;51:3801-7.

[5] García-González C, Uy J, Alnaief M, Smirnova I. Preparation of tailor-made starch-based aerogel microspheres by the emulsion-gelation method. Carbohydrate Polymers. 2012;88:1378-86.

[6] García-González C, Camino-Rey M, Alnaief M, Zetzl C, Smirnova I. Supercritical drying of aerogels using CO_2: effect of extraction time on the end material textural properties. The Journal of Supercritical Fluids. 2012;66:297-306.

[7] Mehling T, Smirnova I, Guenther U, Neubert R. Polysaccharide-based aerogels as drug carriers. Journal of Non-Crystalline Solids. 2009;355:2472-9.

[8] Svagan AJ, Samir MA, Berglund LA. Biomimetic foams of high mechanical performance based on nanostructured cell walls reinforced by native cellulose nanofibrils. Advanced Materials. 2008;20:1263-9.

[9] Glenn GM, Irving DW. Starch-based microcellular foams. Cereal chemistry. 1995;72:155-61.

[10] Chen H-B, Chiou B-S, Wang Y-Z, Schiraldi DA. Biodegradable Pectin/Clay Aerogels. ACS applied materials & interfaces. 2013;5:1715-21.

[11] Chen H-B, Wang Y-Z, Sánchez-Soto M, Schiraldi DA. Low flammability, foam-like materials based on ammonium alginate and sodium montmorillonite clay. Polymer. 2012;53:5825-31.

[12] Dai W, Barbari T. Hydrogel membranes with mesh size asymmetry based on the gradient crosslinking of poly (vinyl alcohol). Journal of Membrane Science. 1999;156:67-79.

[13] Colosi C, Costantini M, Barbetta A, Pecci R, Bedini R, Dentini M. Morphological Comparison of PVA Scaffolds Obtained by Gas Foaming and Microfluidic Foaming Techniques. Langmuir. 2013;29:82-91.

[14] El-Tahlawy K, Venditti RA, Pawlak JJ. Aspects of the preparation of starch microcellular foam particles crosslinked with glutaraldehyde using a solvent exchange

technique. Carbohydrate Polymers. 2007;67:319-31.

[15] Ramaraj B. Crosslinked poly(vinyl alcohol) and starch composite films. II. Physicomechanical, thermal properties and swelling studies. Journal of applied polymer science. 2007;103:909-16.

[16] Hennink W, Van Nostrum C. Novel crosslinking methods to design hydrogels. Advanced drug delivery reviews. 2012;64:223-36.

[17] Galema SA. Microwave chemistry. Chem Soc Rev. 1997;26:233-8.

[18] Işıklan N, Küçükbalcı G. Microwave-induced synthesis of alginate-graft-poly (N-isopropylacrylamide) and drug release properties of dual pH- and temperature-responsive beads. European Journal of Pharmaceutics and Biopharmaceutics. 2012;82:316-31.

[19] Tiwari A, Singh V. Microwave-induced synthesis of electrical conducting gum acacia-graft-polyaniline. Carbohydrate Polymers. 2008;74:427-34.

[20] Singh V, Tiwari A, Pandey S, Singh S. Peroxydisulfate initiated synthesis of potato starch-graft-poly (acrylonitrile) under microwave irradiation. eXPRESS Polymer Letters. 2007;1:51-8.

[21] Singh V, Tiwari A, Tripathi DN, Sanghi R. Microwave assisted synthesis of guar-g-polyacrylamide. Carbohydrate Polymers. 2004;58:1-6.

[22] Socrates G, Socrates G. Infrared and Raman characteristic group frequencies: tables and charts. Third ed: Wiley Chichester; 2001.

[23] Fang J, Fowler P, Tomkinson J, Hill C. The preparation and characterisation of a series of chemically modified potato starches. Carbohydrate Polymers. 2002;47:245-52.

[24] Pushpadass HA, Marx DB, Hanna MA. Effects of extrusion temperature and plasticizers on the physical and functional properties of starch films. Starch-Stärke. 2008;60:527-38.

[25] Xu Y, Zhou J, Hanna MA. Melt-intercalated starch acetate nanocomposite foams as affected by type of organoclay 1. Cereal chemistry. 2005;82:105-10.

[26] Pojanavaraphan T, Magaraphan R, Chiou B-S, Schiraldi DA. Development of biodegradable foamlike materials based on casein and sodium montmorillonite clay.

Biomacromolecules. 2010;11:2640-6.

[27] Donius AE, Liu A, Berglund LA, Wegst UG. Superior mechanical performance of highly porous, anisotropic nanocellulose-montmorillonite aerogels prepared by freeze casting. Journal of the Mechanical Behavior of Biomedical Materials. 2014;37:88-99.

[28] Koebel M, Rigacci A, Achard P. Aerogel-based thermal superinsulation: an overview. Journal of sol-gel science and technology. 2012;63:315-39.

[29] Hostler S, Abramson A, Gawryla M, Bandi S, Schiraldi D. Thermal conductivity of a clay-based aerogel. International Journal of Heat and Mass Transfer. 2009;52:665-9.

[30] Batty W, O'Callaghan P, Probert S. Apparent thermal conductivity of glass-fibre insulant: effects of compression and moisture content. Applied energy. 1981;9:55-76.

[31] Wu Q, Andersson RL, Holgate T, Johansson E, Gedde UW, Olsson RT, et al. Highly porous flame-retardant and sustainable biofoams based on wheat gluten and in situ polymerized silica. Journal of Materials Chemistry A. 2014;2:20996-1009.

[32] Al-Ajlan SA. Measurements of thermal properties of insulation materials by using transient plane source technique. Applied Thermal Engineering. 2006;26:2184-91.

Chapter 9: Biodegradability of Aerogels

9.1 Introduction

One of the most attractive advantages of bio-based polymers is their excellent biodegradability. On the basis of environmental considerations, exploiting the usage of biopolymers is an increasing concerned topic. Bio-based aerogels are a choice that can smooth over the landfill shortage problems initiated by abundant waste of non-biodegradable conventional plastics.

Schiraldi's studies showed that polysaccharide-based pectin aerogel degraded very fast in a compost media with duration of only 10 days and its degree of biodegradability was as high as 50% [1]. However, apart of this work, the biodegradability of this type of low-density materials was seldom reported. Aerogels based on different biodegradable polymers were prepared in the previous chapters. Some of them are made from water-soluble synthesized PVOH, while others are polysaccharide-based. Among those aerogels based on polysaccharides, cellulose fiber has a higher crystallinity than the rests that exhibit similar molecular structures (starch, CMC, agar, et al.). Therefore, their degradable behavior should be different. On the other hand, these polymeric aerogels that have high porosity may show a distinct biodegradability in regard to their corresponding solid materials. According to these considerations, PVOH-, RCF/CMC- and starch-based aerogels have been chosen as representative of different biodegradation behavior of the aerogels prepared along this work. To analyse the effect of porosity, the selected aerogels samples were compressed to make films and their biodegradability was compared with the corresponding aerogels.

9.2 Experimental

Aerogels samples and compressed aerogels films that were investigated were based on PVOH, CMC/RCF and starch, respectively. The most representative compositions, (5P5C, R2.5C2.5 and S5) were chosen. The corresponding aerogels films were prepared using an IQAP LAP PL-15 press (QAP Masterbatch group SL, Barcelona, Spain). Cylinder aerogel was firstly placed between two steel plates covered with a thin polytetrafluoroethylene fabric (thickness: 0.2 mm) and then compressed into a film operating at 25 ^{o}C and 60 bar for 3 minutes.

A micro respirometer system was made following ISO/FDIS 14855-2 method [2], as illustrated in Figure 9.1. Compressed air flow was generated by a pump. A flask filled with sodium hydroxide pellets (Merck KGaA, Damstadt, Germany) was set as a trapper to remove CO_2 in the air before they were injected into a 1000 ml reactive vessel. Prior to the tests, 82 grams of compost composed by 1/3 wt% compost soil, 1/3 wt% soy protein and 1/3 wt% wood pieces were poured into the reactive vessel. Then 5 grams of aerogel or film specimens were embedded into compost. Finally, the reactive vessel was kept in a water base (Precisterm S-387) operating at 65 ^{o}C. During the tests, 20 ml of water was added to each reactive vessel every three days. Aerogel gradually degraded into CO_2, H_2O, CO et al. Water was absorbed by calcium chloride dehydrate (Sigma-Aldrich) and the evolved CO_2 flow was recorded by a K-30 CO_2 sensor (CO_2 Meter, Inc., FL, USA). The compost was also conducted as a blank sample.

9.3 Results and Discuss

The flow of CO_2 released from system was taken as indicative of the degradation rate

of materials. The evolved CO_2 was calculated from the integral values of CO_2 flow rate as displayed in Figure 9.2. All the samples exhibited a similar trend in the decomposition behaviour: a steep increase in the degradation rate occurred in 15 days until a plateau stage after 27 days where the degradation was finished.
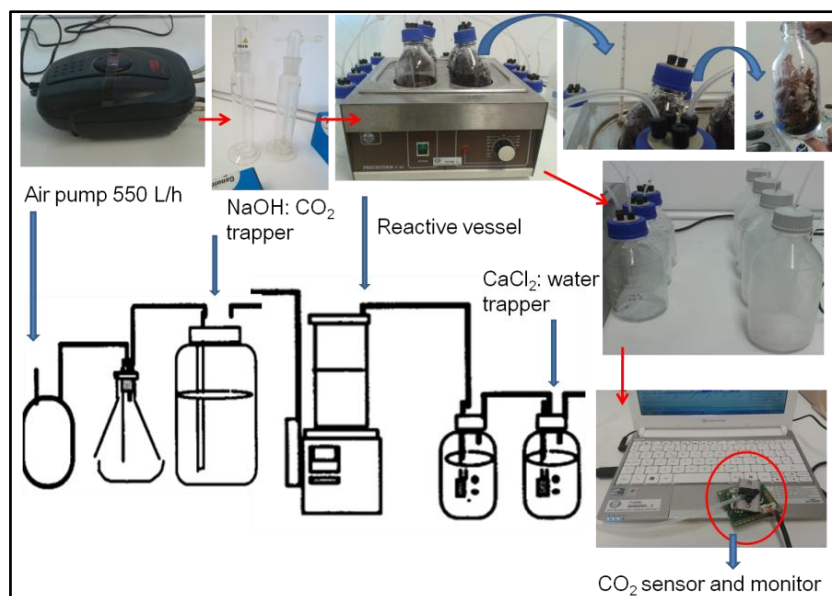

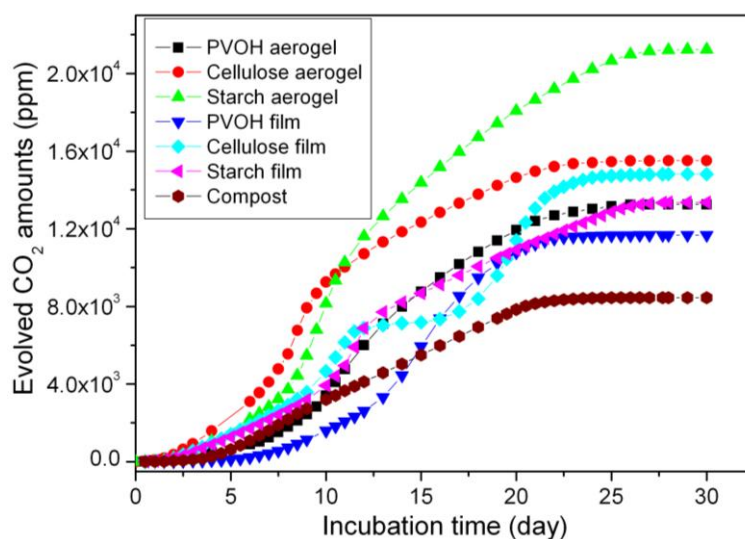Figure 9.1 Illustration of homemade respirometer system

Figure 9.2 Biodegradability behaviors of aerogel samples and compressed aerogel films

Both cellulose and starch based aerogels exhibited a higher decomposition rate and released more CO_2 than the one based on PVOH. This indicated that the natural cellulose and starch have a better biodegradability than synthesized PVOH. On the

other hand, pure starch aerogel decomposed faster than CMC/RCF hybrid aerogel as shown by a change in the slope of the decomposition plot observed after 10 days. This is due to the higher degree of crystalline of RCF in comparison to starch and CMC. The same reason is responsible for the two rapid decomposition steps appeared in the decomposition plot of R2.5C2.5 compressed aerogel film.

The decomposition rates of solid films were lower than their aerogel counterparts. This is due to the higher specific surface area of aserogels. The porous aerogel structure is beneficial to organism cells adhesion, growth and proliferation [3]. As a result, a faster consumption of the matrix occurred in comparison to films, which was shown as increased CO_2 released rate and total CO_2 released amount.

The starch and cellulose films also showed a higher ability to decompose comparing with PVOH, which was in line with previous investigations [4]. It is worth highlighting that the CO_2 production of PVOH-based aerogel or film was lower than that of the compost during the initial decomposition stage. This is most likely attributed to a type of noxious impact produced by the PVOH on the reproduction of microorganism in the compost [5].

9.4 Conclusion

The biodegradability of PVOH-, cellulose- and starch-based aerogels and corresponding compressed solid films were investigated through a homemade micro respirometer system. Bio-based materials based on starch and cellulose had a better biodegradability than that of synthesized PVOH. Aerogels decomposed faster than their solid counterparts due to their porous structures and resultant specific surface areas, which favoured the adhesion, growth and proliferation of microorganism.

References

[1] Chen H-B, Chiou B-S, Wang Y-Z, Schiraldi DA. Biodegradable Pectin/Clay Aerogels. ACS applied materials & interfaces. 2013;5:1715-21.

[2] ISO/FDIS 14855-2:2007(E): Determination of the ultimate aerobic biodegradability of plastic materials under controlled composting conditions-Method by analysis of evolved carbon dioxide-Part 2: Gravimetric measurement of carbon dioxide evolved in a laboratory-scale test.

[3] O'Brien FJ, Harley B, Yannas IV, Gibson LJ. The effect of pore size on cell adhesion in collagen-GAG scaffolds. Biomaterials. 2005;26:433-41.

[4] Solaro R, Corti A, Chiellini E. A new respirometric test simulating soil burial conditions for the evaluation of polymer biodegradation. Journal of environmental polymer degradation. 1998;6:203-8.

[5] Chiellini E, Corti A, D'Antone S, Solaro R. Biodegradation of poly (vinyl alcohol) based materials. Progress in Polymer Science. 2003;28:963-1014.

General Conclusions

Robust foam-like materials based on polymers and sodium montmorillonite clay were prepared through a simple environmentally friendly freeze-drying process in which water was used as solvent. Both biodegradable synthesized and bio-based polymers were utilized in this work, including PVOH, cellulose, xanthan gum, agar, Arabic gum and starch.

Within the polymer-clay aerogels, polymer molecules play a role of glue linking the Na^+-MMT nanoparticles, resulting in higher mechanical performance than pure clay aerogels. On the other hand, Na^+-MMT platelets serve as a physical barrier that increases the heat resistance.

In regard to PVOH-clay aerogels, polymer concentration played the major role on porosities, apparent densities and mechanical properties (compression and impact). Of the different types of flame retardant fillers (ALH, APP, silica gel and K_2CO_3) were investigated, APP and ALH modified PVOH-clay aerogels showed better flame retardant properties according to cone calorimeter tests. Moreover, higher loading of ALH lead to lower peak of heat released rate and fire growth rate.

RCF-CMC composite aerogels exhibited tunable microstructures and mechanical properties by changing RCF/CMC ratio. The mechanical properties of aerogels were increased with the fiber amount up to 3.75 wt%. The addition of RCF not only promoted moisture resistance but also improved the dimensional stability. APP and clay, which were used as addtives, played a synergetic effect on the flame retardancy and thermal stability of cellulosic aerogels.

Within the XG/agar/clay aerogels, the synergistic effect between two polysaccharides made the aerogels display a significant improvement in mechanical properties

compared with those containing a single biopolymer. The highest specific modulus and yield stress were obtained in the 40/60 XG/agar blend (69.4 MPa and 61.9 kPa, respectively) due to its honeycomb-like structure.

Arabic gum-clay and starch-clay systems were afterward investigated. It was found that the viscosity of the mixtures has a decisive effect that determined that final mechanical properties of polymer-clay aerogels. Arabic gum is negatively charged resulting in repulsion with clay nanoscale platelets while starch molecules are neutral showing interactions with clay via hydrogen bonding. Glutaraldehyde was used to enhance the structural integrity and mechanical properties of starch aerogels through crosslinking reaction with starch molecules, which was proved by FTIR analysis. GL level of 5 w/w% was the optimum concentration, which increased the specific modulus more than 30 times.

The biodegradability of representative prepared aerogel samples (P5C5, F2.5C2.5, S5) were investigated. Cellulose or starch based aerogels exhibited a higher biodegradability than PVOH one. Moreover, porous aerogels decomposed faster than their corresponding solid films due to the higher specific surface area.

Outlook

An extensive work would be to expand the functions and modify the drawbacks of the polymer-clay aerogels, such as improving the flexibility, resilience and hydrophobicity.

The polymers and clay used in this work are all moisture sensitive due to their chemical structure with hydroxyl functional groups. According to our study, the moisture content is about 10 wt%, which significantly reduces the mechanical properties. A silylation or fluorination treatment could endow surface or body hydrophobicity to aerogels. Repellent polymer/clay aerogel could be applies as buoy or reusable absorbent.

Polymer-clay aerogels do not have resilience and flexibility, which limiting the reusability. To overcome this drawback, the cell wall structures of aerogels should be modified. Special crosslinking agents could be used to created networks within the aerogels. This part of work should be deeply developed in future.

Publications

1. Liang Wang, Miguel Sánchez-Soto, Jordi J. Bou and Maria Lluisa Maspoch. Foam-like Materials from Renewable Resources. *5th International Conference on Biobased and Biodegradable Polymers*, San Sebastian, 6-9 October 2015.

2. Wang Liang, and Miguel Sánchez-Soto. Green bio-based aerogels prepared from recycled cellulose fiber suspensions. *RSC Advances*, 2015, 5(40): 31384-31391.

3. Wang, L.; Schiraldi, D.; Sanchez, M. Foamlike xanthan gum/clay aerogel composites and tailoring properties by blending with agar. *ACS Industrial & engineering chemistry research*, 2014, 53(18): 7680-7687.

4. Wang L, Sánchez-Soto M, Maspoch ML. Polymer/Clay Aerogel Composites with flame retardant agents: mechanical, thermal and fire behavior. *Materials & Design*, 2013, 52: 609-14.